Model for a cortical circuit associated with childhood absence epilepsy

by

Maliha Ahmed

A thesis
presented to the University of Waterloo
in fulfillment of the
thesis requirement for the degree of
Master of Mathematics
in
Applied Mathematics

Waterloo, Ontario, Canada, 2019

I hereby declare that I am the sole author of this thesis. This is a true copy of the thesis, including any required final revisions, as accepted by my examiners.

I understand that my thesis may be made electronically available to the public.

Abstract

Childhood absence epilepsy is suspected to result from mutations in genes which encode ion channels including sodium channels. Our purpose in this thesis is to explore some of the factors that alter the function of neurons in the cerebral cortex. In particular, we investigate the consequence of these alterations on neuronal network activity associated with this disorder. In this regard, we create a small network consisting of deep layer cortical pyramidal neurons and an interneuron, each described by a single-compartment Hodgkin-Huxley style model. We investigate factors that convert a normal network into a hyperexcitable one, including impairment of $GABA_A$ synapses and sodium channel defects resulting from mutations in *Scn* genes. Our model agrees with experimental results indicating the role of GABA impairment in generating a hyperexcitable network. In particular, our cortical network is capable of generating its own spike-and-wave oscillations analogous to those in a thalamocortical network. Our results also suggest that the co-existence of multiple Na^+-channel mutations alters individual neuronal function to increase or decrease the likelihood of the network exhibiting seizure-like behaviour.

Acknowledgements

First and foremost, I would like to thank my supervisor, Dr. Sue Ann Campbell for her guidance, encouragement, and her incredible patience in supporting me throughout this research.

I would like to thank my graduate committee: Dr. Sue Ann Campbell, Dr. Anita Layton, and Dr. Brian Ingalls for taking the time to read this thesis.

I will always be grateful to Dr. Xiamei Jiang for the insightful conversations during my undergraduate studies and for being one of the biggest reasons behind my interest in applied mathematics.

Thank you to my colleagues and officemates: Jennie Newman, Zahraa Abbas, Lindsey Daniels, Thomas Bury, Kathyrn Fair, Saptarshi Pal, Brendon Phillips, and "extended officemates"– Dr. Sameed Ahmed, Dr. Rui Hu, and Mehrshad Sadria for being such inspiring company. I have learnt a lot from each of them. A special thanks to Manju Mathew, Apinaiya Rasalingam, and Seun Senbore for being there for everything. To all those who gave their support and encouragement, I am extremely grateful.

Lastly, I am thankful to my family– both of my brothers for being so selfless, and my parents for being my strength.

Dedication

This thesis is dedicated to my parents. *JazakAllah Khair* for **everything**.

Table of Contents

List of Tables

List of Figures

Chapter 1

Introduction

Epilepsy is one of the most common non-communicable neurological conditions, affecting over 50 million people worldwide [6]. It is characterized by frequent, unprovoked seizures which are defined as abnormal, excessive or hypersynchronous neuronal activity in the brain [7]. A number of factors are involved in characterizing the various seizure types. Broadly speaking, seizures are divided into two main categories: focal and generalized. Each of these categories consists of a number of subtypes. Focal, or formerly referred to as partial seizures, are seizures that originate in one or more localized regions of the brain, generally limited to a part of one brain hemisphere [8]. While simple partial seizures do not impair consciousness and may be convulsive, complex partial seizures, although not convulsive, do result in a loss of awareness and impaired consciousness [9]. Generalized seizures such as *absence seizures* affect both hemispheres of the brain [10][11].

Childhood absence epilepsy (CAE) is a common idiopathic pediatric epilepsy syndrome accounting for between 2–10% of all cases of epilepsy in children [12]. The condition begins in childhood, typically between the ages of 4 and 10 years, with a peak between 5 and 7 years [13]. It is characterized by brief episodes of impaired consciousness lasting about 5–10 seconds, hundreds of times a day, wherein the child may stare blankly accompanied by an upward roll of their eyeballs, without any convulsive motor activity [14]. Although in most cases the absence seizures resolve in adolescence, about 20% of children with CAE continue to have the condition which may progress into severity [15].

In addition to the observable seizure characteristics of each type of epilepsy, the most common tool used to detect and classify epilepsy type is an electroencephalogram (EEG). An EEG measures electrical activity in the brain and thus is capable of detecting abnormal patterns of activity. The procedure consists of tiny electrodes being placed on the patient's

scalp. These electrodes are capable of detecting electrical charges as a result of brain cell activity. The signals are amplified and recorded for evaluation [16]. EEG activity can be divided into different frequency bands, which are classified as different types of brain waves. Spikes in recordings are clearly distinguishable from other brain activity and are defined as very fast oscillations (lasting less than 80 milliseconds (ms)). The spike-and-wave pattern refers to brief spikes followed by a slower variation, called a slow wave [17], and are typical patterns in EEG recordings observed during epileptic seizures. A regular, symmetrical, generalized spike-and-wave discharge pattern is a signature of absence seizures. In the case of absence epilepsy, patients typically demonstrate bursts of bilateral and synchronous 2.5–4 Hz spike-and-wave activity [15] on the EEG. Figure 1.1 shows the EEG activity recorded in human patients with absence epilepsy.

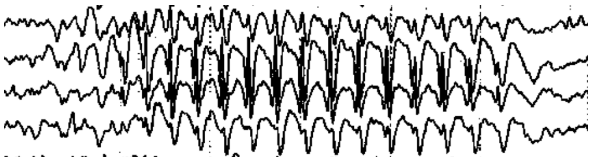

Figure 1.1: Electroencephalographic (EEG) recordings in human patients displaying an approximately 3-Hz spike-and-wave pattern. From [3] via Wikimedia Commons.

The study of childhood absence epilepsy in the clinic is rare for multiple reasons, including the young age of patients, and the nature of the study being potentially invasive. Hence, studies are commonly conducted on animal models, in particular, genetic models of rats and mice [18]. Genetic models refer to animals with genetic defects contributing to some or all symptoms of a disease. Being genetic models, they are helpful in understanding the pathophysiology of absence seizures as they tend to mimic the spontaneously occurring human epilepsy quite well [19]. The two rodent models that have been described and studied the most for CAE are the Wistar Albino Glaxo/Rijswijk (WAG/Rij) rats and the Genetic Absence Epilepsy in Rats from Strasbourg (GAERS) rats [20]. Both of these models, like all genetic models of absence epilepsy, exhibit bilateral and synchronized spike-wave-discharges (SWDs) on the EEG recordings, similar in pattern to ones observed in humans, however they are of a higher frequency, ranging between 7–11 Hz [21, 22].

In addition to the use of animal models, mathematical and computational modelling tools are powerful, especially in the study of neurological disorders such as epilepsy, to understand the dynamics of brain activity during an epileptic seizure. The approach to modelling is largely dependent on the use of the model itself. Broadly speaking, while ranging in complexity and detail, models can be placed in categories of being biophysical or phenomenological. While phenomenological models simply describe an empirical

relationship and convey the phenomena, biophysical models also capture the underlying biophysical mechanisms driving the concerned phenomena. In the case of neuron modelling, whether it is at the single-neuron level or the network level, the standard biophysical model is the conductance-based or Hodgkin-Huxley (HH) type model. In the HH model, with all the variations in properties of different ion channels, action potential generation results implicitly from the dynamics of the model.

Our work in this thesis involves a small network of neurons, each described by a single-compartment HH style model. Our purpose in this thesis was to explore factors that alter the function of individual neurons and give rise to an epileptic network associated with childhood absence epilepsy. In particular, we consider the following two factors: impairment of GABA synapses, and alterations of ion channels to simulate the effect of genetic manipulations. Thus, our approach consists of first defining "normal" (non-epileptic) and "abnormal" (epileptic) neuronal network activity in the cortex. In this regard, working with a simplified model of the HH type allows us to capture the necessary characteristics of the concerned neurons as they work together to play their part in modelling absence epilepsy.

The layout of this thesis is as follows. In Chapter 2, we provide the necessary background in biology, from the structure of the brain to the working components such as neurons. We describe the layered structure of the cerebral cortex and discuss the components comprising the absence circuitry. In Chapter 3, we describe neuron electrophysiology, and review conductance-based modelling, particularly the Hodgkin-Huxley model. We discuss the mechanism of neural communication by describing an action potential, and review synapse models. In Chapter 4, we summarize some of the known genetic mutations associated with absence epilepsy, including mutations in genes encoding sodium and h-channels. In Chapter 5, we describe a thalamocortical model by Traub et al., and discuss its use in this thesis [1]. In Chapter 6, we describe single-compartment models for different deep layer pyramidal neurons and an interneuron, all of which are reductions of neuron models described in the thalamocortical model by Traub et al. in the previous chapter. In Chapter 7, we discuss synaptic models used for AMPA and GABA synapses in our network model. In particular, we describe how synaptic conductances were set and provide a schematic of our reduced cortical network model. In Chapter 8, we discuss the results of modelling impaired GABA synapses as well as modelling sodium channel defects on our cortical network. In Chapter 9, we summarize our work and results, and discuss some of our model limitations as well as future work that could be built on this existing work.

Chapter 2

Background

2.1 Brain structure

The nervous system is divided into two parts, the central nervous system (CNS) and the peripheral nervous system (PNS). The CNS consists of the brain and the spinal cord, and is responsible for integration of all sensory information received, as well as triggering any necessary reactions [23]. The brain is divided into three broader parts: the *hindbrain*, the *midbrain*, and the *forebrain* [24]. The complexity of the functions performed increases with distance in regions further away from the brainstem, and the closer the regions get to the forebrain.

The hindbrain and midbrain are responsible for functions including breathing, control of digestion and heart rate, as well as learning motor skills. On the other hand, more complex functions are performed by parts of the forebrain which is composed of the *diencephalon* and *cerebrum*. The diencephalon is composed of the *thalamus* and *hypothalamus*. The thalamus is involved in processing and integrating information as it reaches higher regions in the brain such as the cerebral cortex. In fact, it acts as a relay station for any information going to or from the cortex, ensuring information is sent to the concerned cortical areas [25]. The cerebrum is the largest part of the brain with a surface known as the *cerebral cortex*. The outermost layer of the cortex is typically known as gray matter, while beneath it are long nerve fibers making a layer known as white matter.

The cerebral cortex is divided into four lobes: frontal, parietal, occipital and temporal as illustrated in Figure 2.1. Each lobe is designed to function in specific ways and holds responsibility for different functions [26]. Located in the front part of the brain, the frontal

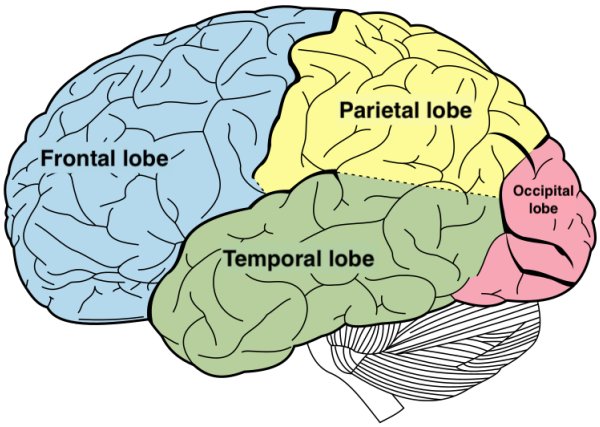

Figure 2.1: Lobes of the cerebrum. From [4] via Wikimedia Commons.

lobe is where higher executive functions are carried out. This includes problem solving, planning, coordination of motor skills, and regulation of emotions [27]. The parietal lobe is responsible for interpreting incoming sensory information as well as spatial and visual perception [24]. The occipital lobe is located at the back of the brain and is involved in processing visual information. This includes receiving visual information and interpreting its properties. The temporal lobe is also involved in processing sensory information, in particular, auditory information, as well as coordinating visual and verbal memory [27].

2.1.1 Neurons

The basic functional unit of the nervous system is a neuron. There are hundreds of billions of neurons working together to keep the nervous system functioning [28]. Although there are several types of neurons, they typically have four morphologically defined regions: the cell body (soma), dendrites, axon, and presynaptic axon terminals, and each region has a distinct function [29]. In general, based on their morphology, neurons are classified into three large groups: unipolar, bipolar and multipolar [30]. Unipolar neurons have a single structure extending away from the cell body, whereas bipolar neurons have a single axon and dendrite extending away from the soma. The most common neuron layout in vertebrates is a multipolar neuron, which typically consists of a single axon and many dendritic structures [29].

The cell body, called the soma, is fundamental to a neuron's survival. It contains the nucleus and is the location of protein synthesis. The dendrites branch out from the soma

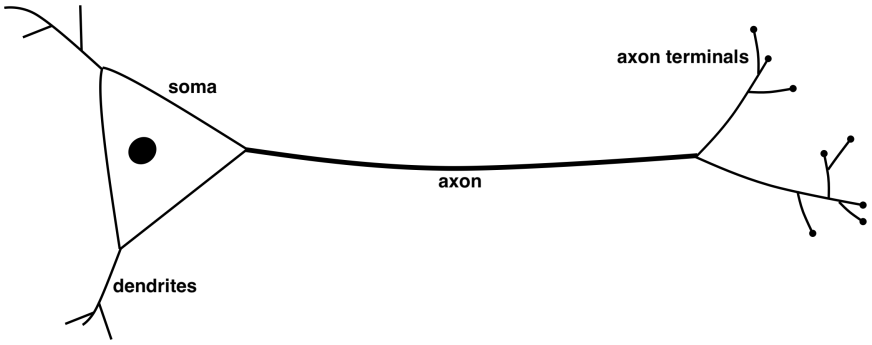

Figure 2.2: An illustration of a typical pyramidal neuron.

in a tree-like fashion. They are essential in receiving incoming signals from other neurons. Most neurons have a single axon extending outward from the soma, and the axon can vary in length from a millimeter to over a meter [31]. Axons conduct electric impulses called *action potentials*. Action potentials are means by which neurons communicate with one another. They are initiated in the axon initial segment, and these signals can propagate down the axon at speeds from 1 to 100m/s [29]. While dendrites are responsible for bringing information into the cell, axon terminals, located in a branch near the end of the axon are responsible for transmission of information to dendrites of other neurons.

2.1.2 Synapses

Axon terminals are the main point of contact with other neurons and their zone of communication is known as a synapse [32]. A presynaptic cell is the neuron transmitting a signal, while a postsynaptic cell is the neuron receiving the signal. The synaptic cleft is a narrow space between the presynaptic and postsynaptic cell. The vast majority of synapses, and those of interest to our work, are *chemical synapses*. In order for communication to occur between neurons, once an action potential reaches the presynaptic terminal, several processes take place. The axon terminal contains vesicles of neurotransmitters which are chemicals involved in neurotransmission. The primary neurotransmitters are *glutamate* and *gamma-Aminobutyric acid* (GABA) [33]. Excitation of the axon terminal causes voltage-gated calcium channels to open, causing an influx of calcium. This stimulates the synaptic vesicles to dock to the presynaptic membrane and release neurotransmitters into the synaptic cleft. The neurotransmitter molecules diffuse across to reach a dendrite of the postsynaptic cell. The molecules bind to specific receptors on the postsynaptic membrane which then activate or inactivate the appropriate ion channels, depending on the type

of neurotransmitter. The neurotransmitter glutamate stimulates two kinds of receptors, α-amino-3-hydroxy-5-methyl-4-isoxazolepropionic acid (AMPA)/kainate, and N-methyl-D-aspartate (NMDA), both of which cause excitation of the membrane. The neurotransmitter GABA, on the other hand, is the major neurotransmitter which results in inhibition. There are in fact, two main receptors for GABA: $GABA_A$ and $GABA_B$. While $GABA_A$ is responsible for fast inhibition, $GABA_B$ synapses activate *indirectly*, following a series of intracellular events [33]. In particular, the transmitter binding event activates an intracellular complex called a G-protein which causes inhibition of the postsynaptic neuron via activation of potassium channels. Thus, the combination of molecules and receptors cause changes in the postsynaptic neuron depending on the type of neurotransmitter involved, resulting in either increasing the postsynaptic neuron's likelihood of firing or decreasing it [34].

2.1.3 Cerebral Cortex

The cerebral cortex is the region of the brain involved in the most complex of tasks and thus naturally requires complex connections within its structure as well as with other areas of the brain. The outermost layer of the cortex commonly known as gray matter consists mostly of cell bodies of neurons, whereas the deeper layer also known as white matter consists of nerve cell axons [25]. The thickness of the human cerebral cortex varies from 1 to 4.5 mm [35], and it is divided into six distinct layers, as shown in Figure 2.3.

The cortex is populated by pyramidal and two types of non-pyramidal neurons, which may be further classified into numerous types, numbering in over 50 [36][37]. Excitatory neurons tend to form synapses with other excitatory neurons with similar properties. Whereas inhibitory neurons innervate surrounding neurons regardless of preference with excitatory neurons. The formation of synapses allows subnetworks to form. Within the subnetwork, excitatory neurons may excite an inhibitory neuron upon stimulation, which in turn inhibits excitation, but since excitatory neurons excite other "like-excitatory neurons", this provides a recurrent excitation back to the original neuron, overcoming the general inhibition. This means that neurons that need to be active can continue to do so, while others continue to undergo inhibition.

Cortical pyramidal neurons are the most numerous type of cortical neurons. They have a cell body shaped like a pyramid, with a dendrite emerging perpendicular towards the cortical surface, known as an apical dendrite. The basal dendrites are dendrites that arise from the base of the cell body and run relatively parallel to the cortical surface. In addition, a single axon emerges from the base of the cell body and runs perpendicularly away from

the cortical surface and terminates either in other cortical layers or in the subcortical white matter [38]. Axons in the cortex can serve as projection fibers that leave the cortex and project to other regions such as the thalamus, brainstem or spinal cord. The importance of pyramidal neurons is such that they are the main source of output of information from the cerebral cortex [39].

The six-layer structure of the cortex consists of different neuron types and functions differing by layer. In general, the first four layers function as input stations while the remaining layers function as output stations with several corticofugal axons (axons that leave the cortex to project outwards). Layer 1, the most superficial layer of the cortex consists of dendrites and axons from numerous neurons. With the presence of numerous dendrites and axons, several synaptic connections also exist within this layer. Layer 2 of the cortex contains some small pyramidal and non-pyramidal neurons. Their dendrites extend upwards towards layer 1, while their axons extend towards the deeper layers to either form local synaptic connections within the cortical layers or in other cortical regions. Layer 3, also known as the external pyramidal layer is mainly populated by pyramidal neurons. Their apical dendrites extend and arborize in layer 1 and their axons extend into the subcortical white matter to project to other cortical areas. Layer 4 is mostly populated by non-pyramidal neurons, and contains some pyramidal neurons. The axons of the pyramidal neurons extend into deeper cortical layers or interlace with other axons in the subcortical regions. On the other hand, axons of the majority of the non-pyramidal neurons remain within the layer.

As the conventional model of cortical processing suggests, sensory information from thalamocortical fibers is received in layer 4, from which it spreads to other cortical layers and regions. For this region, layer 4 is known as the main input station of the cerebral cortex. Consisting of a dominant population of medium and large-sized pyramidal neurons, layer 5 is also known as the internal pyramidal layer. The layer is also the main output station of the cerebral cortex. Meanwhile, the deepest layer of the cortex, layer 6 consists mostly of pyramidal neurons and interneurons. The axons of the pyramidal neurons extend towards the subcortical region, or project towards the thalamus. On the other hand, interneurons are neurons with dendrites and axons that are localized and do not extend to other regions. They are mostly GABAergic neurons which means they make use of gamma-Aminobutyric acid (GABA), an inhibitory neurotransmitter, to target neurons and play a role in synchronized firing [38][40].

The cerebral cortex is not only organized into layers that run parallel to the cortical surface, but also organized into columns that are aligned perpendicular to the cortical surface. Hypothesized by Mountcastle [41], cortical columns represent units of the cerebral cortex in which neurons within the column share receptive field properties. Receptive

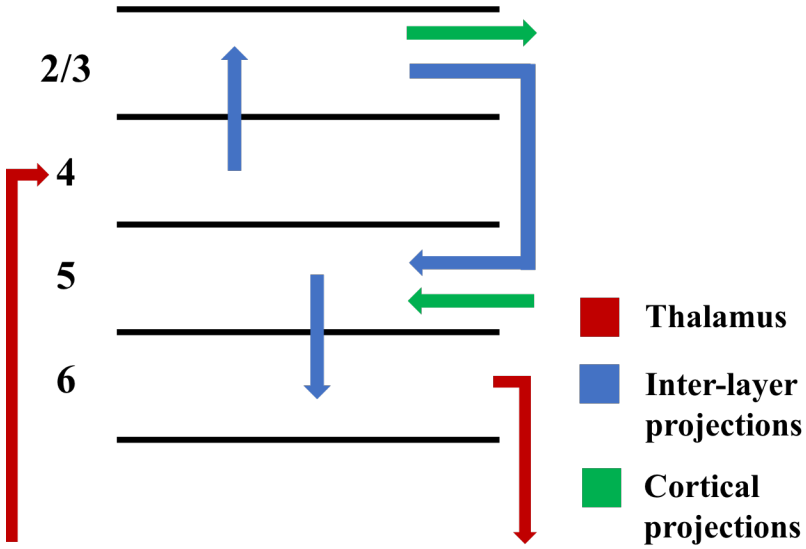

Figure 2.3: Schematic of projections from and within the layered structure of the cortex. Arrows point in the direction of projections.

fields in this context refers to the part of sensory space that invokes certain neuronal responses, such as firing rate, under stimulation [42]. The status of cortical columns as the fundamental unit of the cortex has been discussed extensively due to the lack of convincing evidence confirming its nature of being fundamental, especially since it does not correspond to any specific structure in the cortex [43]. However, the importance of cortical columns continues to be addressed, as they continue to play an important role in the study of the organization of the cortex [43]. In particular, conventional models of cortical processing make use of cortical columns to describe the information pathway within the cortical structure. According to the conventional model, input from the thalamus arrives mainly into layer 4, and also in layer 6. From layer 4, it is projected into layer 2/3. Often the two layers, 2 and 3, are grouped together due to the difficulty in distinguishing them experimentally [44]. The neurons in layer 2/3 then project primarily to layer 5, and also to other cortical areas. Layer 5 neurons tend to have tall tufted apical dendrites, which means the apical dendrites branch out extensively, that reach layer 1. Since layer 1 consists of axons originating from other areas of the cortex, the dendrites from layer 5 form synapses with these axons, allowing integration of feedback from other cortical regions [45]. Neurons in layer 5 also project down to layer 6, where information is integrated and directed to the appropriate cortical regions, and feedback is provided back to the thalamus, thus forming a loop [45]. This layered-structure and schematic of projections is given in Figure 2.3.

2.2 Absence Circuitry

While the pathophysiological mechanisms of absence epilepsy continue to be studied, in the case of absence seizures, the thalamocortical circuit is considered to play an important role in its pathophysiology [46]. The thalamo-cortical-thalamo circuit consists of pathways connecting the thalamus and the cerebral cortex, and the cerebral cortex back to the thalamus, forming a feedback loop between the two structures. The thalamus is characterized as a major sensory and motor relay station for various parts of the brain including the cerebral cortex [47]. Within the thalamus are specialized structures called *nuclei*, to and from which, networks relay information [48]. The *thalamic reticular nucleus*, commonly abbreviated TRN, nRT, RTN or RT, is a thin layer of inhibitory (GABA-ergic) neurons that wraps around the margin of the thalamus [48, 49]. While the TRN is the only thalamic nucleus that does not project to the cortex, one of its primary roles is to regulate thalamo-cortical communication [49]. As illustrated in Figure 2.4, the circuit consists of cortical pyramidal neurons (CT), thalamic relay neurons (TC) and inhibitory neurons in the TRN. Note that in this representation, the node for CT neurons consists of pyramids from all layers. CT neurons make excitatory projections to the TRN as well as to TC neurons, while TC neurons make excitatory projections to CT neurons and to the inhibitory neurons in the TRN. However, projections from the TRN are GABA-ergic and are only made to TC neurons [46, 50].

The thalamocortical circuit has been studied extensively given its importance and involvement as an underlying mechanism in the many dynamic processes defining different brain states [51, 52, 3, 53, 54, 55]. This is governed by the ability of the circuit to generate oscillations of different frequencies and a range of synchrony [56]. Input to the cortical pyramidal neurons, for instance, results in activation of neurons in the thalamic reticular nucleus as well as the thalamic relay neurons. In turn, the TC neurons provide excitatory input to the CT neurons as well as the TRN neurons. In response, the TRN neurons activate and provide inhibition to the TC neurons, forming a negative feedback loop. The interplay between these pathways, dependent heavily on the strength of the feedback stimuli ultimately gives rise to rhythmical activity [56]. As well, changes in one or more components of the circuit can significantly alter the behaviour of neurons locally and distantly located. In particular, while increased excitability of excitatory neurons can result in an increased excitation of the network, decrease in excitation of inhibitory neurons can lead to increased excitation of the network as well [3]. The use of an EEG can help characterize the rhythms and define them based on the location, frequency and nature of the activity, as well as the patient's clinical state [3]. In a spike-and-wave pattern, while the spike component is associated with neuronal firing in the thalamus and cortex, the

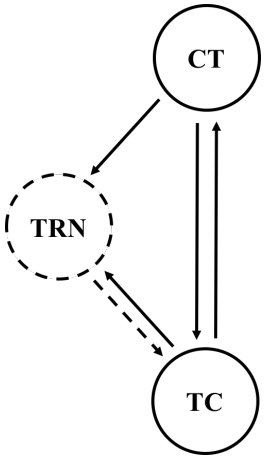

Figure 2.4: The thalamocortical circuit schematic diagram (inspiration drawn from [5]) showing the connections between cortical pyramidal neurons (CT), thalamic relay neurons (TC) and inhibitory neurons in the thalamic reticular nucleus (TRN). Solid circles and arrows indicate excitatory neurons and connections respectively, and dashed circle and arrow indicates an inhibitory neuron and connection respectively.

wave is associated with firing of neurons in the thalamic reticular nucleus.[57, 58]

The cortex, in particular, is integral in the development of spike-and-wave oscillations/discharges (SWDs). It has been shown that thalamic networks consisting of TRN and TC neurons can generate oscillations such as the 7–14 Hz spindle oscillations associated with sleep in humans [59, 60]. The connectivity with the cortex ensures that when the corticothalamic feedback is sufficiently strong, thalamic circuits possess the ability to switch to a slower and hypersynchronized mode of oscillation. In particular, these hypersynchronized oscillations exhibit spike-and-wave EEG patterns [61]. Hypersynchronization refers to the recruitment of a large number of nearby neurons into hyper-excitation due to a hyper-excitable neuron [62]. Paradoxically, this process can be promoted by inhibition [63]. Sufficient excitation of cortical pyramidals, for instance, leads to the activation of GABAergic TRN neurons resulting in abnormality in the form of prolonged inhibition of the network. This evokes inhibitory post synaptic potentials (IPSPs) in TC neurons, further inhibiting the network such that the eventual release from inhibition results in periods of hypersynchronization of excitable neurons [61, 64].

Moreover, in the case of absence epilepsy, many studies reveal the existence of a cortical focus as the origin of paroxysmal activity (occurring suddenly, without warning), followed by rapid propagation towards generalization of activity through intracortical pathways

[21, 58, 65, 20]. Studies involving genetic rodent models of absence epilepsy, namely the GAERS [21] and WAG/Rij [65] rats, provide evidence of the onset of seizure activity in the somatosensory cortex. In particular, depth recordings performed in both cortical and thalamic sites reveal there exists a consistent delay between the onset of spike-and-wave discharges in the somatosensory cortex, and other cortical regions as well as the thalamus [65]. At the start of the SWDs, in the frequency range of 7–11 Hz, intracellular recordings of TC neurons in the GAERS model display excitatory post synaptic potentials (EPSPs) which are followed by inhibitory post synaptic potentials (IPSPs), indicative of excitatory cortical input [21]. While the cortex is considered as the driving source for the origin of SWDs, it is incapable of maintaining rhythmic discharges on its own, nor is the thalamus [5]. Within the cortico-thalamo-cortical circuit, a cortical focus initiates rhythmic discharges, however, once the oscillations are well established, both the cortex and thalamus form an integrated network. In particular, amplification and sustainment of rhythmic discharges is via the cortex and thalamus driving each other.

Chapter 3

Background

3.1 Neuron electrophysiology

Neurons, just like any other living cells, have an electrical voltage (i.e. potential difference) between the inside and outside of the cell. The two sides are separated by the cell membrane. Hence, the potential difference across the membrane is called the membrane potential, V_m, defined as

$$V_m = V_{in} - V_{out}$$

where V_{in} and V_{out} are the intracellular and extracellular potential, respectively. The *resting membrane potential* refers to the potential across the cell membrane when the cell is at rest. Typically neurons have a resting potential in the range of -60 to -70 mV [33]. The potential difference is a result of the difference in ionic concentrations inside and outside the cell. The existence of such a gradient creates the tendency in ions to move from high to low concentrations. However, the cell membrane is a poor conductor of ionic currents due to its structural composition and impermeability to ions. It is composed of two layers of phospholipids, known as a lipid bilayer, with hydrophilic (polar) heads facing the inside and outside of the cell, and hydrophobic (non-polar) tails shielded away and facing each other [33]. A diagram is shown in Figure 3.1. Hence, the movement of ions across the membrane is facilitated by different classes of membrane proteins, namely *ion channels*, and *ion transporters* or *ion pumps*.

Ion channels are crucial in mediating signaling throughout the nervous system. While some channels allow a constant flow of ions (i.e. *leak channels*), others are gated, either by a

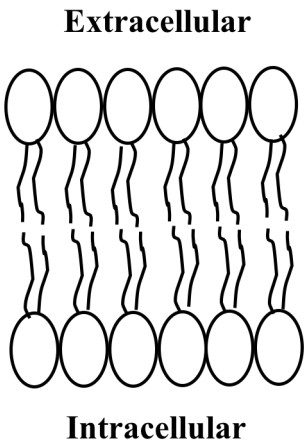

Figure 3.1: Structure of the lipid bilayer with hydrophilic heads facing the inside and outside of the cell, and hydrophobic tails facing each other to form the interior of the cell membrane.

change in voltage, referred to as *voltage-gated channels*, or by chemical substances, referred to as *ligand-gated channels*. Ion channels are typically selective in nature to particular ions and transport the ions along its concentration gradient. Such movement of ions is referred to as *passive transport*. The membrane's permeability to a specific ion is dependent on the number of open channels specific to that ion [29]. Since, sodium, potassium, and chloride ions are found in abundance, they are primarily involved in generating the resting membrane potential. In particular, K^+ ions have a higher intracellular concentration, while ions such as Na^+, Ca^{2+} and Cl^- have a higher extracellular concentration. As a result, upon opening of appropriate channels, Na^+, Ca^{2+} and Cl^- ions have a tendency to diffuse into the cell, while K^+ ions have a tendency to diffuse out of the cell.

The question then arises; how does a difference in concentration for sodium and potassium create a membrane potential? For this we consider the case in which the membrane is only permeable to potassium. In this case, potassium can diffuse through the membrane. Initially, the intracellular and extracellular solutions are electrically neutral, and hence there is no potential difference. With permeability to potassium, K^+ ions move along their concentration gradient towards the outside of the cell. Since K^+ ions are positively charged, their outward movement leaves behind an excess of negative charge, while building an excess of positive charge on the outside. Separation of positive and negative charges across the membrane creates an electric field. As a result, an electrical force also influences the movement of K^+ ions. In particular, they are attracted towards the intracel-

lular negative charges and being repelled by the extracellular positive charges. However, a net movement of K^+ ions towards the outside continues to exist as long as the force due to the concentration gradient is greater than the electrical force attempting to oppose the direction of ionic movement. This means the cell continues to become more negative (with movement of K^+ ions towards the outside) until the electrical driving force balances the chemical driving forces. At this point there is no net movement of ions. The membrane potential at which this occurs is called the *equilibrium, reversal* or *Nernst potential* [33]. The equilibrium potential is different for different ions and is dependent on the concentration gradient of that ion across the cell membrane. The equilibrium potential is proportional to the concentration gradient and can be calculated for any ion using the following equation known as the Nernst equation.

$$E_{ion} = -\frac{RT}{zF}\ln\frac{[C]_i}{[C]_o} \tag{3.1}$$

It was formulated by the German physical chemist, Walther Nernst in 1889 [66]. In this equation, E_{ion} is the Nernst potential for the ion, R is the gas constant, T is the absolute temperature in Kelvin, z is the valence of the ion, F is Faraday's constant, and $[C]_i$ and $[C]_o$ are ion concentrations inside and outside the cell, respectively [33].

Since at rest, neurons are permeable to Na^+ and Cl^-, the resting potential of the neuron is set according to the balance between influx and efflux of sodium, potassium, and chloride ions. Ion concentration difference is also maintained via *ion pumps* which push Na^+ ions out of the cell and K^+ ions into the cell. The Na^+-K^+ pump, for example, pumps one K^+ in for every three Na^+ out of the cell. Since pumps act against the electrical and chemical gradient, they require energy from the breakdown of adenosine triphosphate (ATP). Such movement of ions is called *active transport* [67].

The Nernst equation allows for determining the equilibrium potential in the case of permeability to a single ion species. In particular, this is also the case in which the electrical and diffusive driving forces are in equilibrium. However, more generally, the membrane is permeable to multiple ion species. Moreover, the electrical and diffusive influences on each ion may not necessarily be in equilibrium, meaning the net flow of each ion species across the membrane is nonzero. In this case, as we will see in the following section, describing the current flow through ion channels is necessary to be able to understand the mechanisms underlying the generation of action potentials, especially.

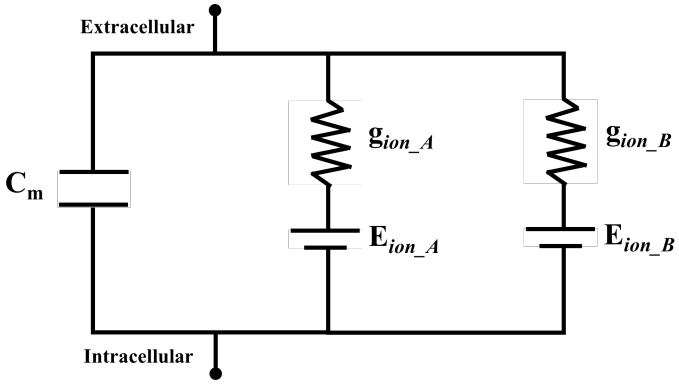

Figure 3.2: A single compartment equivalent electrical circuit representation of a membrane with multiple ion channels.

3.2 Conductance-based Modelling

3.2.1 Hodgkin-Huxley Model

The membrane's permeability to ions and their concentration gradients across the membrane determine the flow of current across the membrane. The understanding of permeability changes is crucial in understanding how action potentials may be generated since it is through the flow of ions through ion channels, and the membrane's permeability, which ultimately establishes the excitability of the neuron.

Making use of Ohm's law, we have that

$$I = \frac{V}{R} = gV$$

where $g = \frac{1}{R}$ is the conductance. This approximation can be viewed as an electrical circuit in which a resistor is in series with a battery. In particular, in an equivalent electrical circuit of a membrane patch, the cell membrane acts as a capacitor since it separates intracellular and extracellular charges along its structure. This is in parallel with a resistor in series with a battery. While the resistor is a model for ion channel permeability, the driving force due to the concentration gradient across the membrane is modelled by a battery. In general, multiple ion channels are modelled by having, in parallel, a resistor and battery for each ion channel. An example of such a circuit is shown in Figure 3.2.

According to the Hodgkin-Huxley model, the current across the membrane has one component associated with the membrane capacitance, and another associated with the

flow of ions through membrane channels. Let Q be the charge distributed across the membrane given by

$$Q = C_m V_m$$

Differentiating this with respect to time gives

$$I_C = C_m \frac{dV_m}{dt}$$

For the component of current associated with ion channels, using Ohm's Law, the voltage difference across the resistor can be given by

$$V_m - E_{ion} = R_{ion} I_{ion}$$

where V_m is the voltage drop across the membrane, E_{ion} is the voltage drop due to the battery (in the biophysical sense, this refers to the reversal potential of the particular ion), and R_{ion} is the resistance. Hence,

$$I_{ion} = g_{ion} \cdot (V_m - E_{ion})$$

where $g_{ion} = \frac{1}{R_{ion}}$ is the ionic conductance.

Using Kirchhoff's current law, the total current flowing through the membrane can be given as the sum of the capacitive current and the ionic current:

$$\begin{aligned} I_C + I_{ion} &= 0 \\ C_m \frac{dV_m}{dt} &= -g_{ion}(V_m - E_{ion}) \end{aligned} \tag{3.2}$$

In case of multiple ion channels, Equation (3.2) would consist of the sum of ionic currents, corresponding to the different ions present,

$$C_m \frac{dV_m}{dt} = -\sum_{i=1}^{k} g_i (V_m - E_i) \qquad \text{for } i\text{= 1 to } k\text{, representing } k \text{ ion channels}$$

As will be the case in our study, any external application of current (e.g. placement of an electrode and injection of current) changes Equation (3.2) to the following:

$$I_C + I_{ion} = I_{app}$$

More generally, this can be written as

$$C_m \frac{dV_m}{dt} = I_{app} - \sum I_{ion} \tag{3.3}$$

Each ion channel is regulated by gates, and in order for ions to flow through, all gates within the channel must be open. The probability that a gate is open or closed may be dependent on the membrane potential (which in our model will always be the case). Let $\mathbf{g}$ represent the fraction of open gates, then,

$$\frac{d\mathbf{g}}{dt} = \frac{\mathbf{g}_\infty(V) - \mathbf{g}}{\tau(V)} \tag{3.4}$$

where

$$\mathbf{g}_\infty(V) = \frac{\alpha(V)}{\alpha(V) + \beta(V)} \qquad \text{and} \qquad \tau(V) = \frac{1}{\alpha(V) + \beta(V)} \tag{3.5}$$

The voltage-dependent rate constants, α(V) and β(V) denote the rate at which a gate goes from the closed to open, and from the open to closed states, respectively. By integrating Equation (3.4) with a fixed V, time-dependent changes for each gate at a given membrane potential can be predicted using the following equation consisting of voltage-dependent values of $\mathbf{g}_\infty$, and τ, with the solution starting at $\mathbf{g}(0)$.

$$\mathbf{g}(t) = \mathbf{g}_\infty(V) + (\mathbf{g}(0) - \mathbf{g}_\infty(V)) \cdot \exp\left(\frac{-t}{\tau(V)}\right)$$

For the purposes of our work, it is important to note that the membrane equations in our model will have the same form as Equation (3.3), and ion channel gating will be represented by Equations (3.4)–(3.5).

3.2.2 Description of an Action Potential

For neurons to communicate with each other, electrical signals caused by changes in the membrane potential need to occur. This transmission of information is known as an *action potential* (sometimes also referred to as a *spike*). Typically, action potentials are generated by a depolarizing current. This refers to an event or stimulus that causes the resting membrane potential (usually between -60 to -70 mV) to move towards 0 mV. When the membrane potential reaches the firing threshold (usually around -55 mV), an action potential is fired. Firing of action potentials follows an "all or none" principle. That is, either firing threshold is not reached or an action potential is fired. Action potentials are characterized by periods of an inward current causing the inside of the cell to become positively charged, followed by an outward current causing the inside of the cell to restore itself back towards resting voltage.

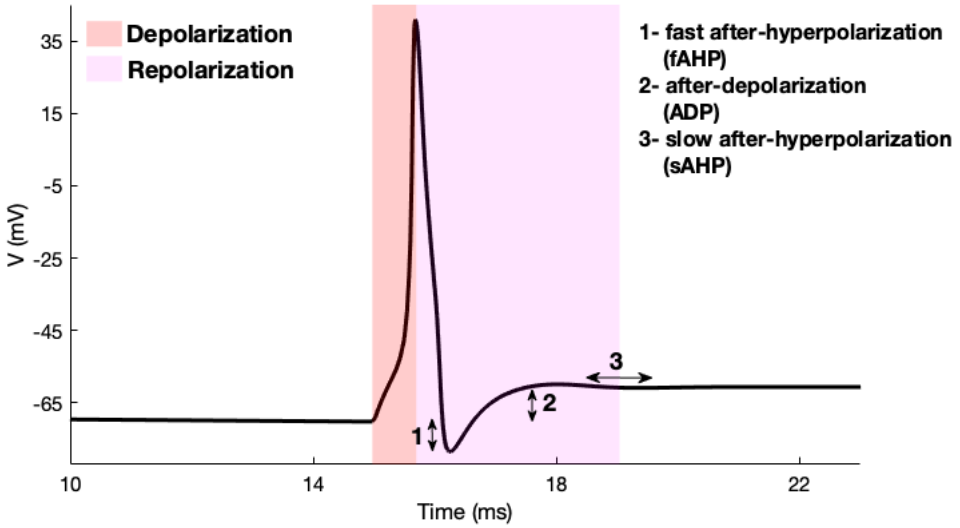

Figure 3.3: Simulation of a typical action potential with shaded regions corresponding to membrane depolarization and repolarization. The three phases (fAHP, ADP, and sAHP) are described in detail below.

The mechanism behind an action potential in a typical neuron is as follows. The onset of a stimulus causes voltage-gated Na^+ channels to open. Since the extracellular concentration of Na^+ ions is greater than the intracellular concentration, Na^+ ions quickly rush into the cell causing the membrane potential to increase towards the reversal potential of sodium, at approximately +60 mV. This movement of membrane potential towards 0 mV is known as *depolarization*. During the course of this phase, other voltage-gated ion channels begin to open and in particular, channels that are specific to K^+ ions. Driven by its concentration gradient, K^+ ions move out of the cell causing the membrane potential to decrease back towards resting voltage, while at about this time, sodium channels begin to close. This phase of membrane potential moving towards resting potential is known as *repolarization*. In fact, due to the relatively slow nature of potassium channels in closing, the membrane potential decreases beyond resting voltage, in a phase known as *hyperpolarization*. Once the potassium channels are closed, the cell returns to its resting membrane potential. An illustration of an action potential is given in Figure 3.3.

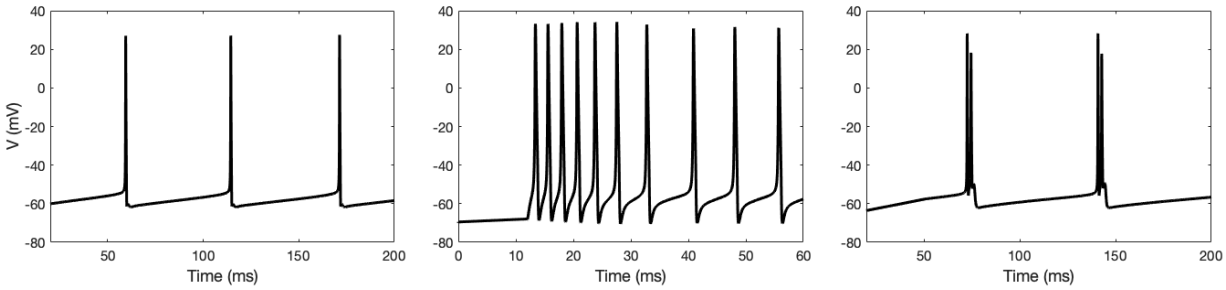

Figure 3.4: Types of neuronal firing patterns. *Left*: tonic or regular spiking, *Middle*: spiking exhibiting adaptation, *Right*: burst firing.

While a typical action potential can be described by voltage-gated Na^+ and K^+ channels, there may in fact be a multitude of ion channels governing the generation of action potentials. Moreover, the differences in different ions can give rise to additional features to an action potential, such as the fast after-hyperpolarization (fAHP), after-depolarization (ADP), and slow after-hyperpolarization (sAHP) phases, illustrated in Figure 3.3. The fAHP phase comprises of the membrane potential undergoing hyperpolarization on a relatively fast timescale. The ADP phase is characterized by a small "depolarizing hump" relative to the resting membrane voltage. The sAHP phase follows the ADP phase wherein the membrane potential is lower that the resting voltage, before returning to the resting voltage.

Although the "all or none" action potential response of a neuron is the same for all neurons, the patterns in which action potentials are fired can vary between neuron types. The three main types of firing patterns are *tonic* (regularly spaced spikes), *adapting* (spikes with increasing interspike intervals), and *bursting* (bursts of spikes consisting of short interspike intervals alternating with long interspike intervals). The interspike interval refers to the period between two subsequent spikes. An illustration of the different types of firing patterns is given in Figure 3.4.

3.3 Multi-compartment Modelling

Models of the Hodgkin-Huxley type are considered to be biophysical models that can describe the effect of input currents on the membrane potential. Input currents can be in the form of an external input through an electrode or synaptic input. In particular, such models can describe the behaviour of neurons taking into account ion channels and their intrinsic

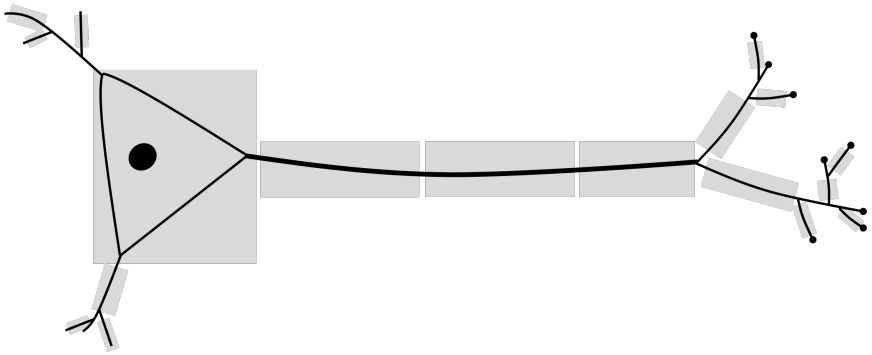

Figure 3.5: Architecture of multi-compartment neuron model.

properties, to generate action potentials (spikes) governed by the dynamics of the model. Single-compartment models are models that do not explicitly include the morphological structure such as dendrites or the axon. With the spatial dimension ignored altogether, the use of single-compartment models is often justified by considering the membrane potential and other biophysical elements of the model as being the same everywhere in the neuron [68]. Another common justification is to let the membrane potential variable represent the voltage at a specific location such as the soma. However, one of the limitations of this is the fact that spikes initiated in the axon is not taken into account. In particular, in the case of cortical pyramidal neurons, initiation of spikes occurs in the Axon Initial Segment (AIS), located in the axon in a region 20–40 μm from the soma [68].

On the contrary, multi-compartment modelling involves, as the name suggests, division of neurons into multiple compartments, as illustrated in Figure 3.5. To give the model a spatial dimension and structure, these multiple compartments are connected to each other with a resistor in between. An equivalent circuit representation is given in Figure 3.6. For more details on compartmental modelling including use of partial differential equations, a comprehensive summary is given in Chapter 2 of [33]. The compartments are each modelled to be small enough that an assumption of uniformity over the entire compartment can be made. While Figure 3.6 illustrates a membrane with a single ion channel, multiple ion channels can be included as being connected in parallel with each other [69]. As well, each compartment is modelled in a similar fashion using Equation (3.2.1). Although inclusion of the spatial dimension adds detail to a neuron model, its effectiveness is largely dependent on the type of result that is to be achieved, whether it is with regards to single neuron activity or perhaps, network behaviour. For the purposes of this work, the neurons in our model will all be single-compartment models.

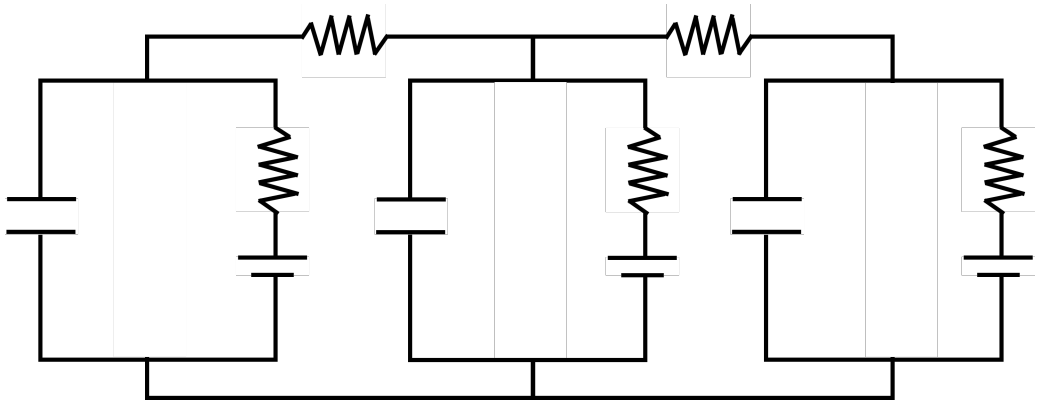

Figure 3.6: A multi-compartment neuron model equivalent to an electrical circuit representation.

3.4 Modelling Synapses

As previously described in Section 2.1.2, synapses involve a number of mechanisms that ultimately result in transmission of electrical signals, allowing neurons to communicate with each other. Therefore, modelling all the processes pertaining to synaptic transmission is a highly demanding task. To simplify this task, synapses can be modelled with a focus on the mechanism of opening of ion channels resulting in postsynaptic currents (PSCs), without the details such as diffusion of neurotransmitter molecules. PSCs that increase the probability of a postsynaptic action potential are excitatory, while those that decrease the probability of a postsynaptic action potential are inhibitory, and this is dependent on the type of ion making up the current. The determining factor for a postsynaptic neuron to generate an action potential is the reversal potential of the postsynaptic current with respect to the threshold for action potential generation in the postsynaptic neuron. If the reversal potential for a PSC is greater than the action potential threshold, this causes the postsynaptic membrane potential to reach beyond threshold, resulting in an increased probability of an action potential. On the other hand, reversal potential for PSCs that are less than action potential threshold keep the postsynaptic membrane potential less than threshold, resulting in a reduced probability of an action potential [70].

Like ionic currents, synaptic currents can be modelled using a conductance, in this case time-dependent, which is open upon the arrival of a presynaptic spike, and its product with a voltage difference, as follows:

$$I_{syn} = g(t) \cdot (V_{post} - V_{rev}) \tag{3.6}$$

where $g(t)$ is the synaptic conductance, V_{post} is the membrane potential of the postsynaptic neuron, and V_{rev} is the reversal potential of the synapse. For excitatory synapses such as AMPA synapses, V_{rev} is approximately 0 mV, whereas for inhibitory synapses such as GABA synapses, V_{rev} = -75 mV [33].

The time-dependent conductance $g(t)$ can be modelled in several ways. A summary of three different models is provided below.

3.4.1 Single-Exponential Decay

One of the most simple models is to assume $g(t)$ rises instantaneously at time t_0, from 0 to $\bar{g}_{syn}$, then decays exponentially with a time constant τ_{syn}:

$$G_{exp}(t) = \bar{g}_{syn} \cdot e^{-\frac{(t-t_0)}{\tau_{syn}}} \tag{3.7}$$

where $\bar{g}_{syn}$ is the maximal synaptic conductance of the connection from a presynaptic neuron to the postsynaptic neuron, and t_0 is the time of the presynaptic spike. This model is quite a simplification since no transmission delay is being accounted for. However, since the process of neurotransmitter release, diffusion across the cleft, binding to receptors, and opening of ion channels, all happen on a very fast timescale, it is reasonable to assume the channels jumping from a closed to open state, instantaneously.

3.4.2 Alpha Function

Another common synapse model is the use of an alpha function such as one given by the following:

$$G_{\alpha}(t) = \bar{g}_{syn} \cdot (t - t_0) \cdot e^{-\frac{(t-t_0)}{\tau_{syn}}} \tag{3.8}$$

where the parameters are the same as the single-exponential decay model.

For both of these models, since the variable t denotes time after presynaptic spiking, there is a need to keep track of spike times. However this may be a computational difficulty, and be an undesirable task.

3.4.3 Destexhe Synapse Model

Developed by Destexhe et al. in 1994, one other way of describing the synaptic conductance is using a gating variable s, where $s(t)$ denotes the fraction of open synaptic channels at

time t [71]. Open synaptic channels refer to postsynaptic receptors that neurotransmitter molecules bind to, followed by the opening of ion channels. In this way, the synaptic conductance is described by

$$G_{Dest}(t) = \bar{g}_{syn} \cdot s(t) \tag{3.9}$$

The kinetic scheme for a process like this is given by

$$\mathrm{C} + \mathrm{T} \underset{\beta}{\overset{\alpha}{\rightleftharpoons}} \mathrm{O}$$

where T represents the neurotransmitter molecule binding to a postsynaptic receptor in the closed state to change to the open state, and α and β are the forward and backward rate constants describing the neurotransmitter binding. Thus, the fraction of bound receptors, $s(t)$ satisfies,

$$\frac{ds}{dt} = \alpha[T](1 - s) - \beta s \tag{3.10}$$

where [T] is time-dependent, and represents the neurotransmitter concentration released into the synaptic cleft upon the arrival of a presynaptic spike. Suppose a presynaptic spike arrives at $t = t_0$ and [T] jumps to T_{max}, and at $t = t_1$, [T] falls back to 0. Then, solving Equation (3.10), we have

$$s(t - t_0) = s_\infty + (s(t_0) - s_\infty)e^{-\frac{(t-t_0)}{\tau_s}}, \qquad t_0 < t < t_1 \tag{3.11}$$

where

$$s_\infty = \frac{\alpha T_{max}}{\alpha T_{max} + \beta} \qquad \text{and} \qquad \tau_s = \frac{1}{\alpha T_{max} + \beta}$$

After the neurotransmitter-mediated pulse is gone, $s(t)$ decays exponentially as

$$s(t - t_1) = s(t_1)e^{-\beta(t-t_1)}, \qquad t > t_1 \tag{3.12}$$

To model the relationship between neurotransmitter release [T] and the presynaptic voltage, it is assumed to take the form given by the following equation [33]:

$$[T](V_{pre}) = \frac{T_{max}}{1 + \exp\left(\frac{-(V_{pre} - V_T)}{K_p}\right)} \tag{3.13}$$

where T_{max} is the maximal concentration of the neurotransmitter in the synaptic cleft, V_{pre} is the presynaptic voltage, K_p is the steepness of voltage dependence, and V_T is the voltage at which the function is half-activated. Destexhe et al. suggest values of T_{max}= 1 mM, V_T= 2 mV and K_p= 5 mV [71]. Using these values and ranging V_{pre} between -85 and 45 mV, Figure 3.7(a) shows [T] as a function of V_{pre}.

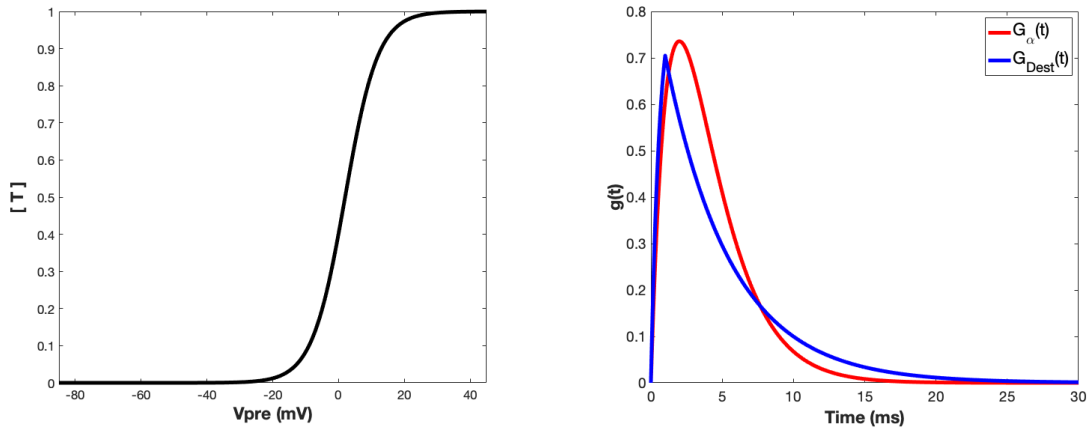

(a) (b)

Figure 3.7: *A*: Plot of neurotransmitter release concentration, [T] as a function of the presynaptic voltage, V_{pre}. *B*: Comparison of synaptic conductance, $g(t)$ using an alpha function model and the Destexhe synapse model.

Chapter 4

Genetic Mutations in Absence Epilepsy

4.1 Mutations in genes encoding sodium channels

Voltage-gated sodium channels are fundamental in membrane depolarization and the initial phase of what constitutes an action potential. In neurons of the central nervous system, these channels are encoded by four vital genes: $Scn1a, Scn2a, Scn3a$ and $Scn8a$ [72]. Mutations in any of these genes plays an important role in impairment and dysfunction leading to various types and degrees of neurological disorders, including epilepsy. The somato-dendritic and axonal regions of neurons not only differ in their function, but also in the distribution of voltage-gated ion channels [73]. In the case of cortical neurons including layer 5 pyramidal neurons, Nav1.2 and Nav1.6 encoded by $Scn2a$ and $Scn8a$ respectively, are among the most prominent sodium channels present in both the axonal and dendritic regions of these neurons [74][75].

One of the most influential studies regarding genetic mutations in absence epilepsy is one by Papale et al. [76]. Mutations in the $Scn8a$ gene were reported with effects associated with absence seizures. $Scn8a$ is responsible for encoding the sodium channel, Nav1.6. This channel contributes largely towards repeated cell firing as well as the conductance of persistent current [77]. For cortical neurons, the axonal initial segment (AIS) being the site of action potential generation and firing, contains a high number of Nav1.6 channels [78][74]. Since membranes containing these channels are more excitable than those containing other sodium channels, any impairment in Nav1.6 function, loss of function in particular, is known to result in reduction of action potential firing due to an increase in threshold for

initiation [79]. According to their study, adult rodents with *Scn8a* mutations exhibited SWDs with burst frequency of 7–9 Hz, a typical signature of absence epilepsy for rodent models. In particular, the effect of three different *Scn8a* mutants was studied, namely $Scn8a^{V929F}$, $Scn8a^{med}$ and $Scn8a^{med-jo}$. The amplitude, frequency of occurrence and duration of SWDs was greater in mice with any of the variant channels as compared to the control case. In order to characterize the seizure phenotype of *Scn8a* mutants, ethosuximide (ETX) was administered. Ineffective against convulsive and focal seizures, typically ETX is used for the treatment of absence epilepsy. The effect of treatment with ETX saw a reduction in the number and duration of SWD episodes in mutants. This further supported the relation between *Scn8a* mutants and their role in absence epilepsy. In addition, it was determined that $Scn8a^{med}$ is a null mutation resulting in a loss-of-function and $Scn8a^{med-jo}$ results in alteration in voltage dependence of activation and inactivation of the sodium current. However, Papale et al. did not report the impact of $Scn8a^{V929F}$ (a chemically induced mutation) on sodium channel activity.

In 2014, similar work was conducted by Oliva et al., in which the effects of $Scn8a^{V929F}$ were determined [80]. A genetic absence epilepsy rodent model of the C3HeB/FeJ strain was used for the purposes of monitoring EEG recordings. The most prominent effect was the exhibition of frequent SWDs in EEG recordings especially associated with absence epilepsy, confirming the role of *Scn8a* mutations in promoting SWDs. To perform biophysical characterization of the variant channel, Nav1.6-V929F, whole-cell patch clamp analysis was conducted in single cells. In particular, ND7/23 cells (dorsal root ganglion neurons) were transfected with Nav1.6 WT and Nav1.6-V929F plasmid. The voltage dependence of activation and inactivation for both the sodium channels was determined using voltage clamp experiments and fit using a Boltzmann equation, as appropriate. In comparison with Nav1.6 WT, expression of the Nav1.6-V929F mutant caused a depolarising shift in activation, and a significant hyperpolarising shift in inactivation. This indicates a decrease in channel activity as a depolarizing shift in activation would result in the neuron requiring a more depolarized response to evoke excitation, while a hyperpolarizing shift in the voltage dependence of inactivation indicates inactivation responses at an even more negative membrane potential. A computational model for a cortical layer 5 pyramidal neuron derived from Hu et al. was also used to investigate the effect of Nav1.6-V929F mutant on firing activity [81]. Results indicated that a larger stimulating current was required to initiate firing in the model expressing Nav1.6-V929F as compared to WT, as well as a lower firing frequency for any given stimulus. This result was interesting as it does not align with intuition which would lean more towards expecting increased excitation in excitatory cortical neurons since seizures are characterized by hyperactivity. Thus, this expressed the need for understanding other possible mechanisms resulting in net excitation ultimately

contributing to SWDs and absence seizures.

For instance, since there is evidence of Nav1.6 expression in interneurons in the cortex including inhibitory neurons [82], it is suggested that the loss of function Nav1.6 mutation in inhibitory neurons would lead to reduced inhibition and thus give rise to SWDs [80]. Furthermore, given the importance of inhibitory cortical interneurons as well as the inhibitory neurons in the thalamus, such as RT cells, in the absence circuitry, loss of $Scn8a$ in the thalamic reticular nucleus in particular causes hypersynchrony of the thalamo-cortical system, playing a key role in invoking absence seizures [83]. In the case of RT cells, results from Makinson et al. show the effect of mutations in the $Scn8a$ gene on thalamic synchronization and firing patterns [83]. Thalamic slices from $Scn8a$ mutant mice exhibited spontaneous oscillatory activity, whereas this activity was not observed in the wild type. In addition, post the deletion of $Scn8a$, RT cells displayed reduced excitation by producing fewer action potentials in both modes of firing- tonic and bursting (see figure 4A and 4C1 from Makinson et al. [83]). The deficiency of $Scn8a$ reduces excitation in the excitatory cortical pyramidal neurons, leading to a deteriorating effect. However, the decrease in activity of inhibitory neurons could result in a net effect of excitation and production of SWDs associated with absence seizures.

In 2018, Ogiwara et al. discovered that mice with $Scn2a$ variant, $Scn2a^{RX/+}$ showed a spontaneous epileptic phenotype of absence-like seizures [84]. Electrocorticography (ECoG) and electromyography (EMG) recordings, measuring the electrical activity from the cerebral cortex and activity produced by skeletal muscles, were more prevalent with a greater incidence in $Scn2a^{RX/+}$ mice than the wild-type. Similarly, in a knockout mutation (where the wild-type gene is made inoperative), $Scn2a^{KO/+}$ mice, showed a similar ECoG-EMG activity resembling absence seizures. In particular, the epileptic phenotype was dependent on Nav1.2 deficiency particularly in excitatory neurons. Since Nav1.2 is abundantly expressed in glutamatergic neurons including neocortical pyramidal neurons, examination of $Scn2a$ deficiency in cortical pyramidal neurons was a reasonable measure. Voltage-clamp analysis of $Scn2a^{KO/+}$ hippocampal pyramidal neurons showed an approximately 45% decrease in maximum sodium conductance density. Furthermore, using current-clamp recordings, action potential properties of excitatory and inhibitory neurons in the neocortical layer 2/3 and hippocampal CA1 region were investigated. While peak amplitude of single action potentials and spike trains was lower by approximately 25% in $Scn2a^{KO/+}$ mice than the control case, there were no significant differences in electrophysiological properties of neocortical and hippocampal inhibitory neurons between the genotypes.

4.2 Mutations in genes encoding h-channels

H-channels, first identified in the heart, are voltage-gated ion channels involved in modulating excitability in regions of the brain [85]. They are also partly gated by the binding of cAMP [86]. Cyclic AMP is an intracellular signaling molecule that activates certain proteins enabling the activation of the h-channels [70]. Interestingly, unlike most other voltage-gated ion channels, h-channels activate in response to membrane hyperpolarization, and their activation occurs much more slowly as compared to most other ion channels [87][85]. Although structurally similar to potassium channels, these channels largely conduct sodium currents, hence producing a depolarizing response to membrane hyperpolarization [88]. Thus, overall, h-channels function in stabilizing membrane potential to either input- excitatory or inhibitory. In response to an inhibitory input (hyperpolarizing input), h-channels activate and through the entry of cations into the cell, depolarize membrane potential back towards rest, whereas depolarizing inputs deactivate h-channels open at rest, and return the membrane potential towards rest by the removal of a net depolarizing current (via its deactivation) [85][88].

H-channels are encoded by four genes, $Hcn1$ to $Hcn4$ [89], with $Hcn1$ primarily significant in cortical pyramidal neurons and $Hcn2$ in neurons in the thalamus [90]. To investigate the effects of h-channel alterations, several studies have been conducted in different types of neurons, with different results, depending on the investigation conducted. With regards to absence seizures, some of the most significant results that have motivated several studies have come from earlier work conducted by Ludwig et al. which involved use of $Hcn2$-deficient mice [91]. In their investigation, mice lacking Hcn subtype 2 were generated. Given that h-channels encoded by $Hcn2$ are abundant in the thalamus, their results showed a near complete loss of the Hcn current in the thalamocortical relay neurons of these mice. This further suggested that the h-current, I_h, is primarily generated by $Hcn2$ in the thalamocortical (TC) neurons. In addition, it was also found that the TC neurons with $Hcn2$-deficiency were more hyperpolarized than the wild type, indicating the contribution of I_h to the resting membrane potential. In comparison to wild type, TC neurons in $Hcn2$-deficient mice responded to the same depolarizing input with bursts, whereas the wild type responded with tonic firing, increasing in frequency with increasing input. This shows how the lack of $Hcn2$ contributes towards oscillatory activity in thalamocortical networks. To further classify their results and the association with absence epilepsy, EEG recordings from freely moving $Hcn2$-deficient mice displayed frequent bilaterally synchronous spike-and-wave discharges, typical of absence seizures.

The results of the study by Ludwig et al. provided important insight into the mechanisms of absence epilepsy, especially towards investigating the contributions of I_h to hy-

perexcitability in cortical neurons. One such study is by Strauss et al. in which pyramidal neurons from the somatosensory neocortex of WAG/Rij rats were investigated [92] . The approach involved evaluating the contribution of I_h in excitatory behaviour as associated with absence epilepsy. To test for differences in Hcn activity between epileptogenic and non-epileptogenic cortices, the h-current was blocked using application of ZD7288, a selective Hcn channel blocker, in cortical layer 2/3 pyramidal neurons. Neurons from epileptogenic cortices displayed lower sensitivity to ZD7288, thus indicating presence of a much smaller I_h conductance than in neurons from non-epileptogenic cortices. Furthermore, upon investigation of firing properties, all neurons exhibited a train of single action potentials in response to depolarizing inputs. However, depolarizing inputs post application of ZD7288 resulted in a change in the firing pattern from regular spiking to burst firing. The bursting pattern ranged from 1–4 bursts at the beginning followed by regular spiking, to repetitive bursting. This result suggests strongly that reduction of I_h induces burst discharges. The authors also showed in their study the influence for lower I_h conductance on increasing membrane resistance and thus affecting the membrane potential. These changes affected by I_h ultimately suggest an increase in excitability of cortical neurons as well as contribute towards the generation of SWDs and absence seizures in WAG/Rij rats.

Another study using WAG/Rij rats was conducted by Kole et al., building upon the results previously obtained by Strauss et al. [93]. The study by Kole et al. focused on investigating whether changes in I_h contribute towards generation of generalized seizures, by tracking I_h expression with respect to seizure onset. WAG/Rij rats, and Wistar rats (which do not typically show SWD seizures) were used. Layer 5 pyramidal neurons from the primary somatosensory cortex from each animal type were further investigated for comparison. In order to track Hcn channel expression, ECoG recordings were conducted, at three stages of development. The recordings showed the first occurrence of spike-wave discharges at a later stage in development. Subsequently, at the same stages of recordings, $Hcn1$ expression was tracked, showing a reduced $Hcn1$ expression earlier in development than the first SWD occurrence. This suggests that a reduction in $Hcn1$ expression precedes the onset of seizures. In addition, the firing pattern of layer 5 pyramidal neurons of both the Wistar and WAG/Rij rats was investigated at the developmental stage during which SWDs were observed in the WAG/Rij animals. With a somatic current injection, while regular spiking was observed in the Wistar neurons, in a significantly large proportion of WAG/Rij neurons, burst firing was observed, with increase in frequency with increased input. Interestingly, similar to the results in Strauss et al., post application of the Hcn channel blocker ZD7288, the firing behaviour of the Wistar neurons changed from regular spiking to repetitive bursting. To explain the behaviour observed by such I_h-mediated changes, Kole et al. suggested that the loss of $Hcn1$ channels reduces the threshold for

dendritic Ca^{2+} spikes, giving rise to burst discharges. As well, similar to observations by Strauss et al., the authors found a significantly larger somatic and dendritic input resistance in the WAG/Rij neurons than Wistar neurons. This may well be a possible reason for an increase in neuronal excitability, despite reduced I_h causing a more hyperpolarized resting membrane potential [94].

Chapter 5

Traub's Model

5.1 Introduction

In 2005, Traub et al. constructed a network model consisting of 3,560 multi-compartment neurons of multiple types to study population phenomena in the thalamocortical network [1]. Neuronal types included superficial pyramidal neurons in layers 2/3, layer 4 spiny stellate neurons, layer 5 tufted pyramidal neurons, layer 6 nontufted pyramidal neurons, superficial and deep layer cortical interneurons, thalamocortical relay neurons (TC), and neurons in the thalamic reticular nucleus (TRN). Within this population variety, neurons had different intrinsic properties such as regular spiking (RS), fast rhythmic bursting (FRB), intrinsic bursting (IB), and low threshold spiking (LTS). The purpose of their study was to be able to replicate different population phenomena including thalamocortical sleep spindles, and synchronized population bursts resembling electrographic seizures (seizures that are evident on EEGs), amongst other network behaviours. The use of multi-compartment neurons allowed for a range of intrinsic neuronal properties to be taken into account. In this model, connectivity of network components varied in being chemical (via chemical synapses) and electrical (via gap junctions). In addition, Traub et al. also investigated the necessity of gap junctions (these are narrow gaps between pre- and post-synaptic neurons, containing ion channels through which ion flow is regulated directly by membrane depolarization) between the axons of pyramidal neurons for population synchronization.

This model is particularly useful for its coverage on topics including slow sleep oscillations and the transition to seizures, and some of the model predictions are consistent with experimental recordings as well. With the incorporation of neurons from different layers, this model takes into account the layered structure of the cortex. This serves the

purpose of our investigation well since we would also like to explore the role of the cortex in initiation and propagation of seizures across the cortex through the interaction of neurons in the different layers. The diversity in neuron types, and the inclusion of firing behaviours of isolated neuron models based on experimental data provide a useful baseline activity for our investigation. Furthermore, some of the simulations performed pertain to the cortex only (with the thalamus disconnected), and include the behaviour of cortical neurons in different layers. In particular, such baseline activity is essential in our context of introducing gene defects at the single-neuron level and exploring the effects on behaviour of a cortical network.

5.2 Model Components

All of the neurons in Traub's model were described using multiple compartments, ranging from 57 to 144 compartments. In addition, many of the compartments were grouped together to form "levels" such that compartments within the same level had the same membrane conductance density. For instance, level 0 was the axon, level 1 was the soma, and levels 2 up to 18 were for the dendrites. Although the types of conductances were the same for all of the neurons, the membrane conductance density distributions, as well as the details of the kinetics differed between neuron types. The incorporated Ca^{2+}, Na^{+}, and K^{+} currents included in the model are summarized in Table 5.1.

Current	Current Description
I_h	anomalous rectifier/ hyperpolarization-activated mixed cation current
I_{Naf}	fast and transient inactivating Na^{+} current
I_{Nap}	persistent Na^{+} current
I_{Kdr}	delayed rectifier K^{+} current
I_{Ka}	transient inactivating K^{+} current
I_{K2}	slowly activating and inactivating K^{+} current
I_{Km}	muscarinic receptor-supressed K^{+} current
I_{Kc}	fast voltage and Ca^{2+}-dependent K^{+} current
I_{Kahp}	slow Ca^{2+}-dependent K^{+} current
I_{CaT}	low-threshold inactivating Ca^{2+} current
I_{CaL}	high-threshold Ca^{2+} current
I_{Leak}	leak current

Table 5.1: Description of currents used in Traub's model for all cell types

Since our focus is on the cortical component in the absence circuitry, for our model, we will only be concerned with the layer 5 and layer 6 pyramidal neurons and the deep

interneuron in the cortex. Henceforth, the phrase "all neuron types" will refer specifically to these four neurons: layer 5 tufted intrinsically bursting (IB), layer 5 regular spiking (RS), layer 6 non-tufted regular spiking (NRS) pyramidals, and the deep low-threshold spiking (LTS) interneuron.

The soma for all neuron types was modelled as a cylinder with a surface area of $2\pi rl$, where r is the radius and l is the length. The radius was 9 μm for both IB and RS, 8 μm for NRS, and 7.5 μm for LTS neurons, while the length was 25 μm for both IB and RS, and 20 μm for both NRS and LTS neurons.

The principal equation describing the change in membrane potential is given by the following equation,

$$C_m \frac{dV}{dt} = I_{hold} + I_{app} - I_h - I_{Naf} - I_{Nap} - I_{Kdr} - I_{Ka} - I_{K2} - I_{Km} - I_{Kc} - I_{Kahp} - I_{CaT} - I_{CaL} - I_{Leak} - I_{syn} \tag{5.1}$$

where C_m is the membrane capacitance (in $\mu \mathrm{F}/cm^2$) with a value of 0.9 for all pyramidals and 1.0 for the deep LTS interneuron. I_{hold} is the input current required to hold and maintain the voltage of the neuron (also used in this context for setting the resting membrane potential), I_{app} is a steady applied current, and I_{syn} is a sum of AMPA- and GABA-mediated synaptic currents (described in Chapter 7). A consistent set of units were maintained such that voltage is given in mV, current in $\mu \mathrm{A}/cm^2$, membrane conductance densities in mS/cm^2, and time in msec.

5.2.1 Summary of Currents

Except where noted, all currents were modelled using the Hodgkin-Huxley formalism as described in section 3.2.1. The details describing each current are given below.

I_h

The kinetics for the hyperpolarization-activated mixed cation current, I_h were based on data in Huguenard and McCormick [95]. In their work, the current was derived from voltage-clamp recordings of guinea pig thalamic relay neurons maintained in vitro as a thalamocortical slice. The current is modelled as follows:

$$I_h = g_h \cdot m_h \cdot (V - V_h) \tag{5.2}$$

where V_h is the reversal potential for this mixed cation current equal to -43 mV for all cortical pyramidal neurons and -40mV for the deep LTS interneuron in the model, and g_h is the maximal conductance. The steady state activation function, and the time constant for all neuron types were described by

$$m_{h\infty} = \frac{1}{1 + \exp\left(\frac{V+75}{5.5}\right)} \qquad \tau_{mh} = \frac{1}{\exp(-14.59 - 0.086 \cdot V) + \exp(-1.87 + 0.0701 \cdot V)}$$

I_{Naf}

The fast and transient inactivating Na^+ current was described using a Hodgkin-and-Huxley style equation

$$I_{Naf} = g_{Naf} \cdot (V - V_{Na}) \cdot m_{Naf}^3 \cdot h_{Naf} \tag{5.3}$$

where V_{Na} is the equilibrium potential for Na^+ equal to 50 mV for all neurons, g_{Naf} is the maximal conductance, m_{Naf} is the activation variable, and h_{Naf} is the inactivation variable. The kinetics for this current were based on quantitative data in Martina and Jonas [96].

The steady state activation, and inactivation functions for all pyramidal neurons were described by

$$m_{Naf\infty} = \frac{1}{1 + \exp\left(\frac{-V-38}{10}\right)} \qquad h_{Naf\infty} = \frac{1}{1 + \exp\left(\frac{V+62.9}{10.7}\right)}$$

The activation and inactivation time constants for all pyramidal neurons took the following form,

$$\tau_{mINaf} = \begin{cases} 0.025 + 0.14 \cdot \exp\left(\frac{V+30}{10}\right) & , V \leq -30\text{mV} \\ 0.02 + 0.145 \cdot \exp\left(\frac{-V-30}{10}\right) & , V > -30\text{mV} \end{cases}$$

$$\tau_{hINaf} = 0.15 + \frac{1.15}{1 + \exp\left(\frac{V+37}{15}\right)}$$

While the steady state activation function for the deep LTS interneuron was the same as $m_{Naf\infty}$, the inactivation function was described by

$$h_{Naf\infty L} = \frac{1}{1 + \exp\left(\frac{V+58.3}{6.7}\right)}$$

The activation and inactivation time constants for the LTS interneuron took the following form,

$$\tau_{mINafL} = \begin{cases} 0.0125 + 0.1525 \cdot \exp\left(\frac{V+30}{10}\right) & , V \leq -30\text{mV} \\ 0.02 + 0.145 \cdot \exp\left(\frac{-V-30}{10}\right) & , V > -30\text{mV} \end{cases}$$

$$\tau_{hINafL} = 0.225 + \frac{1.125}{1 + \exp\left(\frac{V+37}{15}\right)}$$

I_{Nap}

The persistent, depolarization-activated Na^+ current, I_{Nap} was described using the following equation,

$$I_{Nap} = g_{Nap} \cdot (V - V_{Na}) \cdot m_{Nap} \tag{5.4}$$

The kinetics for this current were based on quantitative data in Martina and Jonas [96]. The steady state activation was described by the following Boltzmann equation for all neurons,

$$m_{Nap\infty} = \frac{1}{1 + \exp\left(\frac{-48-V}{10}\right)}$$

The decay time constant, τ_{mNap} was described for all neuron types by

$$\tau_{mNap} = \begin{cases} 0.025 + 0.014 \cdot \exp\left(\frac{V+40}{10}\right) & , V \leq -40\text{mV} \\ 0.02 + 0.145 \cdot \exp\left(\frac{-V-40}{10}\right) & , V > -40\text{mV} \end{cases}$$

I_{Kdr}

The delayed rectifier K^+ current, I_{Kdr} was described using

$$I_{Kdr} = g_{Kdr} \cdot (V - V_K) \cdot m_{Kdr}^4 \tag{5.5}$$

where V_K is the equilibrium potential for K^+, assumed to be -95 mV for all pyramidals and -100 mV for the LTS interneuron, and g_{Kdr} is the maximal conductance. The kinetics were based on data in Martina et al. [97].

The steady state activation function, $m_{Kdr\infty}$ for all pyramidals, and $m_{Kdr\infty L}$ for the interneuron was described by the following,

$$m_{Kdr\infty} = \frac{1}{1 + \exp\left(\frac{-V-29.5}{10}\right)} \qquad m_{Kdr\infty L} = \frac{1}{1 + \exp\left(\frac{-V-27}{11.5}\right)}$$

The decay time constant, τ_{mKdr} was for all neurons by

$$\tau_{mKdr} = \begin{cases} 0.25 + 4.35 \cdot \exp\left(\frac{V+10}{10}\right) & , V \leq -10\text{mV} \\ 0.25 + 4.35 \cdot \exp\left(\frac{-V-10}{10}\right) & , V > -10\text{mV} \end{cases}$$

I_{Ka}

The transient inactivating K^+ current, I_{Ka} was described using the equations presented by Huguenard and McCormick [95]:

$$I_{Ka} = g_{Ka} \cdot (V - V_K) \cdot m_{Ka}^4 \cdot h_{Ka} \tag{5.6}$$

The steady state activation and inactivation functions for all neurons were described by

$$m_{Ka\infty} = \frac{1}{1 + \exp\left(\frac{-V-60}{8.5}\right)} \qquad h_{Ka\infty} = \frac{1}{1 + \exp\left(\frac{V+78}{6}\right)}$$

The decay time constants for activation and inactivation for all neuron types were described by

$$\tau_{mKa} = 0.185 + \frac{0.5}{\exp\left(\frac{V+35.8}{19.7}\right) + \exp\left(\frac{-V-79.7}{12.7}\right)}$$

$$\tau_{hKa} = \begin{cases} \frac{0.5}{\exp\left(\frac{V+46}{5}\right)+\exp\left(\frac{-V-238}{37.5}\right)} & , V \leq -63\text{mV} \\ 9.5 & , V > -63\text{mV} \end{cases}$$

I_{K2}

The slowly activating and inactivating K^+ current, I_{K2} equations followed Huguenard and McCormick [95] and McCormick and Huguenard [98]:

$$I_{K2} = g_{K2} \cdot (V - V_K) \cdot m_{K2} \cdot h_{K2} \tag{5.7}$$

The steady state activation and inactivation functions were described, for all neurons by

$$m_{K2\infty} = \frac{1}{1 + \exp\left(\frac{-V-10}{17}\right)} \qquad h_{K2\infty} = \frac{1}{1 + \exp\left(\frac{V+58}{10.6}\right)}$$

The decay time constants for activation and inactivation were described by

$$\tau_{mK2} = 4.95 + \frac{0.5}{\exp\left(\frac{V-81}{25.6}\right) + \exp\left(\frac{-V-132}{18}\right)}$$

$$\tau_{hK2} = 60 + \frac{0.5}{\exp\left(\frac{V-1.33}{200}\right) + \exp\left(\frac{-V-130}{7.1}\right)}$$

I_{Km}

The muscarinic receptor-supressed K^+ current, I_{Km} was described using the equation presented by Traub et al. [99]:

$$I_{Km} = g_{Km} \cdot (V - V_K) \cdot m_{Km} \tag{5.8}$$

The forward and backward rate functions for all neuron types were defined as

$$\alpha_{mKm} = \frac{0.02}{1 + \exp\left(\frac{-V-20}{5}\right)} \qquad \beta_{mKm} = 0.01 \cdot \exp\left(\frac{-V-43}{18}\right)$$

I_{Kc}

The fast voltage and Ca^{2+}-dependent K^+ current, I_{Kc} was described using the following equation:

$$I_{Kc} = g_{Kc} \cdot (V - V_K) \cdot m_{Kc} \cdot \Gamma(\chi) \tag{5.9}$$

The equation involved a voltage dependent activation variable, m_{Kc} as well as a Ca^{2+}-dependent term, $\Gamma(\chi)$, where $[Ca^{2+}]_i$ is denoted by χ, and $\Gamma(\chi) = \min\,(0.004{\cdot}\chi,\ 1.0)$ [100].

The forward and backward rate functions were defined, for all pyramidal neurons, as

$$\alpha_{mKc} = \begin{cases} 0.053 \cdot \exp\left(\frac{V+50}{11} - \frac{V+53.5}{27}\right) & , V \leq -10\text{mV} \\ 2 \cdot \exp\left(\frac{-V-53.5}{27}\right) & , V > -10\text{mV} \end{cases}$$

$$\beta_{mKc} = \begin{cases} 2 \cdot \exp\left(\frac{-V-53.5}{27}\right) - \alpha_{mKc} & , V \leq -10\text{mV} \\ 0 & , V > -10\text{mV} \end{cases}$$

Whereas for the deep LTS interneuron, $\alpha_{mKcL} = 2 \cdot \alpha_{mKc}$ and $\beta_{mKcL} = 2 \cdot \beta_{mKc}$.

I_{Kahp}

The slow Ca^{2+}-dependent K^+ current, I_{Kahp} responsible for afterhyperpolarization, was described using kinetics presented by Traub et al. [100].

$$I_{Kahp} = g_{Kahp} \cdot (V - V_K) \cdot m_{Kahp} \tag{5.10}$$

The forward rate function, for all neurons, was Ca^{2+} dependent, and thus was a function of χ.

$$\alpha_{mKahp} = \min(0.0001 \cdot \chi, 0.01) \qquad \beta_{mKahp} = 0.01$$

I_{Cat}

The low-threshold Ca^{2+} current, I_{Cat} was modelled using the following Hodgkin-Huxley type equation,

$$I_{Cat} = g_{Cat} \cdot (V - V_{Ca}) \cdot m_{Cat}^2 \cdot h_{Cat} \tag{5.11}$$

where g_{Cat} is the maximal conductance and V_{Ca} is the reversal potential for Ca^{2+} with a value of 125 mV, for all neuron types.

The steady state activation and inactivation functions for all pyramidals were Boltzmann style, and were described by

$$m_{Cat\infty} = \frac{1}{1 + \exp\left(\frac{-V-56}{6.2}\right)} \qquad h_{Cat\infty} = \frac{1}{1 + \exp\left(\frac{V+80}{4.0}\right)}$$

The steady state activation and inactivation functions for deep LTS were modelled similarly, and described by

$$m_{Cat\infty L} = \frac{1}{1 + \exp\left(\frac{-V-52}{7.4}\right)} \qquad h_{Cat\infty L} = \frac{1}{1 + \exp\left(\frac{V+80}{5.0}\right)}$$

The time constants for activation and inactivation, for all pyramidal cells, were described by

$$\tau_{mCat} = 0.204 + \frac{0.333}{\exp\left(\frac{-V-131}{16.7}\right) + \exp\left(\frac{V+15.8}{18.2}\right)}$$

$$\tau_{hCat} = \begin{cases} 0.333 \cdot \exp\left(\frac{V+466}{66.6}\right) & , V \leq -81\text{mV} \\ 9.32 + 0.333 \cdot \exp\left(\frac{-V-21}{10.5}\right) & , V > -81\text{mV} \end{cases}$$

The time constants for activation and inactivation, for the interneuron, were described by

$$\tau_{mCatL} = 1 + \frac{0.333}{\exp\left(\frac{V+27}{10}\right) + \exp\left(\frac{-V-102}{15}\right)}$$

$$\tau_{hCatL} = 28.3 + \frac{0.33}{\exp\left(\frac{V+48}{4}\right) + \exp\left(\frac{-V-407}{50}\right)}$$

I_{Cal}

Similar to the low-threshold Ca^{2+} current, the high-threshold current I_{Cal} was also modelled using a Hodgkin-Huxley style equation.

$$I_{Cal} = g_{Cal} \cdot (V - V_{Ca}) \cdot m_{Cal}^2 \tag{5.12}$$

The forward and backward rate functions, for all neurons, were described by

$$\alpha_{mCal} = \frac{1.6}{1 + \exp(-0.072 \cdot (V - 5))} \qquad \beta_{mCal} = 0.1 \cdot \frac{\frac{V+8.9}{5}}{\exp\left(\frac{V+8.9}{5}\right) - 1}$$

I_{Leak}

The leak current for all neuron types were described as simple ohmic currents:

$$I_{Leak} = g_{Leak} \cdot (V - V_{Leak}) \tag{5.13}$$

where the g_{Leak} is the constant conductance and V_{Leak}, the equilibrium potential, was assumed to be -70 mV for all pyramidals and -65 mV for the deep LTS interneuron.

Ca^{2+} dynamics

Calcium dynamics are defined as presented in the work by Traub et al. [99]. A simple proportional model of Ca^{2+} diffusion was used, with Ca^{2+} concentration denoted by χ (in μmol/L) and the change in χ was described by:

$$\frac{d\chi}{dt} = -\phi_\chi \cdot I_{Ca} \cdot U_{ICa} - \beta_\chi \cdot \chi$$

$$\text{where} \quad \phi_\chi = \frac{5200}{Area * Depth} \qquad \text{and} \quad U_{ICa} = \frac{Area\ \mu m^2 \cdot 1 \times 10^{-8} cm^2}{\mu m^2} \cdot \frac{1\text{nA}}{1 \times 10^{-3} \mu A}$$

Here, the change in calcium concentrations was dependent only on I_{Cal} (in $\mu A/cm^2$). The factor U_{ICa} is used to convert the units of current from $\mu A/cm^2$ to nA. The calcium concentration was calculated beneath the soma-dendritic membrane. The area (in μm^2) and depth (in μm) varied depending on the neuron. The area is calculated according to the measurements given in section 5.2. The depth at which the calcium concentration was calculated was $12{\times}10^{-3}$ μm for the IB and RS neuron, $4{\times}10^{-3}$ μm for the NRS neuron, and $2{\times}10^{-4}$ μm for the LTS interneuron. The decay time constant for $[Ca^{2+}]$ was 50 ms for the deep LTS interneuron, and 100 ms for all pyramidal neurons. The constant 5200 is used to convert current (in nanoamperes), time (in milliseconds), and volume (in cubic micrometers) to concentration of Ca^{2+} ions (in μmol/L). In particular, Faraday's constant is used to convert charge to moles, and volume is converted from cubic micrometers to litres. The conversion of units for this constant is derived using:

$$5200\ \frac{\mu\text{mol}\cdot\ \mu m^3}{\text{L}\cdot\ \text{msec}} = \frac{1{\times}10^6\ \mu\text{mol}}{1.92988 \times 10^5\ \text{C}} \cdot \frac{1 \times 10^{-12}\ \text{C}}{1\ \text{msec}} \cdot \frac{1 \times 10^{15}\ \mu m^3}{1\ \text{liter}}$$

The maximal conductance values for each of the currents given in Traub's model are presented in Table 5.2.

Tufted RS	
Parameter	Value (mS/cm^2)
g_{Naf}	200
g_{Nap}	0.16
g_{Kdr}	170
g_{Kc}	28.8
g_{Ka}	20
g_{Km}	8.5
g_{K2}	0.5
g_{Kahp}	0.2
g_{Cal}	1.6
g_{Cat}	0.1
g_h	0.1
g_{Leak}	2.8

Tufted IB	
Parameter	Value (mS/cm^2)
g_{Naf}	200
g_{Nap}	0.16
g_{Kdr}	170
g_{Kc}	16
g_{Ka}	20
g_{Km}	11.9
g_{K2}	0.5
g_{Kahp}	0.2
g_{Cal}	4
g_{Cat}	0.1
g_h	0.1
g_{Leak}	2.8

Non-Tufted RS	
Parameter	Value (mS/cm^2)
g_{Naf}	200
g_{Nap}	0.08
g_{Kdr}	170
g_{Kc}	15
g_{Ka}	122.5
g_{Km}	4.2
g_{K2}	0.1
g_{Kahp}	0.2
g_{Cal}	0.2
g_{Cat}	0.1
g_h	0.25
g_{Leak}	2

Deep LTS	
Parameter	Value (mS/cm^2)
g_{Naf}	60
g_{Nap}	0.16
g_{Kdr}	100
g_{Kc}	25
g_{Ka}	1
g_{Km}	0.5
g_{K2}	0.5
g_{Kahp}	0.1
g_{Cal}	0.1
g_{Cat}	0.1
g_h	0.1
g_{Leak}	2.4

Table 5.2: Maximal ionic conductance densities as given in Traub et al. [1] and Cunningham et al. [2]; Tables A4, A5, and A6 from Traub et al. [1] and Supplementary Material in Cunningham et al. [2].

Chapter 6

Single-Compartment Models for Cortical Neurons

Our work began with using Traub's model as a starting point and reducing it on multiple levels. At the larger, network-level, we reduced from a 3560-neuron model to a 4-neuron model with each neuron of a different type. In particular, from the variety of neurons of different layers, we chose to only include the layer 5 tufted regular spiking (RS) pyramidal, layer 5 tufted intrinsically bursting (IB) pyramidal, layer 6 non-tufted regular spiking (RS) pyramidal, and a deep low-threshold spiking (LTS) interneuron. In this regard, in our reduced model we interpreted any input of current into our layer 5 neurons as projections from other (upper) layers. Furthermore, Traub's single-neuron models ranged in number of compartments from 57 to 144 compartments which included a single-compartment soma, a 6-compartment branched axon, and multiple dendritic compartments. At the single-neuron level, we made a reduction from a multiple compartments to a single-compartment, representing the soma. Each neuron was described by a Hodgkin-Huxley style model, exactly the way described by Traub et al. [1]. Our goal was to retain the firing behaviour of these neurons with a simpler model that does not account for spatial structure. In particular, the goal for our single-compartment models was to exhibit similar frequency of firing as compared to the multi-compartment model, for input of currents similar to those given in Traub's model simulations. For our reduced model, the types of conductances governing single-neuron dynamics were kept the same. However, the membrane conductance densities (mS/cm^2) required modification such that our single-compartment models reproduced the behaviour of Traub's multi-compartment models. It is important to note that we understand that these choice of modified parameters are not unique, and it is likely that different sets of parameters could lead to similar results as well. However, our approach is

reasonable since our analysis is qualitative in nature.

6.1 Layer 6 Non-tufted Regular Spiking Pyramidal Neuron

According to Traub's model, the non-tufted pyramidal neurons were morphologically characterized as neurons with thin apical dendrites which do not produce branching formations that reach Layer 1. While their intention was for the neuron model to resemble the structure of neurons of such type typically found in layer 5, as reported in the work by Mason and Larkman [101], Traub's model placed these neurons in layer 6. In this regard, the the firing patterns of these neurons resembled those recorded by Mason and Larkman for slender layer 5 non-tufted neurons in rodents. The firing patterns consists of burst-tonic spiking (see Figure A6 from Traub et al. [1]). This type of firing is described as one with an initial doublet (or triplet) followed by regular spiking. In order to model these neurons, Traub et al. used kinetics of membrane conductances as used for layer 2/3 pyramidal neurons in their previous work [99].

In our attempt to reproduce Traub's model of this layer 6 pyramidal neuron by reducing the multi-compartmental model to a single-compartment model, membrane conductance densities were modified. Without any changes, the behaviour of the single-compartment model using the parameters corresponding to the soma compartment in Traub's model (also given in Table 5.2) is shown in Figure 6.1, in response to different values of depolarizing current. The resulting behaviour consisted of fast-spiking, drastically different from the expected firing pattern for this type of neuron. To prevent this behaviour, some of the membrane conductance densities were changed, based on the effect on individual currents on membrane potential. The holding current was set to 0 μA/cm^2, and the leak conductance was increased to 2.6 mS/cm^2 to increase the resting membrane potential. Since the slowly activating and inactivating potassium current, I_{K2} has a strong effect on decreasing the response to a depolarizing current, its conductance was increased, resulting in reduced frequency of firing, however with an usual, irregular initial burst (Figure 6.2*B,C,D*). In an attempt to resolve this, the conductance of I_{Km} was increased from a value of 4.2 to 15 (Figure 6.2*E*). In addition, given the transient nature of the fast inactivating current, I_{Ka}, its conductance was increased to 150 mS/cm^2 to reduce the initial burst (Figure 6.2*F*), overall giving similar results to that in Traub's model. The resulting modified single-compartment model is given in Figure 6.3.

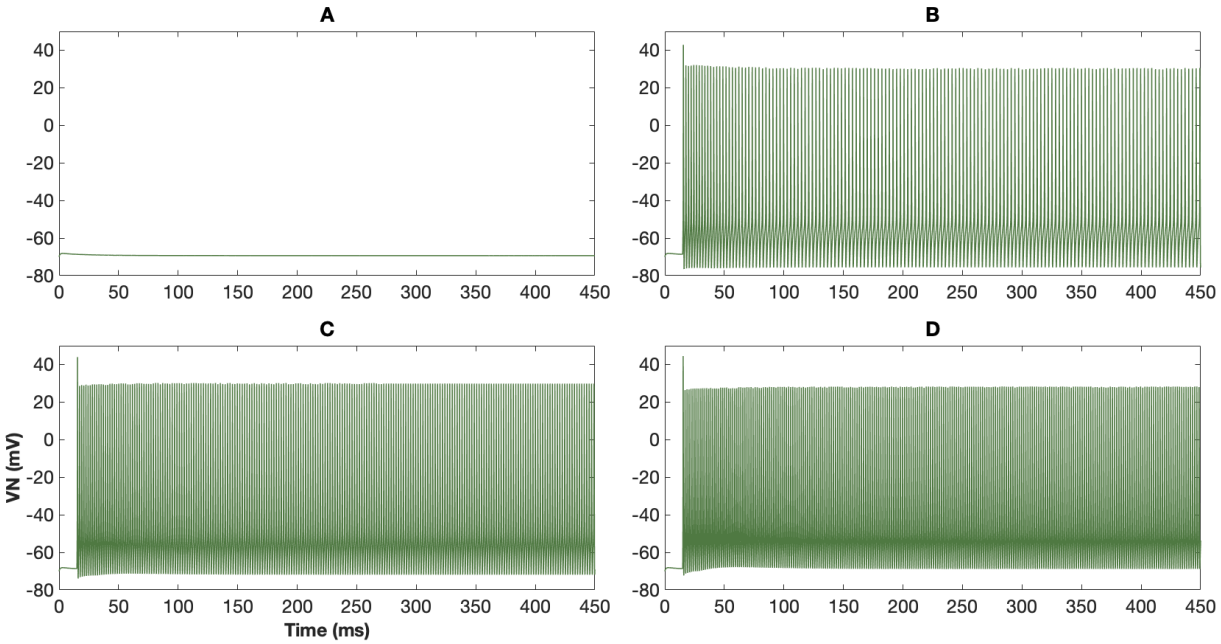

Figure 6.1: Single-compartment model for layer 6 non-tufted RS pyramidal neuron using soma compartment conductance density values from Traub's model. Units of applied current are $\mu A/cm^2$. **A**: I_{app}= 0, **B**: I_{app}= 50 ,**C**: I_{app}= 80, **D**: I_{app}= 100

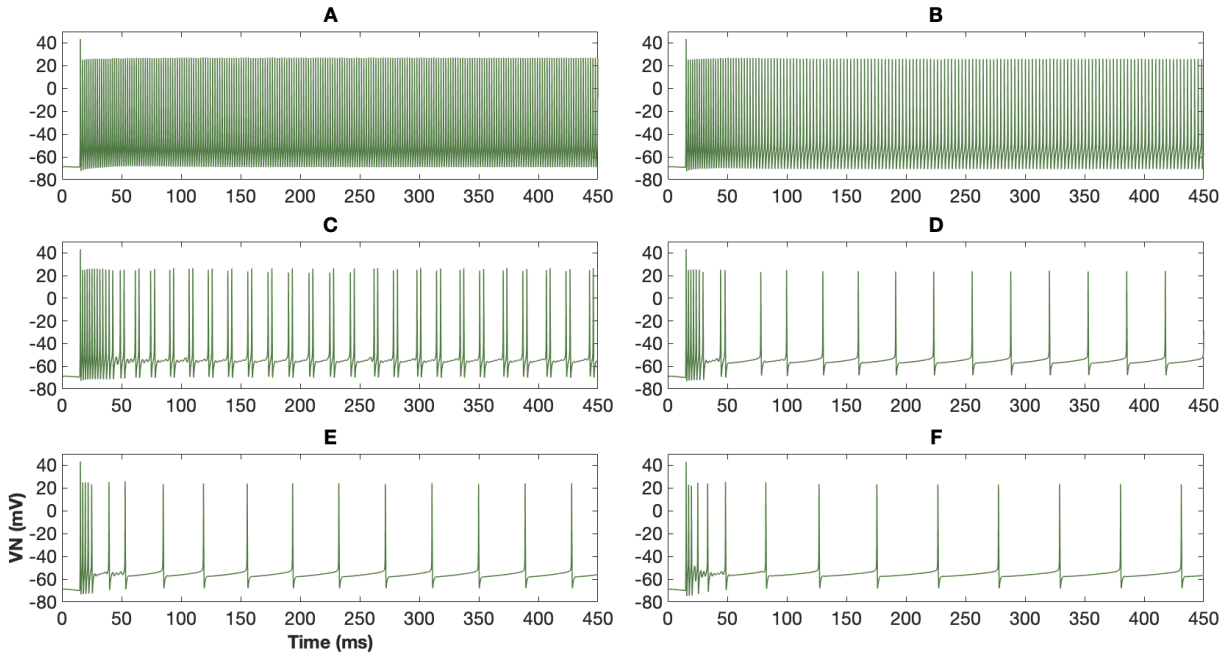

Figure 6.2: Stages of modification of membrane conductance densities for the single-compartment layer 6 non-tufted RS neuron model, with a fixed constant applied current, I_{app}= 100 $\mu A/cm^2$. Units of conductance are mS/cm^2. **A**: g_{K2}=1, **B**: g_{K2}=10, **C**: g_{K2}=25, **D**: g_{K2}=45, **E**: g_{K2}=45 and g_{Km}=15, **F**: g_{K2}=45, g_{Km}=15, and g_{Ka}=150

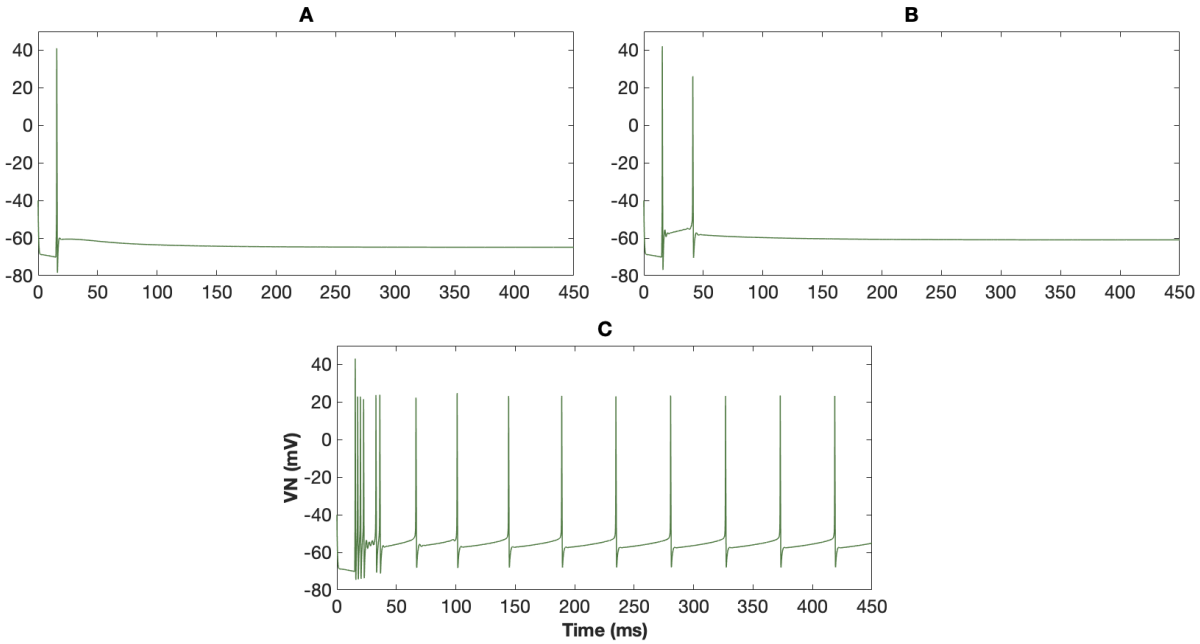

Figure 6.3: Firing behaviour of the single-compartment model for layer 6 non-tufted RS pyramidal neuron, using our modified conductance densities. Units of applied current are $\mu A/cm^2$. **A**: I_{app}= 50, **B**: I_{app}= 70 ,**C**: I_{app}= 102

6.2 Layer 5 Tufted Intrinsically Bursting Pyramidal Neuron

Traub's model for the layer 5 intrinsically bursting (IB) neuron was based on work by Larkum et al. [102]. The work presented in the latter paper involved investigating action potential patterns and their correlation with depolarizing inputs of current in dendrites and soma, and the underlying membrane mechanisms. Their motivation stemmed from the understanding of non-homogeneity in distribution of voltage-gate ion channels across the somato-dendritic membrane of pyramidal neurons [103]. In Traub's model, current injection occurred in the distal apical dendrites (dendrites which emerge apically from the cell body). The resulting behaviour was slow depolarizations and bursts generated in the dendrite, also known as dendritic bursts. This was also in agreement with experimental work on burst firing mechanisms in rat neocortical pyramidal neurons by Williams and Stuart [104]. In their study, bursting was characterized as strong or weak, depending on the initial burst of action potentials as well as the firing pattern which followed. According to their definition, strong bursting consisted of an initial burst of 2–6 action potentials, followed by repeated bursting consisting of 2–3 actions potentials per burst. Williams and Stuart also reported that dendritic depolarization strengthened burst firing, in which case, bursting was sustained. On the contrary, somatic injection resulted in diminished bursting over time (see Figure 7 of Williams and Stuart [104]). These definitions and observations are also captured in Traub's multi-compartment model of the layer 5 IB pyramidal neuron, in response to dendritic depolarization.

As per Traub's model, most of the voltage-dependent conductance kinetics were very similar to the layer 6 pyramidal neuron, while bursting was largely dependent on the high-threshold calcium conductance, g_{Cal}. Traub's model also demonstrated generation of single or multiple bursts depending on the strength of applied current, as shown in Figure A4 of [1]. Bursting behaviour begins at depolarizations of over 1 nA (equivalent to 70 $\mu A/cm^2$) in strength, and is sustained for strengths of applied current larger than 1.5 nA (equivalent to 104 $\mu A/cm^2$). Since our single-compartment model does not take into account neuron morphology except for the soma, modelling dendritic injection was not possible. Hence, membrane conductance densities were adjusted in order for neuronal firing behaviour to resemble Traub's model results. The firing behaviour of our single-compartment model for these neurons, without any conductance modifications is given in Figure 6.4.

Our conductance density modifications began by keeping the holding current at the same value of -14 $\mu A/cm^2$ (equivalent to -0.2 nA in Traub's model), while the leak conductance was reduced to 2 mS/cm^2 to further decrease the resting membrane potential to

match Traub's model value of -80 mV. As was the case for the layer 6 non-tufted neuron where g_{Km} was one of the key conductances involved in reducing fast spiking, its value for this neuron was increased as well from 11.9 to 30 mS/cm^2 (Figure 6.5A). In order to invoke bursting, g_{Cal} had to increased considerably as well (Figure 6.5B). The bursting interval was larger than required, and since the slow Ca^{2+}-dependent potassium current, I_{Kahp} contributes in prolonging the phase between bursts, its conductance value was increased to 3.5 (Figure 6.5C). The conductance of the transient inactivating K^+ current, g_{Ka} was reduced slightly (Figure 6.5D), resulting in repeated bursts, consisting of 2 action potentials, similar to the firing behaviour from Traub's model. The final simulations post modification of conductances in given in Figure 6.6.

In comparison with Traub's model, the resting membrane potential for our single-compartment model stays relatively the same at -80 mV. However, whereas the initial burst in Traub's model is followed by the peak amplitude reaching nearly -75 mV, our single-compartment model is unable to capture similar dynamics as nearly all the bursts are followed by peak amplitudes as high as -65 mV. These differences could be due to the simplicity in our model's setup. Given the absence of numerous compartments resulting in a lack of contribution of either depolarizing or repolarizing effects of the multitude of currents, the differences in our results are relatively unsurprising.

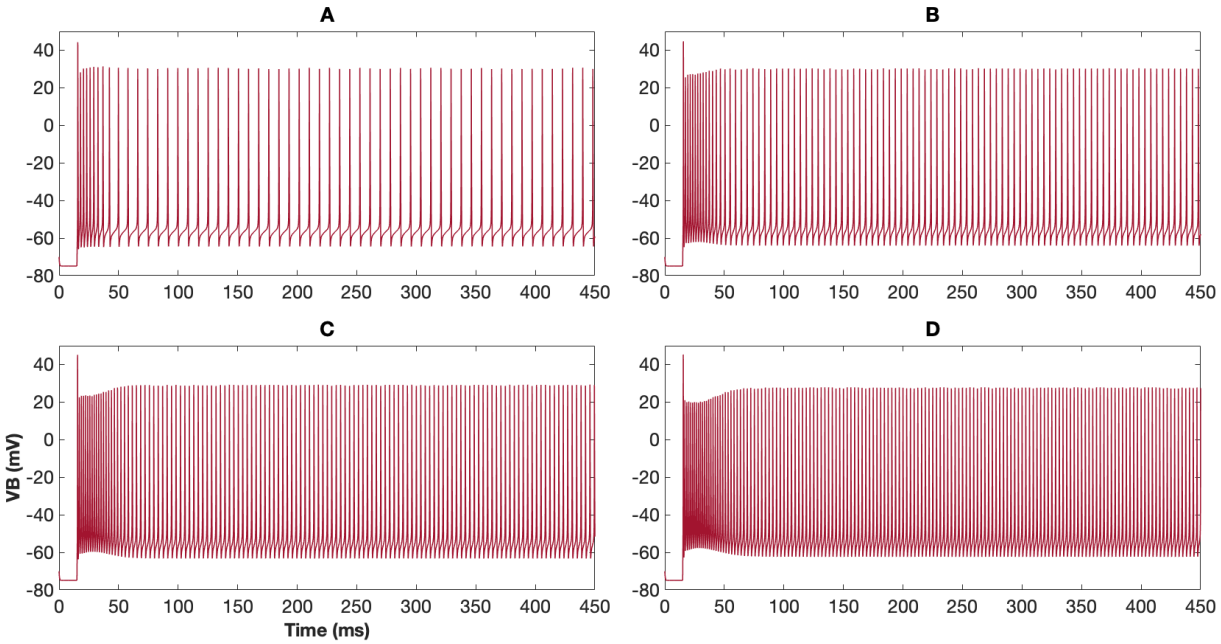

Figure 6.4: Single-compartment model for layer 5 tufted IB pyramidal neuron using soma compartment conductance density values from Traub's model. Units of applied current are $\mu A/cm^2$. **A**: I_{app}= 63, **B**: I_{app}= 77 ,**C**: I_{app}= 91, **D**: I_{app}= 104

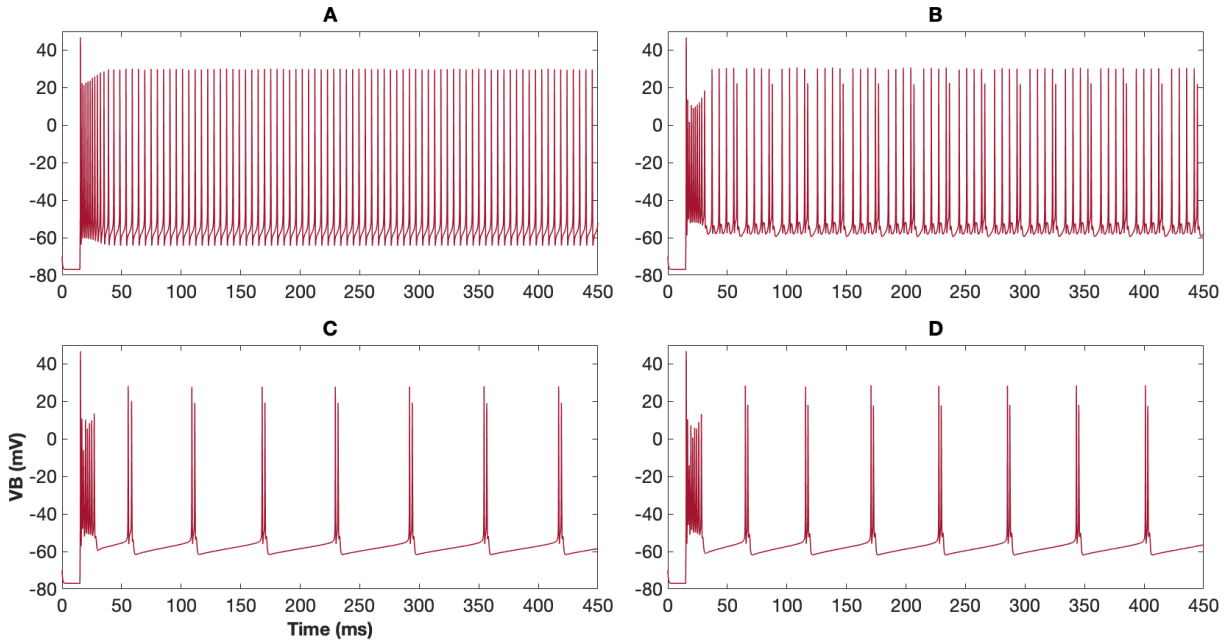

Figure 6.5: Stages of modification of membrane conductance densities for the single-compartment layer 5 tufted IB pyramidal neuron, with a fixed constant applied current, I_{app}= 105 $\mu A/cm^2$. Units of conductance are mS/cm^2. **A**: g_{Km}=30, **B**: g_{Km}=30, and g_{Cal}=10, **C**: g_{Km}=30, g_{Cal}=11.5, and g_{Kahp}=3.5, **D**: g_{Km}=30, g_{Cal}=11.5, g_{Kahp}=3.5, and g_{Ka}=15

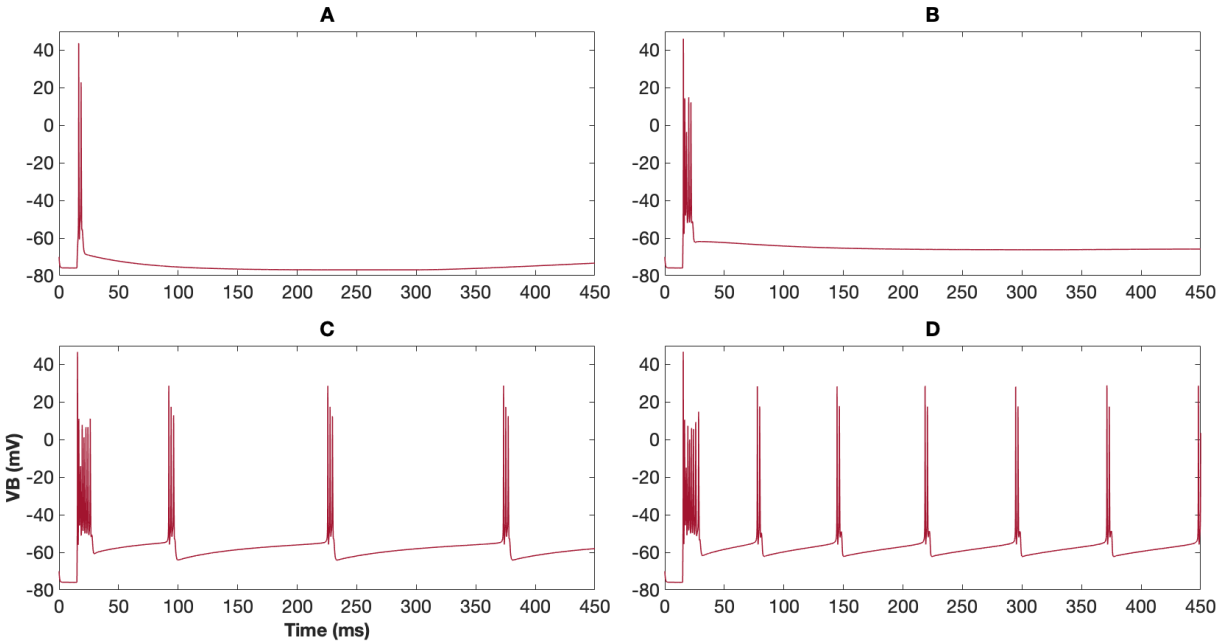

Figure 6.6: Firing behaviour of the single-compartment layer 5 tufted IB pyramidal neuron, using our modified conductance densities. Units of applied current are $\mu A/cm^2$. **A**: I_{app}= 30, **B**: I_{app}= 70, **C**: I_{app}= 97, **D**: I_{app}= 100

6.3 Layer 5 Tufted Regular Spiking Pyramidal Neuron

Tufted neocortical pyramidal neurons in layer 5 also exhibit regular spiking in some cases [104]. As reported in the study by Williams and Stuart, regular firing is typically invoked by somatic depolarizations, with the frequency of firing increasing with increased depolarization (see Figure 2 of Williams and Stuart [104]). For the layer 5 tufted regular spiking (RS) pyramidal neuron in Traub's model, although it was not clear whether the applied current is dendritic or somatic, it is likely that the injection site is at the soma. While the compartmental architecture of this neuron was the same as the layer 5 IB pyramidal neuron, one of the key differences between the two neuron models was the high-threshold calcium conductance, which was lower for the RS pyramidal neuron. Also, the conductance density for the fast voltage and calcium dependent K^+ current, I_{Kc} was higher as compared to the layer 5 IB neuron. The firing behaviour of the layer 5 RS pyramidal neuron can be seen in Figure A5 of [1].

We simulated the firing behaviour of this neuron using conductance densities for the soma compartment as reported in Traub's model, in our single-compartment model with results given in Figure 6.7. Unsurprisingly, similar to the behaviour of the layer 5 IB and layer 6 RS pyramidal neurons, the firing was very rapid. In fact, for an applied current of 70 μA/cm^2, repeated bursts were evoked. Thus, a similar approach of modifying conductance densities took place. The holding current was kept the same at -28 μA/cm^2 (equivalent of -0.4 nA from Traub's model), and the leak conductance was also kept the same at 2.8 mS/cm^2, to keep the resting membrane potential at -81 mV. Using the adjusted conductance densities of the layer 5 IB pyramidal neuron as a starting point, some of the conductances for the layer 5 RS pyramidal neuron were modified. In order to reduce the fast spiking nature and the initial burst firing, both g_{Ka} and g_{Km} were increased significantly (see Figure 6.8A). Since there is no bursting involved, the high-threshold calcium conductance was reduced, and simultaneously, g_{Kahp} was also reduced (Figure 6.8B). The result of the modified single-compartment model is given in Figure 6.9.

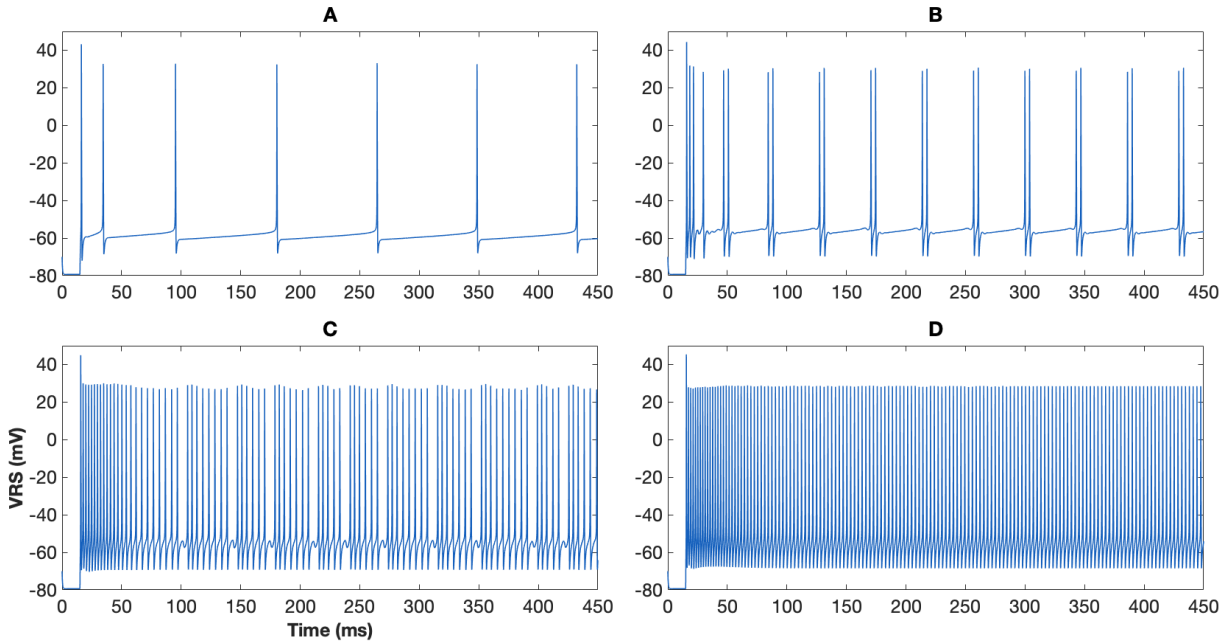

Figure 6.7: Single-compartment model for layer 5 tufted RS pyramidal neuron using soma compartment conductance density values from Traub's model. Units of applied current are $\mu A/cm^2$. **A**: I_{app}= 55, **B**: I_{app}= 70 ,**C**: I_{app}= 85, **D**: I_{app}= 100

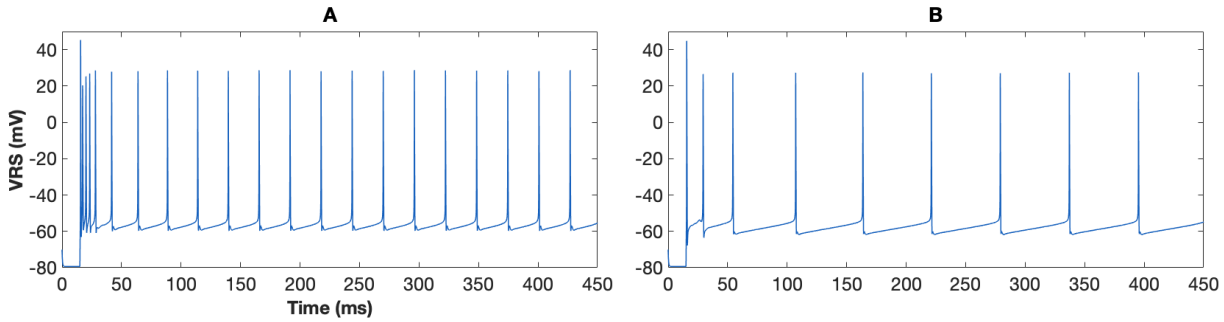

Figure 6.8: Stages of modification of membrane conductance densities for the single-compartment layer 5 RS pyramidal neuron, with a fixed constant applied current, $I_{app} = 95\mu A/cm^2$. Units of conductance are mS/cm^2. **A**: g_{Kc}=15, g_{Ka}=20, g_{Km}=30, g_{Cal}=8 and g_{Kahp}=1.5, **B**: g_{Kc}=15, g_{Ka}=40 and g_{Km}=70, g_{Cal}=8 and g_{Kahp}=1.5

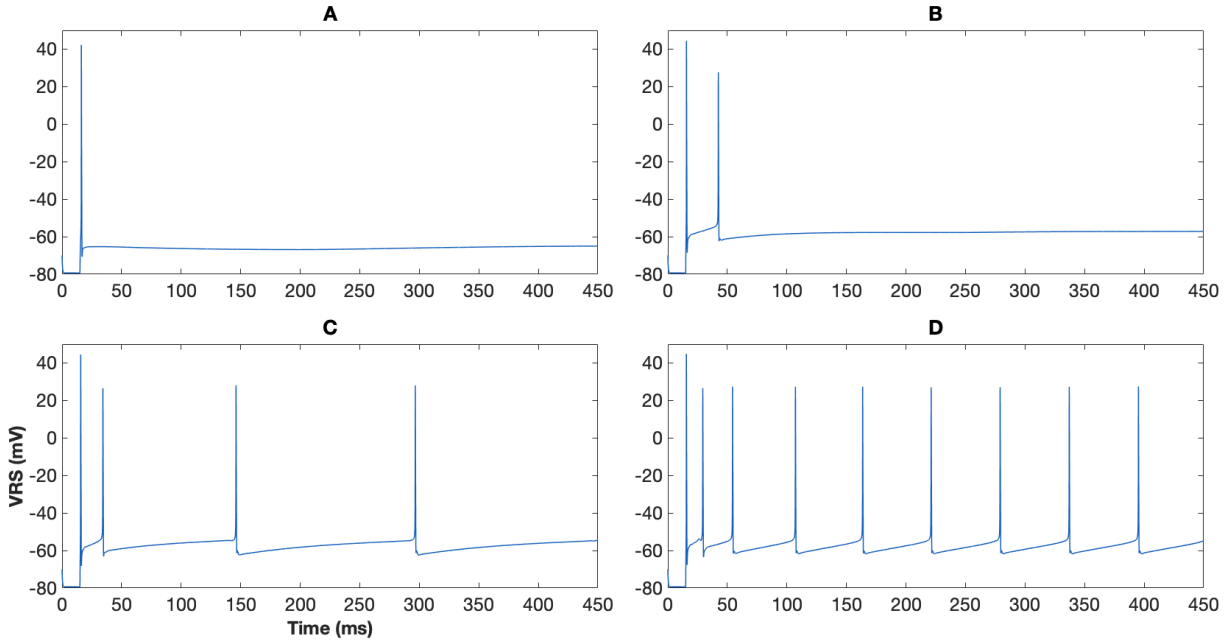

Figure 6.9: Firing behaviour of the single-compartment layer 5 RS pyramidal neuron, using our modified conductance densities. Units of applied current are μA/cm^2. **A**: I_{app}= 55, **B**: I_{app}= 84, **C**: I_{app}= 88, **D**: I_{app}= 95

6.4 Deep Low-Threshold Spiking Interneuron

One of the most common types of inhibitory interneurons found in the cortex are low-threshold spiking (LTS) interneurons [105]. Low-threshold spiking cells generally require relatively small depolarizations above resting potential to elicit action potential firing. While interneurons usually tend to project locally, some layer 4 interneurons branch extensively and extend vertically into layers 2/3 and 5 [40, 105]. LTS cells are also characterized to exhibit brief bursting, with an initial burst of action potentials in response to depolarizing input currents [106]. In addition to low-threshold spikes from hyperpolarized potentials due to depolarizing input, low-threshold spiking in response to hyperpolarizing input at depolarized potentials is also one of the characteristics [107]. They also display spike-frequency adaptation in spiking behaviour following low-threshold spikes [106].

Traub's model of deep layer LTS cells was based on a model by Cunningham et al. [2]. However, it is unclear what layer(s) "deep" exactly corresponds to. The response of a single model interneuron to a brief depolarizing current pulse is given in the supplemental material of Cunningham et al. [2]. The initial burst of low-threshold spikes, followed by spike-frequency adaptation, as described in the experimental work by Kawaguchi [107, 106] is evident in this firing response. However, the response of the model interneuron to hyperpolarizing input is not provided, which makes it unclear if the model is capable of achieving this response or not. The firing behaviour of the model deep LTS interneuron, is given in Figure A2 of [1]. Using the conductance densities for the soma compartment as reported in Traub's model, the response of our single-compartment model is given in Figure 6.10.

Since the default firing behaviour consisted of a single spike, in order to increase spiking, g_{Nap} was increased to 120 mS/cm^2. Conductance density for the persistent sodium current needed to be increased further to result in more spiking, and a higher peak membrane potential amplitude. The changes from 120 to 170 mS/cm^2 are shown in Figure 6.11*A–B*. Minimal spike-frequency adaptation, a common feature of LTS cells, is also evident in these simulations. Although the peak membrane potential amplitude reaches the appropriate value of approximately 35 mV, the spike frequency needed to be reduced. The conductances of both I_{Km} and I_{K2} were increased gradually, shown in Figure 6.11*C–D*. The afterdepolarization activity indicated that the fast voltage and calcium-dependent potassium current conductance, g_{Kc} needed to be reduced (Figure 6.11*E*). Lastly, the conductances of both I_{Km} and I_{K2} were increased further to reduce the spike frequency (Figure 6.11*F*). The results of the modified single-compartment model is given in Figure 6.12.

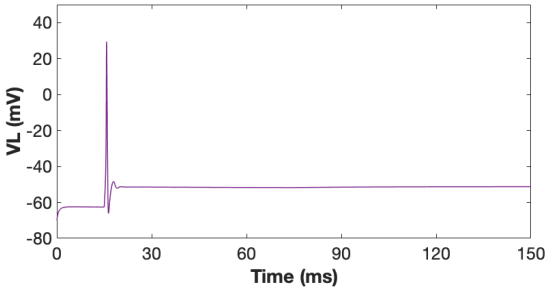

Figure 6.10: Single-compartment model of deep LTS interneuron using soma compartment conductance density values from Traub's model. Units of applied current are $\mu A/\text{cm}^2$ with a value of 42.

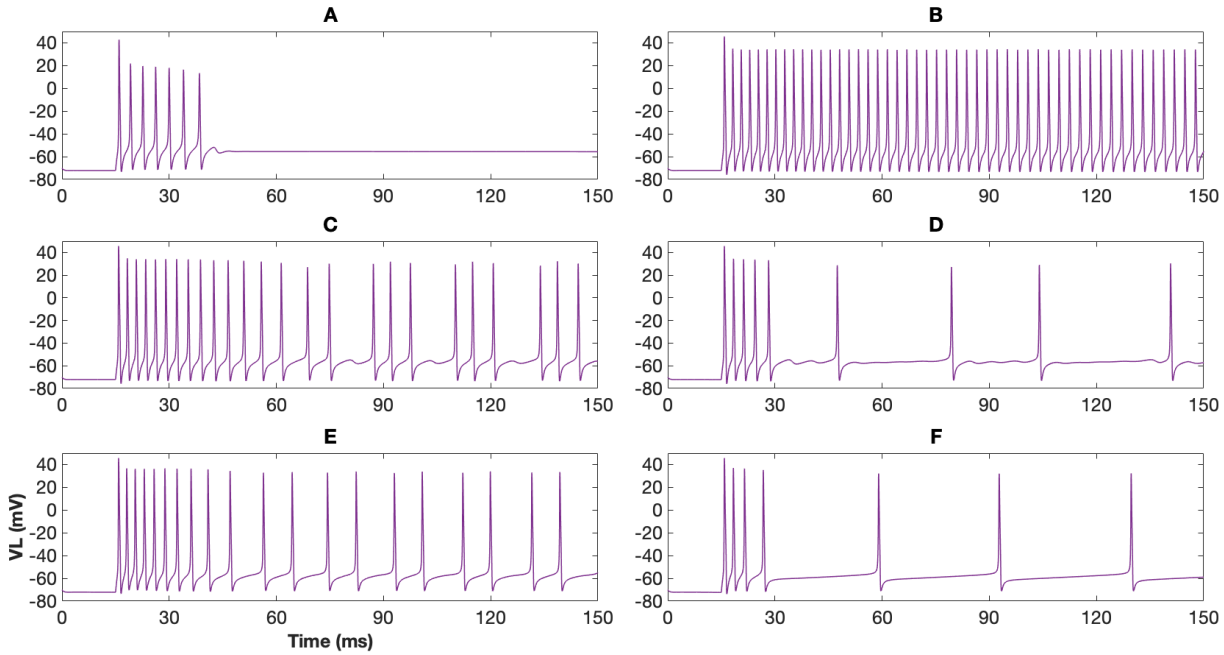

Figure 6.11: Stages of modification of membrane conductance densities for the single-compartment deep LTS interneuron, with a fixed constant applied current, I_{app}= 42 $\mu A/\text{cm}^2$. Units of conductance are mS/cm^2. **A**: g_{Naf}=120, **B**: g_{Naf}=170, **C**: g_{Naf}=170, g_{Km}=g_{K2}=2, **D**: g_{Naf}=170, g_{Km}=g_{K2}=4, **E**: g_{Naf}=170, g_{Km}=g_{K2}=4, g_{Kc}=15, **F**: g_{Naf}=170, g_{Km}=g_{K2}=9, g_{Kc}=15

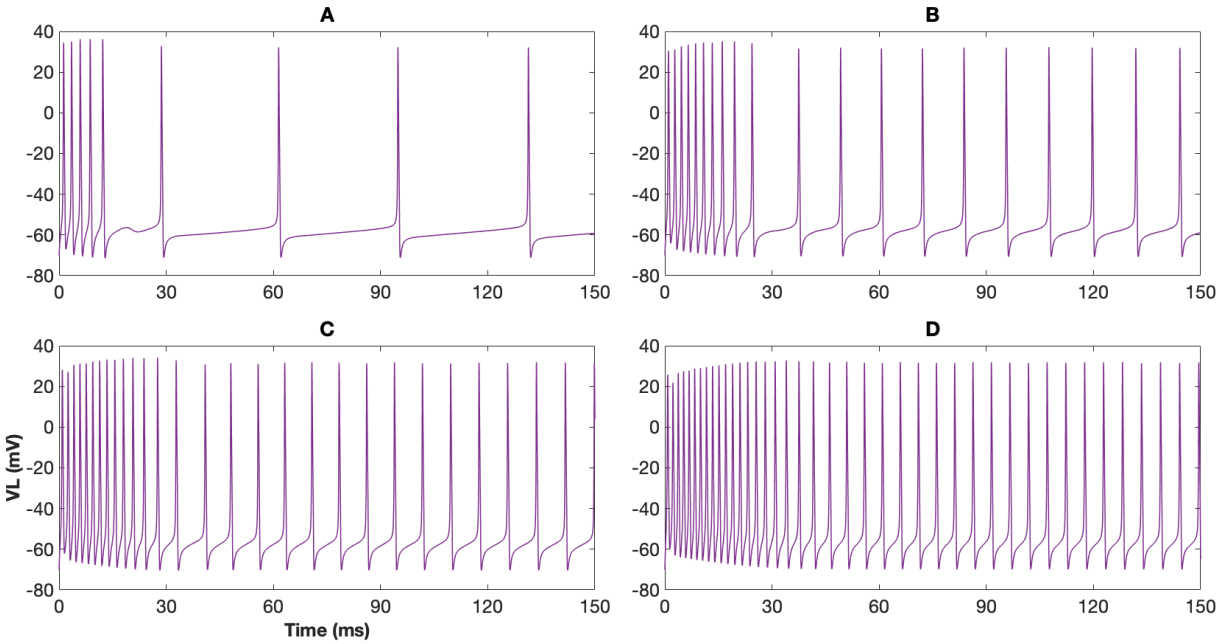

Figure 6.12: Firing behaviour of the single-compartment deep LTS interneuron, using our modified conductance densities. Units of applied current are $\mu A/\text{cm}^2$. **A**: I_{app}=42, **B**: I_{app}=55, **C**: I_{app}=65, **D**: I_{app}=80

The following parameters were used for all of our single-compartment neuron models, modified from the parameters for the soma compartment as given in Traub et al. [1].

Tufted RS	
Parameter	Value (mS/cm^2)
g_{Naf}	200
g_{Nap}	0.16
g_{Kdr}	170
g_{Kc}	15
g_{Ka}	40
g_{Km}	70
g_{K2}	0.5
g_{Kahp}	1.5
g_{Cal}	8
g_{Cat}	0.1
g_h	0.1
g_{Leak}	2.8

Tufted IB	
Parameter	Value (mS/cm^2)
g_{Naf}	200
g_{Nap}	0.16
g_{Kdr}	170
g_{Kc}	15
g_{Ka}	15
g_{Km}	30
g_{K2}	0.5
g_{Kahp}	3.5
g_{Cal}	11.5
g_{Cat}	0.1
g_h	0.1
g_{Leak}	2

Non-Tufted RS	
Parameter	Value (mS/cm^2)
g_{Naf}	200
g_{Nap}	0.08
g_{Kdr}	170
g_{Kc}	15
g_{Ka}	150
g_{Km}	45
g_{K2}	45
g_{Kahp}	0.2
g_{Cal}	0.2
g_{Cat}	0.1
g_h	0.25
g_{Leak}	2

Deep LTS	
Parameter	Value (mS/cm^2)
g_{Naf}	170
g_{Nap}	0.16
g_{Kdr}	100
g_{Kc}	15
g_{Ka}	1
g_{Km}	9
g_{K2}	9
g_{Kahp}	0.1
g_{Cal}	0.1
g_{Cat}	0.05
g_h	0.1
g_{Leak}	2.4

Table 6.1: Maximal ionic conductance densities for each current, for each of the single-compartment neuron models.

Chapter 7

Synaptic Models

7.1 AMPA Synapse

According to Traub's model, the time course for AMPA conductances took the form of an alpha function as given in Section 3.4 by Equation (3.8). In this case, $\bar{g}_{syn}$ is the AMPA conductance scaling constant (maximal synaptic conductance), t is time after a presynaptic spike, and τ_{syn} is the decay time constant. To maintain consistency in units, the default units of nS were converted to mS/cm^2 by dividing by the area of the postsynaptic neuron.

Although in appearance the conductance $G_\alpha(t)$ is a simple non-linear function of time, its use is undesirable. Instead, we have made use instead of the nonlinear Destexhe synapse model, $G_{Dest}(t)$, given by Equations (3.9)–(3.13). Our motivation behind this is to remain within the realm of being biologically plausible, especially since the Destexhe model is by definition, biophysical in nature, with its kinetics similar to the manner in which ion channel modelling is defined.

As per Destexhe [71], we are working under the condition of a neurotransmitter pulse of duration 1 ms and amplitude of 1 mM. This means T_{max}= 1 mM and t_1= 1 ms, and as well, we are using $V_T = 2$ mV and $K_p = 5$ mV.

The decay time constant, defined as $\frac{1}{\beta_A}$, is between 4.5–5.3 ms [33][108]. This gives a range for the decay rate of conductance, β_A (in ms^{-1}),

$$\frac{1}{5.3} \leq \beta_A \leq \frac{1}{4.5} \tag{7.1}$$

According to Ermentrout et al., the rise time constant ($\tau_{sA} = \frac{1}{\alpha_A + \beta_A}$) in cortical pyramidal

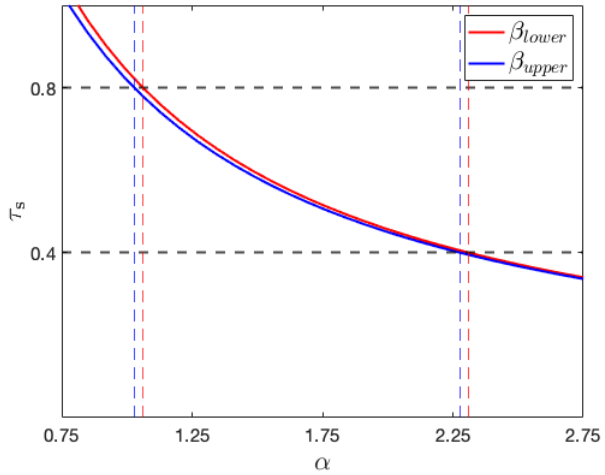

Figure 7.1: Rise time constant, τ_s, as a function of the rise rate of conductance, α, for the lower and upper bound on decay rate of conductance, β.

neurons is between 0.4–0.8 ms [33].

$$0.4 \leq \tau_{sA} \leq 0.8 \tag{7.2}$$

$$0.4 \leq \frac{1}{\alpha_A + \beta_A} \leq 0.8$$
$$\frac{1}{0.4} - \beta_A \geq \alpha_A \geq \frac{1}{0.8} - \beta_A$$

Using Equation (7.2) with both $\beta_{Aupper} = 0.222\ ms^{-1}$ and $\beta_{Alower} = 0.1886\ ms^{-1}$ gives a range for the rise rate of conductance, α_A (in $mM^{-1}ms^{-1}$). Thus, as β_A ranges from 0.1886–0.222 ms^{-1}, α_A ranges from 1.0614–2.3114 $mM^{-1}ms^{-1}$ to 1.0280–2.2780 $mM^{-1}ms^{-1}$, respectively.

Figure 7.2 shows how the Destexhe model compares for the upper and lower bounds on α_A and β_A. We chose an average value of 0.6 ms for τ_{sA}, and 0.2173 ms^{-1} for β_A, taken from results on excitatory synaptic currents in excitatory cortical neurons by Hestrin [108]. This gives a value for α_A equal to 1.4493 $mM^{-1}ms^{-1}$. Since the rise and decay time for AMPA synapses on cortical inhibitory neurons is about twice as fast as cortical pyramidal neurons, the rise and decay rate of conductances for synaptic connections to the interneuron are chosen to be $2{\cdot}\alpha_A$ and $2{\cdot}\beta_A$ [108].

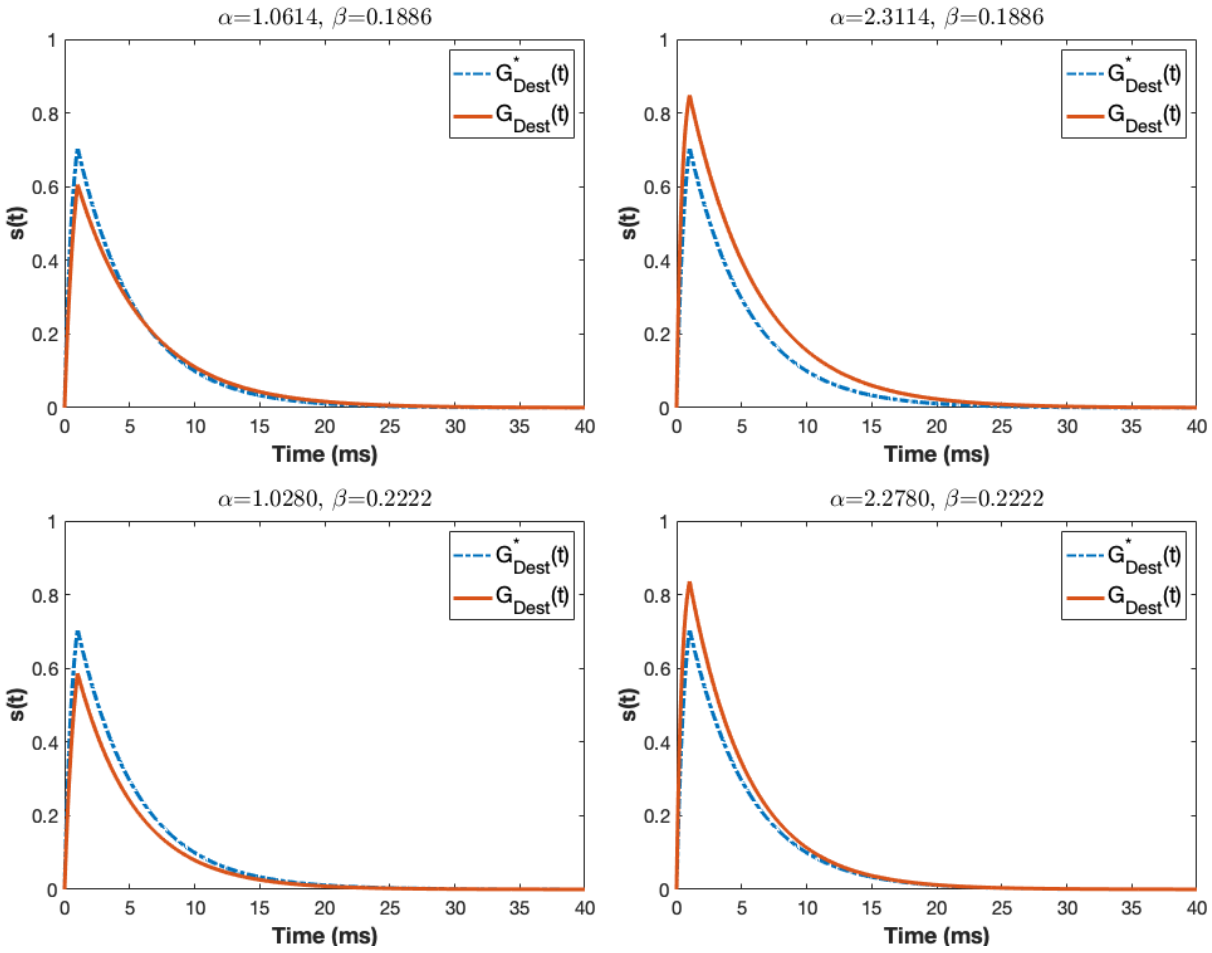

Figure 7.2: Gating variable $s(t)$ from Destexhe's synapse model using minimum and maximum values of rise and decay rates of conductance, α and β. Note: $G^*_{Dest}(t)$ is the model using our chosen average rise and decay rates, $\alpha = 1.4492\ mM^{-1}ms^{-1}$ and $\beta = 0.2173\ ms^{-1}$.

Presynaptic Neuron Type	Postsynaptic Neuron Type	α_A $(mM^{-1}ms^{-1})$	β_A (ms^{-1})
Pyramidal	Pyramidal	1.4493	0.2173
	Interneuron	2.8985	0.4346

Table 7.1: Values of rise and decay rates of conductance for different AMPA synapses in our model.

7.2 GABA Synapse

According to Traub's model, the time course for $GABA_A$ conductances took the form of a single exponential decay model as given in Section 3.4 by Equation (3.7). In this case, the maximal synaptic conductance was mediated by GABA binding to $GABA_A$ receptors. Since only $GABA_A$ connections are considered in our model, henceforth $GABA_A$ will be referred to simply as GABA.

By similar reasoning as in the case of the AMPA synapse, Traub's use of the exponential decay model for the GABA synapse, was replaced instead with the nonlinear Destexhe synapse model, $G_{Dest}(t)$. The decay time constant, τ_G was chosen to be 20 ms in Traub's model for synapses on all cortical neurons from the LTS interneuron. This was done under their assumption that the time course of dendritic inhibitory post synaptic conductances (IPSCs) was longer as compared to the soma and regions close to the soma. Since our model does not include a spatial component, the decay time constant was chosen appropriately. According to Destexhe et al. [71], fitting of their model to whole-cell recordings of $GABA_A$ currents in hippocampal neurons gave a decay time constant of about 5.6 ms. Furthermore, decay times of inhibitory synaptic conductances in Purkinje neurons vary from a slow decay time of 12.5 ms to a fast decay time of 8.5 ms [109]. For pyramidal neurons in the somatosensory cortex, the decay time constant is given as approximately 8 ms [110]. For our model, we chose a value of 8 ms, which is appropriate keeping in mind the typical numbers in the literature. Thus, this gives $\beta_G = 0.125\ ms^{-1}$. As for the rise rate of conductance, α_G, we chose a value of 5 $mM^{-1}ms^{-1}$ as given by Destexhe et al. [71].

Presynaptic Neuron Type	Postsynaptic Neuron Type	α_G $(mM^{-1}ms^{-1})$	β_G (ms^{-1})
LTS	all cortical neurons	5	0.125

Table 7.2: Values of rise and decay rates of conductance for GABA synapses in our model.

7.3 Synaptic Dynamics

All synaptic dynamics in our model followed the Destexhe synapse model, given by Equations (3.9)–(3.13). We note that the maximal conductance is the maximum conductance from a single active synapse from neuron of type i to neuron of type j. The synaptic current in this instance is

$$I_{syn\_ij}(t) = \bar{g}_{syn\_ij} \cdot (V_j - V_{rev}) \cdot s_i(t)$$

where the synaptic current, I_{syn_ij} is from neuron i to neuron j, $\bar{g}_{syn\_ij}$ is the maximal conductance, s_i(t) denotes the fraction of open synaptic channels, V_j is the membrane potential of neuron j, and V_{rev} is the reversal potential for the postsynaptic current. Such a connection is illustrated in Figure 7.3.

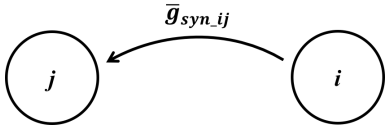

Figure 7.3: Single-synapse model from neuron of type i to neuron of type j.

If neuron j receives input from N neurons of type i, then the total synaptic current is given by the following equation, and such a connection is illustrated in Figure 7.4.

$$I_{syn\_ij}(t) = \bar{g}_{syn\_ij} \cdot (V_j - V_{rev}) \cdot \sum_{k=1}^{N} s_{i,k}(t) \tag{7.3}$$

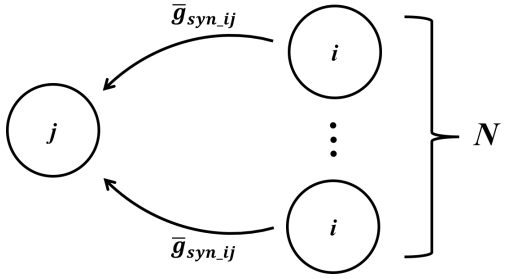

Figure 7.4: Multiple-synapse model from N neurons of type i's to neuron of type j.

If all N neurons of type i are active at the same time, then the maximal conductance received by neuron j is equal to $N \cdot \bar{g}_{syn\_ij}$. In our reduced network model, each neuron type

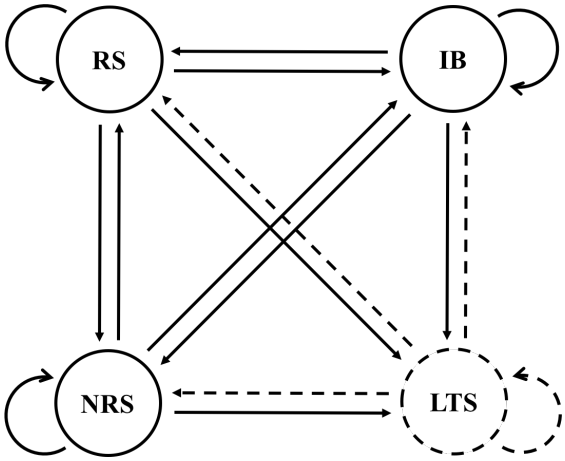

Figure 7.5: Schematic of our reduced network model. Solid lines denote excitatory synapses and dashed lines denote inhibitory synapses. Note: RS: layer 5 tufted regular spiking, IB: layer 5 tufted intrinsically bursting, NRS: layer 6 non-tufted regular spiking (pyramidal neurons), LTS: deep layer low-threshold spiking (interneuron).

(pyramidal and interneuron) receives input from a single neuron of all the other types. So, in order to represent these multiple synapses with a single synapse, we need the synaptic current to have the following form:

$$I_{syn\_ij}(t) = N \cdot \bar{g}_{syn\_ij} \cdot (V_j - V_{rev}) \cdot s_i(t) \tag{7.4}$$

A schematic of the reduced network model is given in Figure 7.5.

First and foremost, for each synapse, we define the baseline maximal conductance as the minimum value that allows spiking in a single presynaptic neuron to evoke some level of spiking in a single postsynaptic neuron. Although neuronal responses are integrative in nature due to input from a relatively large number of nearby neurons, our small network is incapable of taking this feature into account. Hence, our definition of baseline activity consisting of "some level of spiking in a single postsynaptic neuron" refers to our way of compensating for the small size of our network as well as the limited synaptic input to each neuron in our network. Using Traub's maximal synaptic conductances as a starting point, it was noted that for almost all synapses in our reduced model, baseline synaptic activity was not achieved. To rectify this, we used a scaling factor to scale all of Traub's values. Multiple simulations were performed for each synapse, and it should be noted that GABA synaptic conductances were set such that spiking in the interneuron evoked an inhibitory response on the excitatory pyramidals. Some of the simulated results are given in Figure

7.6. The modified maximal synaptic conductances as they compare to those in Traub's model are given in Table 7.3. While the AMPA conductances in Traub's model range from 1.0–2.0 nS, and ours from 12.0–70.0 nS, it should be noted that our values are reflective of the fact that our model consists of single synapses from each neuron type. Similarly, GABA conductances in Traub's model range from 0.01–0.05 nS while ours are in the 100–350 nS range. According to a cortical network model by Lytton and Sejnowski [111], the maximal excitatory conductance for a single neuron was 5000 nS, with 10 nS per synapse. For inhibitory synapses, their model uses a maximal conductance of 100 nS for a single neuron with 1 nS per synapse. In this regard, our range for AMPA and GABA synapses seems reasonable, especially since our model is a reduction of a much larger network.

Presynaptic neuron	Postsynaptic neuron	Traub's baseline (nS)	Our baseline (nS)
IB	IB	2.0	30.0
	RS	2.0	60.0
	NRS	2.0	40.0
	LTS	2.0	12.0
RS	RS	1.0	30.0
	IB	1.0	65.0
	NRS	1.0	40.0
	LTS	2.0	14.0
NRS	NRS	1.0	18.0
	IB	1.0	60.0
	RS	1.0	70.0
	LTS	2.0	16.0
LTS	LTS	0.05	100.0
	RS	0.02	100.0
	IB	0.05	350.0
	NRS	0.01	115.0

Table 7.3: Baseline maximal synaptic conductance values for all synapses in the reduced network model given in Figure 7.5.

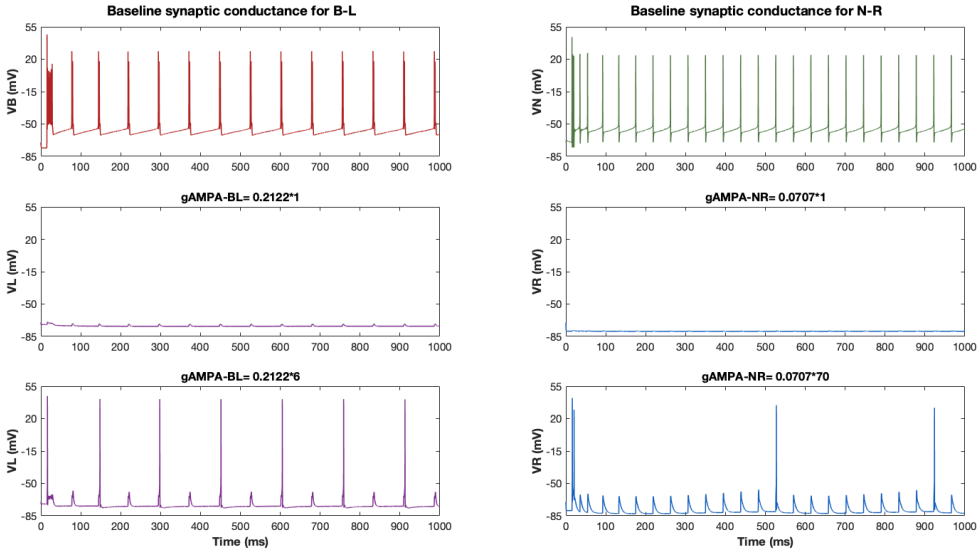

(a)

(b)

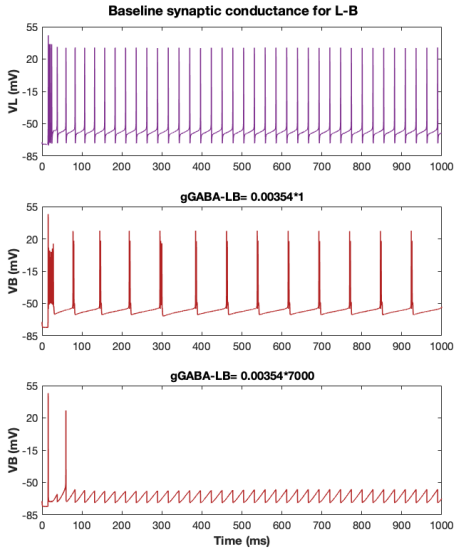

(c)

Figure 7.6: Simulations exhibiting firing activity of neurons for different synapses to set baseline synaptic conductances. (a): synapse from layer 5 intrinsically bursting neuron (IB) to deep low-threshold spiking interneuron (LTS), (b): synapse from layer 6 regular spiking neuron (NRS) to layer 5 regular spiking neuron (RS), (c): synapse from LTS to IB.

Chapter 8

Results

8.1 Numerics

All model simulations were performed on macOS using MATLAB's standard solver for ordinary differential equations (ODEs), ode45. This function is based on an explicit Runge-Kutta formula, the Dormand-Prine method, which combines calculation of fourth- and fifth-order accurate solutions. In general, systems with solutions with slowly changing parts together with rapidly changing components are known as being *stiff*. Since our models consisted of rapid changes characterized by spiking, we could classify them as being relatively stiff. For stiff systems, in general, Runge-Kutta methods either fail or the computation is time intensive with a small step size. Even though our models did not fail with the use of function ode45, we performed the same simulations with MATLAB's ODE solver for stiff systems, ode15s. This function is a multi-step implicit solver with the maximum order of the numerical differential formulas set to a default value of 5. A comparison of solutions using both functions, ode45 and ode15s is shown in Figure 8.1. It is seen that the difference between both solutions is relatively small. Since both solutions are qualitatively alike and the computation time is nearly the same (elapsed computation time using ode45 was on average 0.5% less than using ode15s for producing Figure 8.1), we chose to use ode45 for all our simulations.

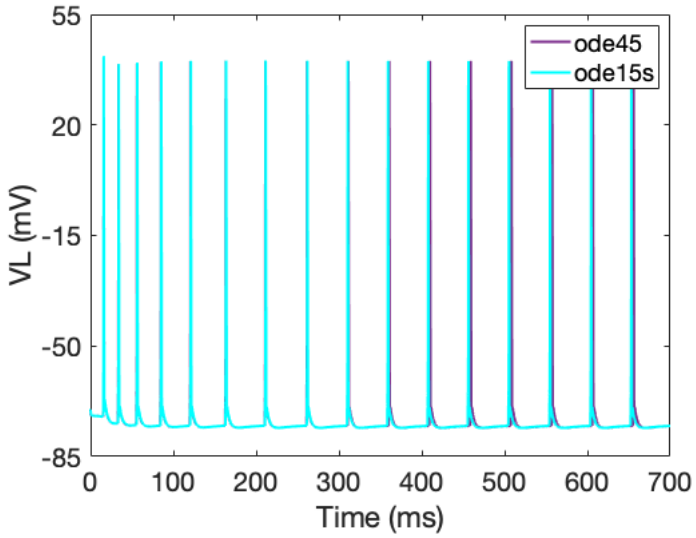

Figure 8.1: Comparison of solution using MATLAB's ODE solvers ode45 (for non-stiff systems) and ode15s (for stiff systems).

8.2 Isolated single neurons

To begin our investigation of our network's behaviour, we first consider the behaviour of the individual neurons. In this regard, first and foremost, the firing rate versus input current (f-I curves) for all four neuron types were generated. The firing rate for layer 5 and 6 RS neurons, and the interneuron was defined as the number of spikes per second, while for the layer 5 IB neuron, it was defined as the number of bursts per second. The input current to all neurons was varied over the range of 0 and 130 $\mu A/cm^2$ (corresponding to 1.2 to 1.8 nA depending on the neuron type), in increments of 0.25 $\mu A/cm^2$. We chose this range based on two observations: first, beyond this range the layer 5 IB neuron only exhibited an initial burst followed by spikes with a large after-depolarization, and second, this range provided sufficient excitation to all our other cortical neurons whereas values beyond this range only increased the firing frequency even further. For a better comparison of firing/bursting rate of all neuron types, the f-I curves are plotted together for a defined frequency range of 0 to 60 Hz, as shown in Figure 8.2.

As can be noted, the firing curves for layer 5 RS and layer 6 RS neurons are similar in the sense that both neurons require similar amounts of stimulating current to initiate firing. While the layer 5 IB neuron requires the largest current input to initiate firing, the interneuron requires the smallest current and also produces more action potentials for most

inputs. This reflects the intrinsic nature of the interneuron well since it is a low-threshold spiking neuron, thus, requiring a relatively smaller stimulus to initiate firing. Qualitatively speaking, the firing behaviour of all neurons was comparable to firing patterns reported in experimental works [104][37]. To illustrate their firing behaviours, as isolated single neurons, each neuron is given a fixed, constant input of current for the duration of the simulation. The size of input currents was chosen based on the range of 0 and 130 $\mu A/cm^2$ used for computing the f-I curves, such that the values were towards the relatively high end of this range. With no synaptic connectivity between each other, each neuron has its own firing frequency as seen in Figure 8.3. As was observed earlier in Chapter 6, the layer 6 RS and the interneuron both exhibit fast spiking when the depolarizing current is turned on (in this case, fast spiking is observed in the first 30 ms), followed by regular spiking.

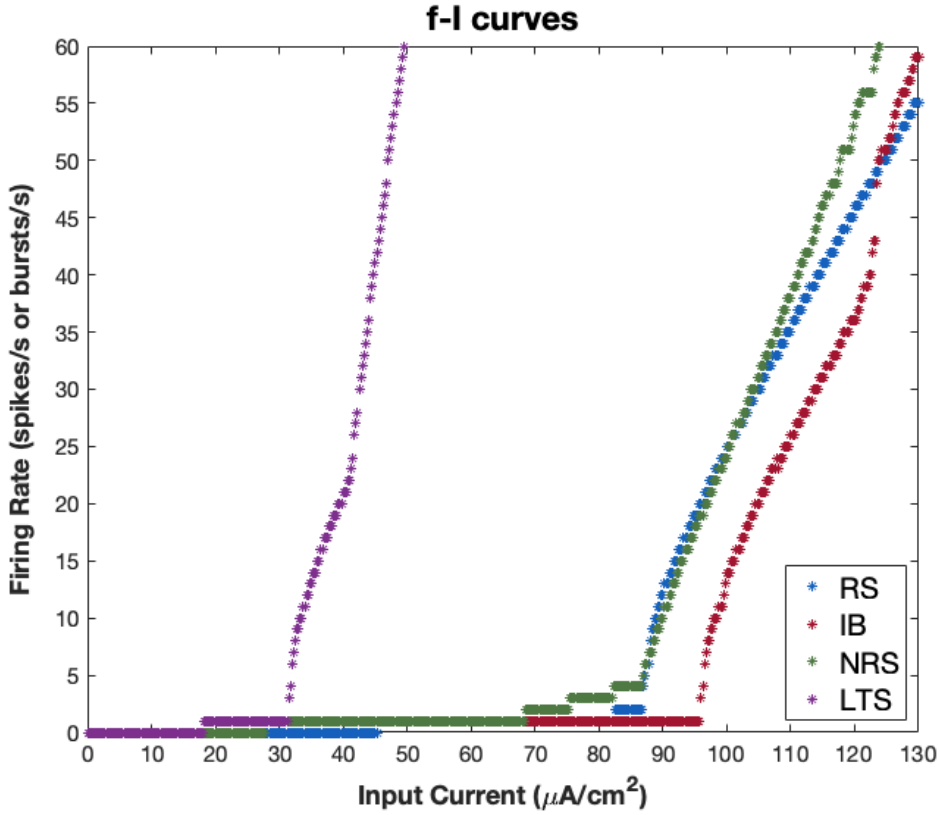

Figure 8.2: Firing rate vs input current (fI-curves) for all neuron types. Note: RS: layer 5 tufted regular spiking, IB: layer 5 tufted intrinsically bursting, NRS: layer 6 non-tufted regular spiking (pyramidal neurons), LTS: deep low-threshold spiking (interneuron)

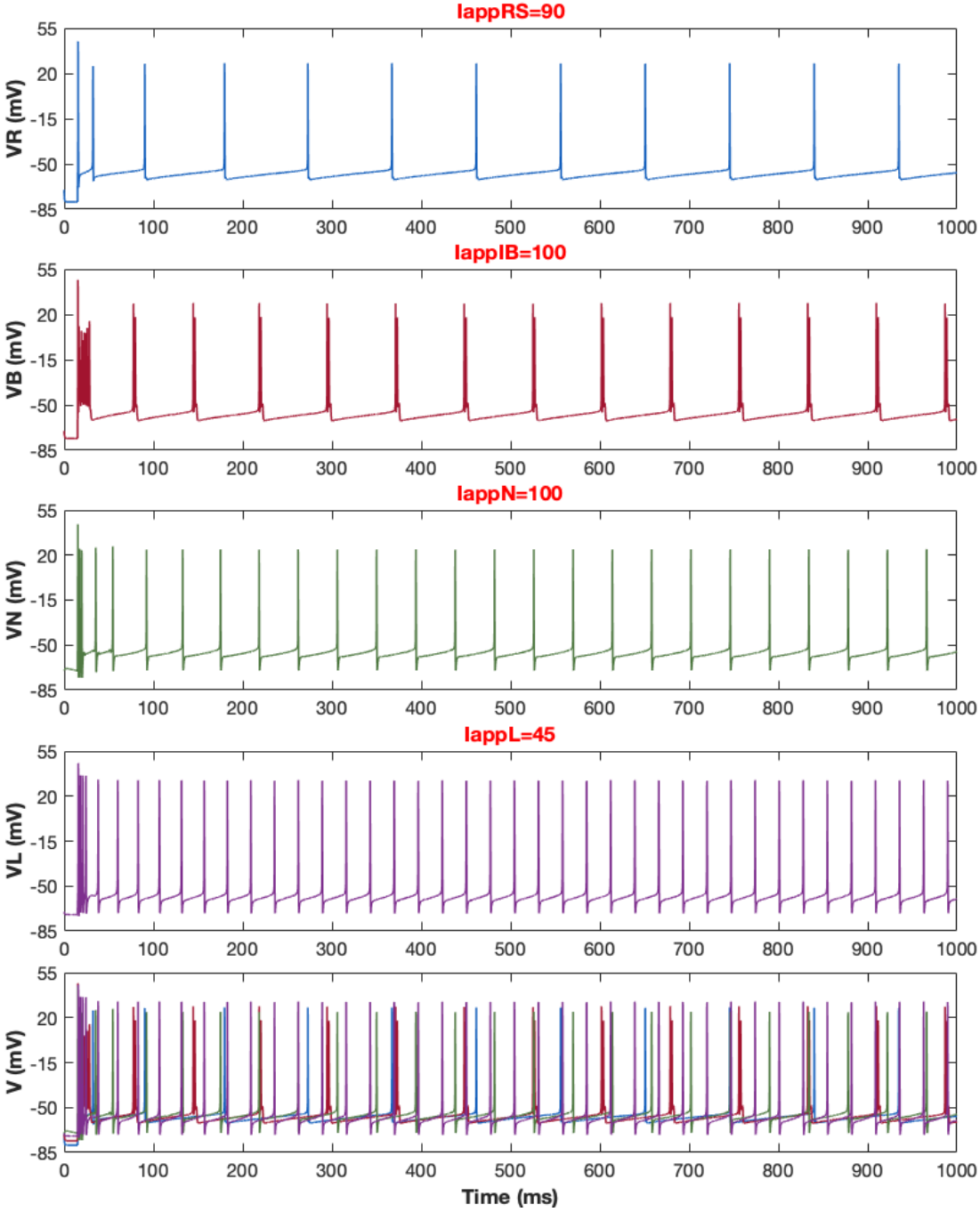

Figure 8.3: Input to all pyramidal neurons and interneuron, with no connectivity between neurons. The colours indicate neuron type as given in Figure 8.2. Units of applied current are $\mu A/cm^2$.

8.3 Default state: inhibited network

With all synapses active, including those from the interneuron to all pyramidal neurons, this is the default state and we label it as the "inhibited network". We test its behaviour for cases of applied current to different neurons. Figure 8.4(a)–(b) illustrates network behaviour for input to layer 5 pyramidal neurons only and input to layers 5 and 6 pyramidal neurons, respectively. In both cases, network activity is synchronized and without any applied current to the interneuron, all neurons exhibit regular firing. While application of current to the layer 6 pyramidal neuron reduces its membrane potential maximum significantly, the neuron exhibits a strong after-depolarization as well as an increased after-hyperpolarization. Subsequently, in the layer 5 IB neuron, after-depolarization is removed, while appearing in the layer 5 RS neuron. The action potentials of the interneuron are qualitatively the same in both the cases. A closer look at the action potentials comparing cases (a) and (b) is given in Figure 8.4(c).

The synchronized nature of firing of all neurons is a result of the synaptic connectivity between all of them since the baseline connectivity was set such that spiking in one neuron results in a response in the other, with some periodicity. The type of firing (regular spiking) of all neurons is interesting to note given that one of the neurons has bursting properties by default. However, its bursting behaviour being transformed into regular spiking does not come as a surprise since a network consisting of only the layer 5 IB neuron and the interneuron reveals activity consisting of alternating bursts consisting of 5 spikes and 2-spike bursts (see Figure 8.6(a)). This behaviour is a result of a negative feedback loop from the inhibitory neuron's ability to suppress bursts into single spikes. Interestingly, input to the interneuron removes the 5-spike bursts in (a) to 2-spike bursts. Since our full network includes synapses from all pyramidal neurons to the interneuron, the otherwise alternating activity of the IB neuron as seen in Figure 8.6 is lost due to the recurrent excitatory feedback from other pyramidal neurons resulting in the interneuron's repetitive spiking.

Figure 8.5(a)–(c) shows the network behaviour when the interneuron has a nonzero applied current. As the input is increased from 43 to 50 $\mu A/cm^2$, oscillations in activity of all pyramidal neurons arise, and eventually are fully suppressed as the interneuron spikes repetitively. Since increasing the input to the interneuron increases its firing frequency, consequently, the pyramidals are unable to recover from the hyperpolarizing response before the interneuron fires again, as a result inhibiting the firing of all excitatory pyramidals.

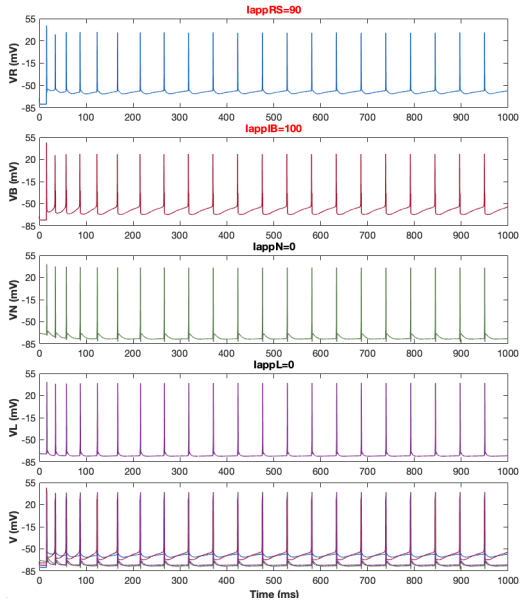

(a) Input to layer 5 (RS and IB) pyramidal neurons only

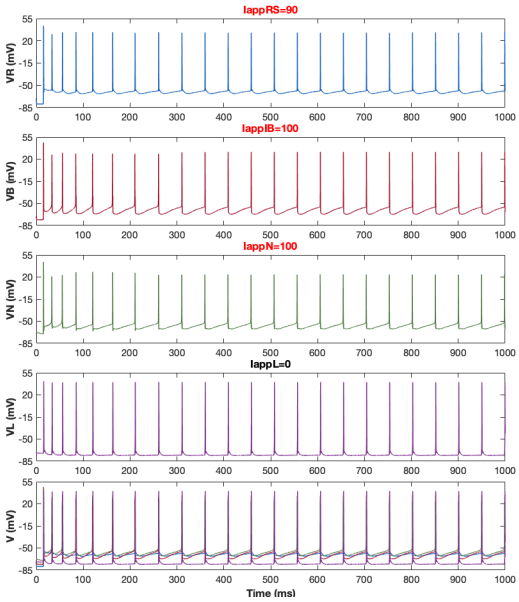

(b) Input to pyramidal neurons only

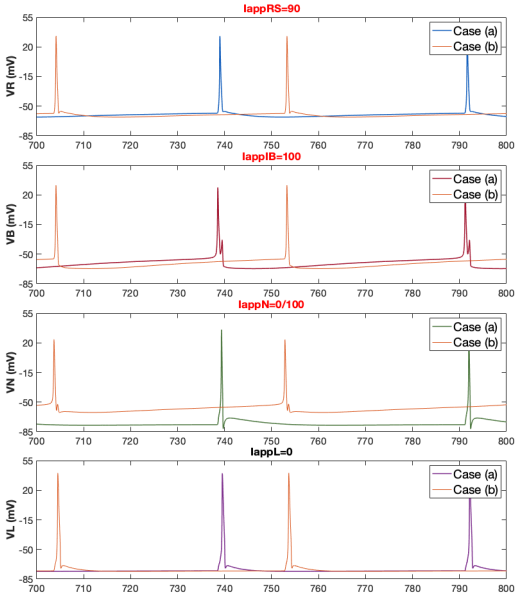

(c) Comparison of cases (a) and (b)

Figure 8.4: Default state of network with full connectivity between all neurons. (a)–(c): variation of input to pyramidal neurons with no input to interneuron. Units of applied current are $\mu A/cm^2$.

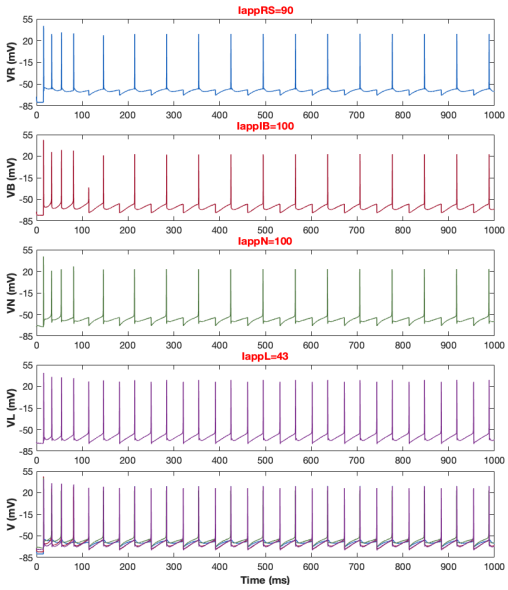

(a) Input to all neurons with I_{appL}= 43 $\mu A/cm^2$

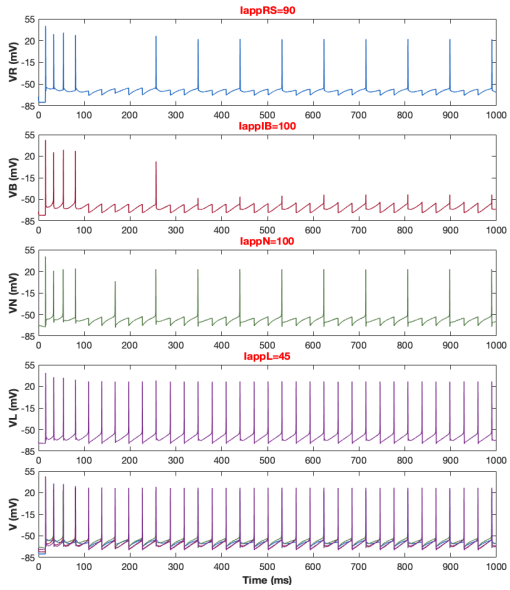

(b) Input to all neurons with I_{appL}= 45 $\mu A/cm^2$

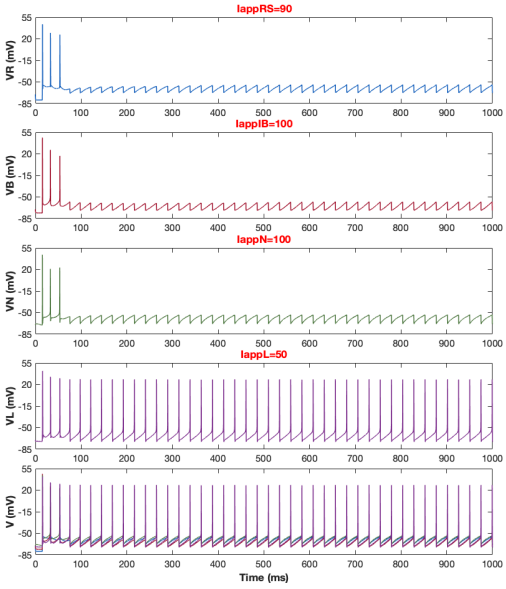

(c) Input to all neurons with I_{appL}= 50 $\mu A/cm^2$

Figure 8.5: Default state of network with full connectivity between all neurons. (a)–(c): variation of input to interneuron with input to all pyramidal neurons as in Figure 8.4(b). Units of applied current are $\mu A/cm^2$.

8.4 Modelling impaired GABA synapses

Investigating network behaviour in the case of complete disinhibition is very reasonable as there is evidence of impaired GABA inhibition in the case of absence epilepsy. In particular, efficacy of intracortical GABAergic mechanisms has been shown to be reduced significantly in cortical slices of rodent models of absence epilepsy compared to non-epileptic controls [112]. In addition, sudden generalized bilaterally synchronous spike-and-wave discharges have been reported in EEG recordings from the cortex following blockade of $GABA_A$ receptors with penicillin, indicating the vital role of disinhibition in generating SWDs. In Figure 8.7, inhibition is progressively reduced by 50, 75, 90 and 100 percent. By this we mean reducing the GABA conductance strength for synapses from the interneuron to pyramidal neurons. In all these simulations, there was no applied current to the interneuron. Interestingly, as inhibition is reduced, the nature of firing of all neurons changes from regular spiking to bursting. The firing frequency of the network also reduces significantly by 61% from 23 Hz to 9 Hz. As a disinhibited network, the expected behaviour of all neurons was an increase in firing frequency. However, given the result of bursts, we hypothesized that perhaps the bursting was a consequence of the existence of an intrinsically bursting neuron in our population. Thus, we considered its removal such that we had a R-N (layer 5 RS and layer 6 RS pyramidal neurons) network only.

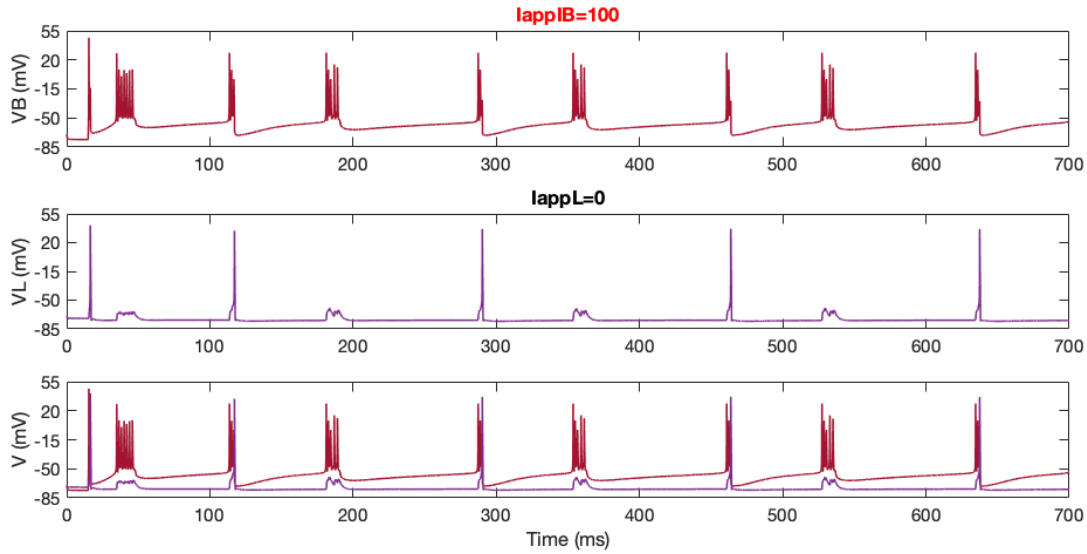

(a) Input to IB pyramidal neuron only

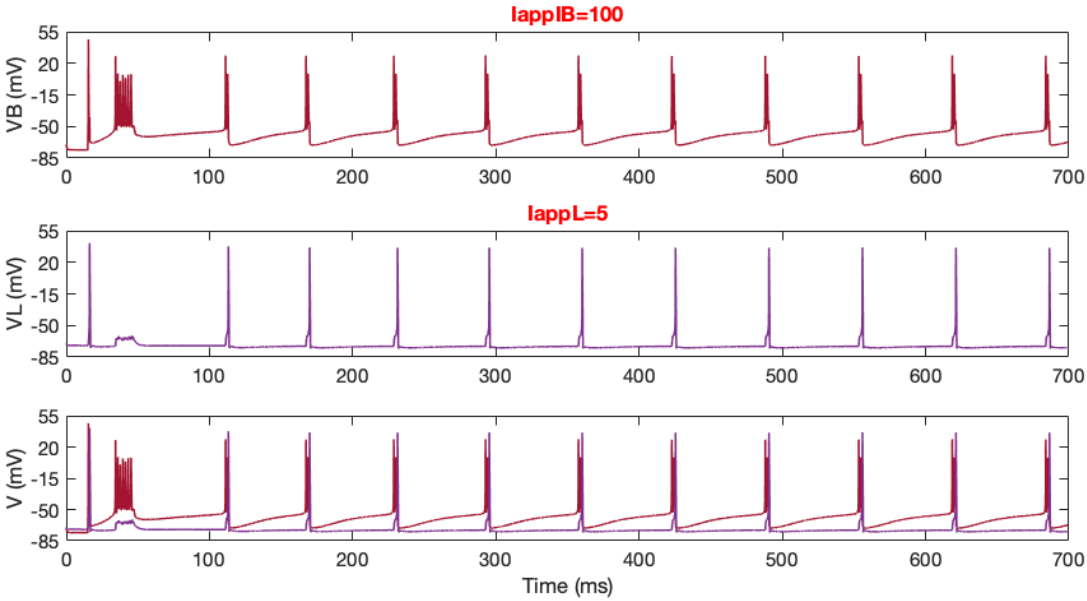

(b) Input to both IB pyramidal neuron and interneuron

Figure 8.6: Network consisting of layer 5 IB neuron and LTS interneuron only. Units of applied current are $\mu A/cm^2$.

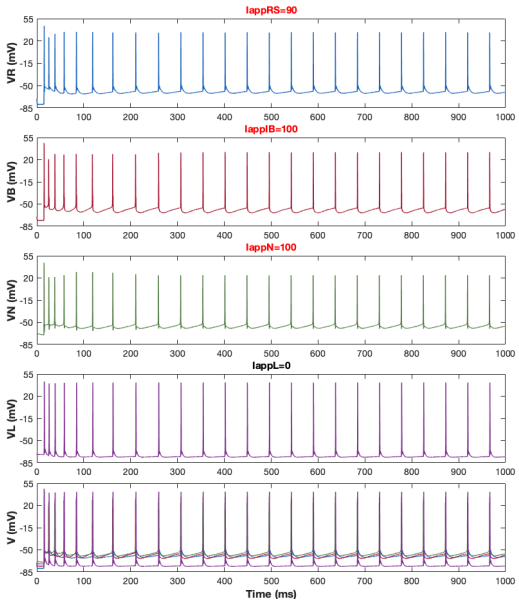

(a) Inhibition strength reduced by 50%

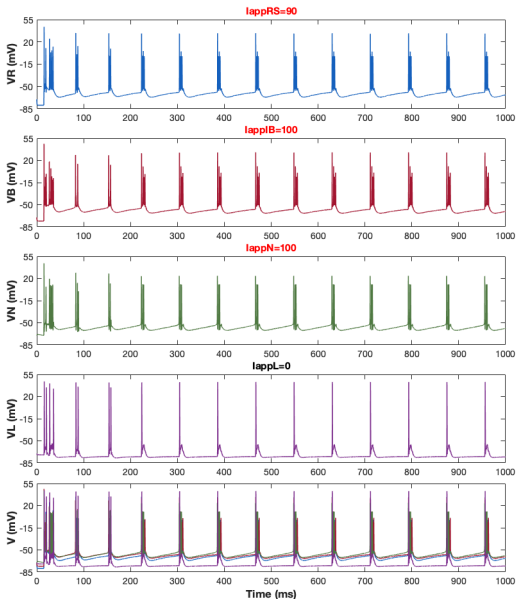

(b) Inhibition strength reduced by 75%

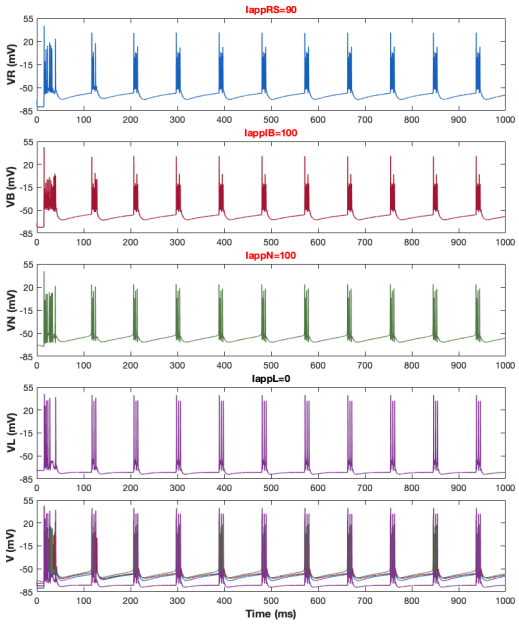

(c) Inhibition strength reduced by 90%

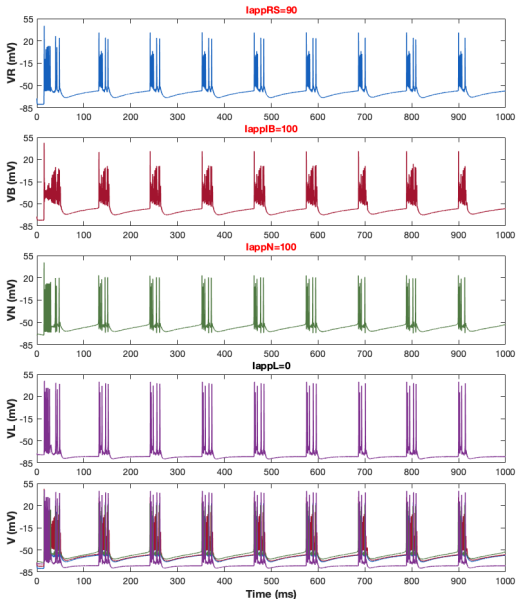

(d) Complete disinhibition

Figure 8.7: Network with full connectivity between all neurons, with varying strengths of inhibition. Strength of inhibition refers to magnitude of synaptic conductance from LTS interneuron to all pyramidal neurons. Units of applied current $\mu A/cm^2$.

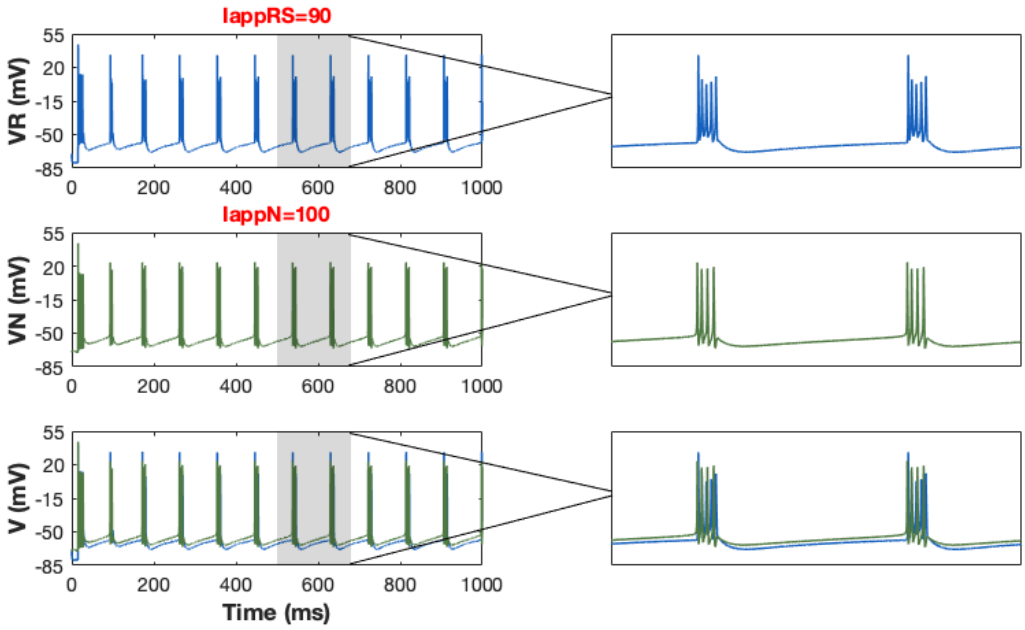

Figure 8.8: Network consisting of layer 5 RS pyramidal neuron and LTS interneuron only with input to both neurons. Units of applied current are $\mu A/cm^2$.

With input to both neurons in the R-N network, both neurons exhibit synchronized bursts (see Figure 8.8). This indicates that for our neural population, burst discharges are network-induced responses in neurons that would otherwise in isolation exhibit regular spiking firing properties. This result is in agreement with some bursting behaviours found in the literature. In general, bursting may be an intrinsic property resulting from interactions among ionic currents governing the dynamics of a neuron, or it may be a network phenomenon governed by synaptic interactions of individual neurons.

In addition, there exist bursting patterns that are of qualitatively different types when generated by different mechanisms. For our neural population, two bursting types were observed, namely, square-wave bursting (for the RS, IB, and LTS neurons) and parabolic bursting (for the NRS neuron). Square-wave bursting is characterized by states of depolarized repetitive firing during which action potentials ride on a depolarized plateau, and a silent phase during which there is no firing. Parabolic bursting refers to bursting during which the firing frequency increases and decreases through the course of the burst. While the bursting frequency was the same for all neurons as they exhibited synchronized activity, the number of action potentials in the "active" (spiking) phase of the burst differed

between neurons. For the RS and IB neuron, in addition to action potentials, bursts also consisted of subthreshold membrane potential oscillations. This type of activity refers to when the membrane potential is below action potential threshold, however, voltage fluctuations occur, which may be due to intrinsic properties of the neuron or due to postsynaptic potentials [113]. Given that none of the neurons in our population exhibit such behaviour in isolation, we can attribute these subthreshold oscillations as behaviour induced by synaptic connectivity between the neurons. On the other hand, for the NRS and LTS neuron, bursts consisted only of action potentials with an average of 7 and 5 action potentials per burst, respectively. Given in Table 8.1 are the average lengths of inter-burst interval (IBI) and burst interval, for all neurons in a network with complete disinhibition.

Neuron Type	Inter-burst Interval (ms)	Burst Interval (ms)
RS	85.841	29.839
IB	85.197	29.298
NRS	85.759	26.077
LTS	85.534	28.724

Table 8.1: Average inter-burst interval (IBI) and burst interval lengths for all neurons in a network with complete disinhibition.

Without any GABAergic inhibition, as individual neurons receive feedback from all other neurons in the network, the depolarization from this feedback is over their threshold potentials for a period of time that is sufficiently long to generate bursts. On the contrary, in the presence of inhibition, the network consists of strong inhibitory feedback loops from the interneuron to all pyramidal neurons. As a result, as pyramidal neurons receive external stimuli, the excitatory synapses formed with other pyramidal ensure strong excitation to each other, and to the interneuron as well. Consequently, firing of pyramidal neurons is rapidly damped by strong inhibition by the interneuron, making it difficult for the pyramidal neurons to produce bursts of action potentials. Bursting activity of the network also drives the activation of certain ion channels, which play a role in the mechanism producing these bursts. For instance, to compare the inhibited and disinhibited network, the concentration of calcium is plotted against time in Figure 8.9. As expected, there is a significant increase (about 3–5 times) in $[Ca^{2+}]$ in the disinhibited case. This is expected because of the typical role of calcium in producing bursts. In some cases, the mechanism underlying bursts involves a slow inward current, such as I_{Nap} or I_{Cat} which works towards depolarizing the membrane potential, producing a burst. In particular, the depolarized plateau that action potentials ride on are attributed to the influx of Ca^{2+} which depolarizes the membrane and facilitates repetitive firing. The activation of these currents is followed by the slow activation of voltage or calcium-dependent outward currents such as I_{Km} or

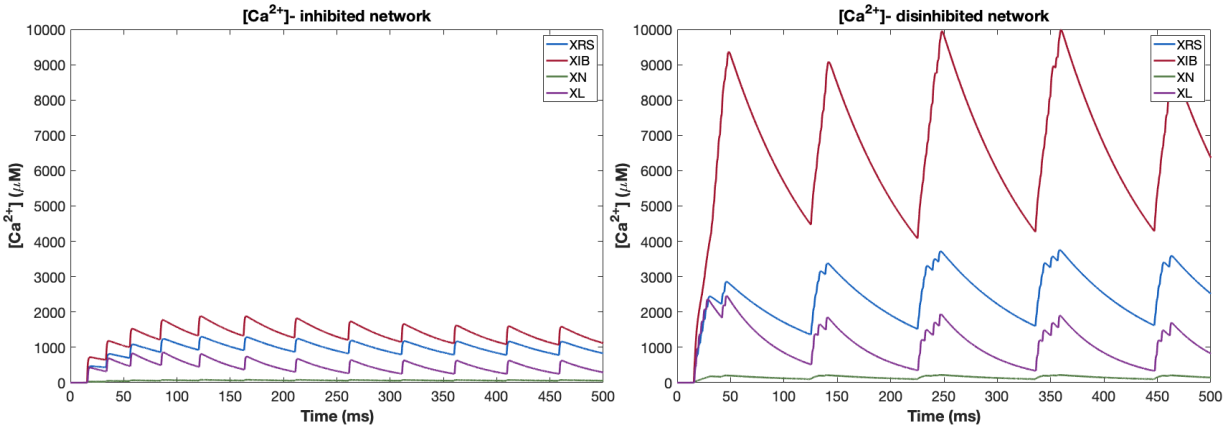

Figure 8.9: Time course of $[Ca^{2+}]$ concentration for each neuron in the inhibited network $(Left)$ and disinhibited network $(Right)$. Note: RS: layer 5 regular spiking, IB: layer 5 intrinsically bursting, N: layer 6 regular spiking (pyramidal neurons), L: deep layer low-threshold spiking (interneuron).

I_{Kc}, therefore repolarizing the neuron back towards resting potential.

An analysis of all gating variables for individual neurons was performed for both the inhibited and disinhibited network, to try and understand the role of the various ionic currents. Interestingly, while qualitatively the time course for all gating variables was different between both cases, the magnitudes were similar for all activation variables except for m_{Km}, m_{K2} and m_h. Figure 8.10(b) shows the time course of m_{Naf} and m_{Cat}. As shown in Figure 8.10(a), throughout the duration of the burst, the activation variables m_{Km} and m_{K2} increase in magnitude, and at the end of the burst, begin to slowly decay. The significant aspect of these gating variables is the change in their magnitude at the start and end of the burst, which is greater between the inhibited and disinhibited case. This result seems to indicate that the slow activation of I_{Km} and I_{K2}, upon sufficient activation, is able to terminate bursts, as these are outward currents.

As is the case in absence epilepsy, with a disinhibited cortical network, synchronized discharge of all neurons is very evident in our network as well. In fact, our network is able to generate its own form of spike-and-wave oscillations within the disinhibited regime, where the spikes are interpreted as synchronized burst discharges of all neurons and the waves as periods of quiescence.

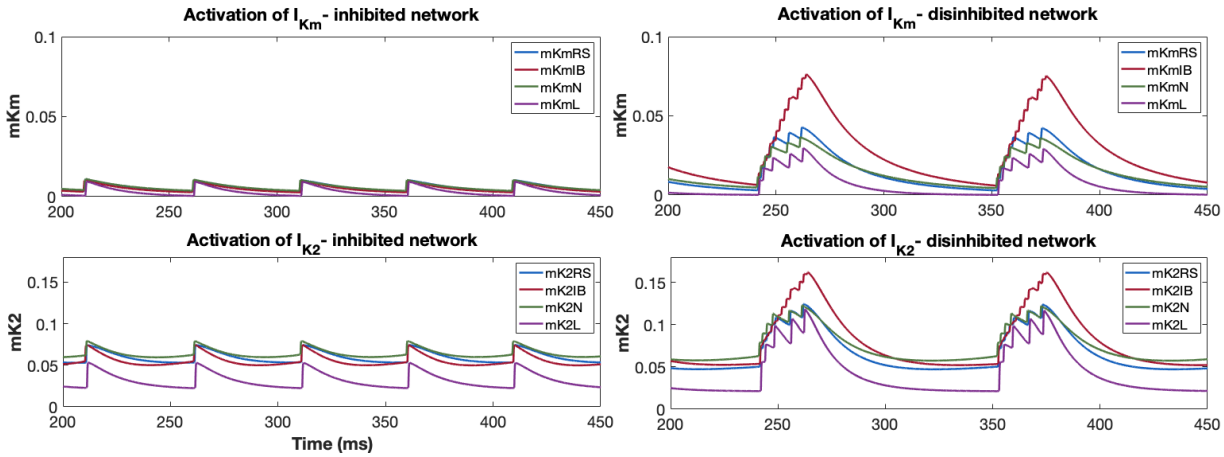

(a) Time course of activation variables for the muscarinic receptor-suppressed K^+ current (m_{Km}) and slowly activating and inactivating K^+ current (m_{K2}) for each neuron from 200 to 450 ms.

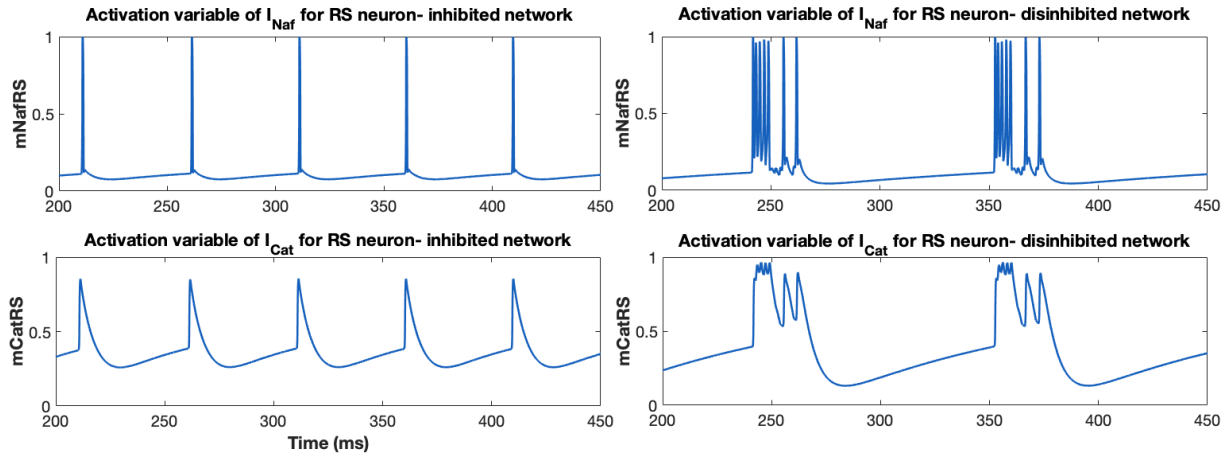

(b) Time course of activation variables for the fast and transient inactivating Na^+ current (m_{Naf}) and low-threshold inactivating Ca^{2+} current (m_{Cat}) for RS neuron from 200 to 450 ms.

Figure 8.10: Time course of activation variables for each neuron in the inhibited network (*Left*) and disinhibited network (*Right*). Note: *RS*: layer 5 regular spiking, *IB*: layer 5 intrinsically bursting, *N*: layer 6 regular spiking (pyramidal neurons), *L*: deep layer low-threshold spiking (interneuron)

8.5 Modelling sodium channel defects

Variant forms of a gene are called alleles. Some of these variants can be spontaneous where alterations of a gene found at the same place on a chromosome arise from mutations, while some alleles can be chemically induced. A species possessing two different alleles of a particular gene is known as a heterozygote. We know from experimental data that mutations in *Scn2a* and *Scn8a* genes lead to functional changes in subtypes of the sodium channels, Nav1.2 and Nav1.6 respectively, resulting in a channelopathy such as absence epilepsy.

In the 2009 study by Papale et al., EEG recordings from mice carrying *Scn8a* mutations revealed appearance of spike-wave discharges in heterozygotes with the $Scn8a^{V929F}$[1] allele, as well as heterozygotes with $Scn8a^{med}$[2] and $Scn8a^{med-jo}$[3] alleles [76]. Since $Scn8a^{med}$ is a loss-of-function null allele, we interpret this as the shutoff of the sodium channel it encodes [114].

$Scn8a^{med-jo}$ is a missense mutation, which refers to a point mutation resulting in an amino acid substitution, and it has been implicated in alterations in voltage dependence of activation and inactivation [115]. In particular, voltage clamp procedures performed on Xenopus oocytes to study the electrophysiological effects of $Scn8a^{med-jo}$ revealed the effect on the voltage dependence of channel gating [115]. Accordingly, the $Nav1.6^{med-jo}$ channel demonstrated an approximately 14 mV depolarizing shift in activation. For the sodium channel activation, while the half-activation ($V_{1/2}$) for the wild-type channel was -23.9 $\pm$ 1.9 mV, for the mutant channel it was -9.8 $\pm$ 1.5 mV. The slopes of the curves were $k = 4.4 \pm 0.8$ and 4.1 ± 0.6 for the wild-type and mutant channels respectively. The voltage dependence of inactivation exhibited a shift that was similar in nature to the shift in activation since in voltage-gated sodium channels, activation and inactivation are coupled. The $V_{1/2}$ for the wild-type channel was -51.1 $\pm$ 0.6 mV with $k = 5.7 \pm 0.3$ and for the mutant channel, it was -44.3 $\pm$ 0.9 mV with $k = 5.0 \pm 0.3$.

At the time of the study by Papale et al., while $Scn8a^{V929F}$ was known to be implicated in absence epilepsy, its functional impact on sodium channel activity was not known [76]. However, in 2014, examination of $Nav1.6^{V929F}$ by Oliva et al. suggested alterations in voltage dependence of activation and inactivation of the channel, similar in nature to $Nav1.6^{med-jo}$, with depolarizing shifts in activation of approximately 6 mV and a hyperpolarizing shift in inactivation of approximately 12 mV. Accordingly, their results

[1] A chemically induced allele; synonym for $Scn8a^{8J}$ allele
[2] A spontaneous allele; *med* stands for motor end plate disease
[3] A spontaneous allele; symbol *jo* stands for jolting

suggested $V_{1/2}$ of activation for the wild-type channel, for dorsal root ganglion neurons used in their study, was -15.2 ± 1.7 mV with $k = 9.37 \pm 1.4$, and for the mutant channel it was -9.33 ± 1.6 mV with $k = 7.53 \pm 0.6$. Whereas, $V_{1/2}$ for inactivation for the wild-type channel was -36.58 ± 2.2 mV with $k = -7.32 \pm 0.2$ and for the mutant channel it was -48.37 ± 1.9 mV with $k = -6.11 \pm 0.2$.

Nav1.2 and Nav1.6 channels, encoded by *Scn2a* and *Scn8a* respectively, are found abundantly in hippocampal and cortical neurons, including layer 5 pyramidal neurons. In fact, Nav1.6 channels are also expressed in inhibitory interneurons in the cortex. However, many of the existing computational models for *Scn8a* mutations exclusively model the effect on electrophysiological properties of these channels in excitatory hippocampal and cortical neurons. Given that the effect of *Scn8a* mutations is overall an adverse one, many of the existing conclusions point towards investigating these mutations in the inhibitory neurons in the cortex as well, as even intuitively, debilitated activity of excitatory neurons is less likely to give rise to burst discharges as compared to inhibitory neurons. Keeping this in mind, we considered *Scn2a* variants only for our set of excitatory pyramidal neurons, while *Scn8a* variants were introduced only for the inhibitory interneuron.

Our investigation was directed at examining the functional consequences of variant Nav1.2 and Nav1.6 channels in our pyramidal neurons and interneuron, respectively, and especially the consequences of changes at the single-neuron level on network behaviour. Firstly, since $Scn8a^{med}$ is a null allele, we modelled its effect on the interneuron by setting the maximal sodium conductance density for the transient Na^+ current, g_{Naf} to 0. To model the effects of $Scn8a^{med-jo}$ and $Scn8a^{V929F}$, since the voltage-dependence on activation and inactivation is altered, we introduced absolute shifts in half-activation voltages for the transient Na^+ current, as given in Equation (8.1). In this regard, the shifts were the same amount as those observed in the literature for both mutations. Table 8.2 summarizes the changes in half-activation voltages for the variant channels the way they appear in our model.

$$m_{Naf\infty L} = \frac{1}{1 + \exp\left(\frac{-V-38+V_{shift-m}}{10+k_{shift-m}}\right)} \qquad h_{Naf\infty L} = \frac{1}{1 + \exp\left(\frac{V+58.3+V_{shift-h}}{6.7+k_{shift-h}}\right)} \tag{8.1}$$

Following the results from Ogiwara et al. for hippocampal pyramidal neurons, we modelled the effects of $Scn2a^{KO/+}$[4] in all pyramidal neurons in our model by reducing the maximal conductance density for the persistent Na^+ current, g_{Nap} by 40% [84].

[4] $KO/+$ stands for a knockout mutation where the wild-type gene is made inoperative

Channel Type	Voltage-dependence of activation		Voltage-dependence of inactivation	
	$\Delta V_{1/2}$	Δslope	$\Delta V_{1/2}$	Δslope
$Nav1.6^{med-jo}$	14.1	0.3	6.8	-0.7
$Nav1.6^{V929F}$	5.87	1.84	-11.79	-1.21

Table 8.2: Absolute shifts in half-activation voltages for variant Nav1.6 channels.

Since the literature on genetic mutations giving rise to epileptogenic effects is not clear about whether these mutations co-exist or are isolated incidents, our approach was to investigate different combinations of variants inserted into our model. We tested for the effects of *Scn8a* mutant alleles individually, on our inhibited network, as well as the effects of $Scn2a^{KO/+}$ in combination with each of the three *Scn8a* variants. Thus, in total giving six unique cases to consider.

Firstly, the effect on individual neurons was determined, as given in Figures 8.11–8.12. For all pyramidal neurons, while the initial spike or burst occurs approximately at the same time and for the same duration as the wild-types, subsequent firing occurs with a delay. The average interspike interval (ISI) for the layer 5 RS increased by 75.31%, and the inter-burst interval (IBI) length for the layer 5 IB neuron increased by 40.37%. There is a slight increase in average ISI length for the layer 6 RS neuron as well by 7.18%. In fact, the change in their response is such that with a greater stimulation (applied current), their behaviour resembles the wild-type case even more, which indicates a positive shift in their f-I curves. There is almost no change in the peak amplitude of all pyramidal neurons. Interestingly, the effect of *Scn8a* variants on the interneuron result in diminishing firing altogether. Even with an increased input current, at most the interneuron fires a single action potential (not shown here).

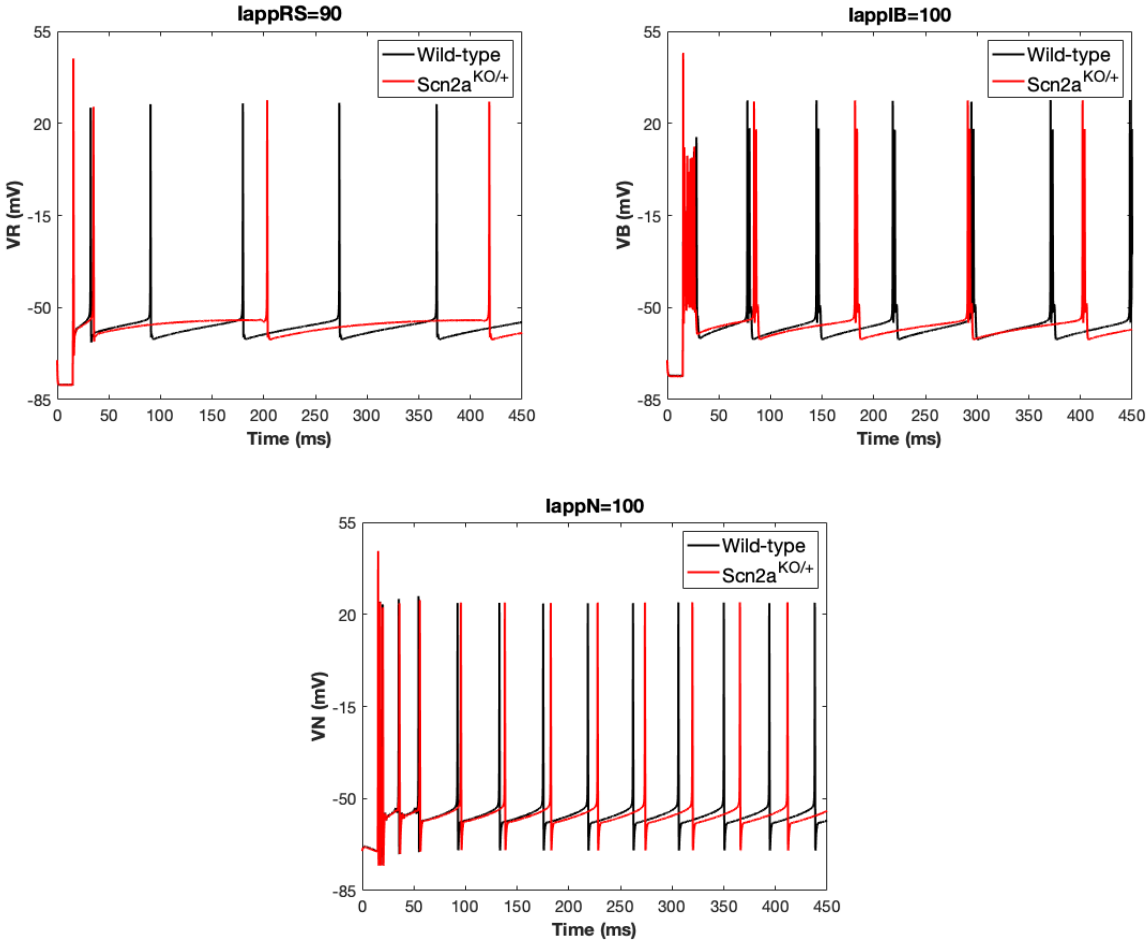

Figure 8.11: Effect on the three pyramidal neuron types by modifying the persistent sodium current, representing $Scn2a$ mutation.

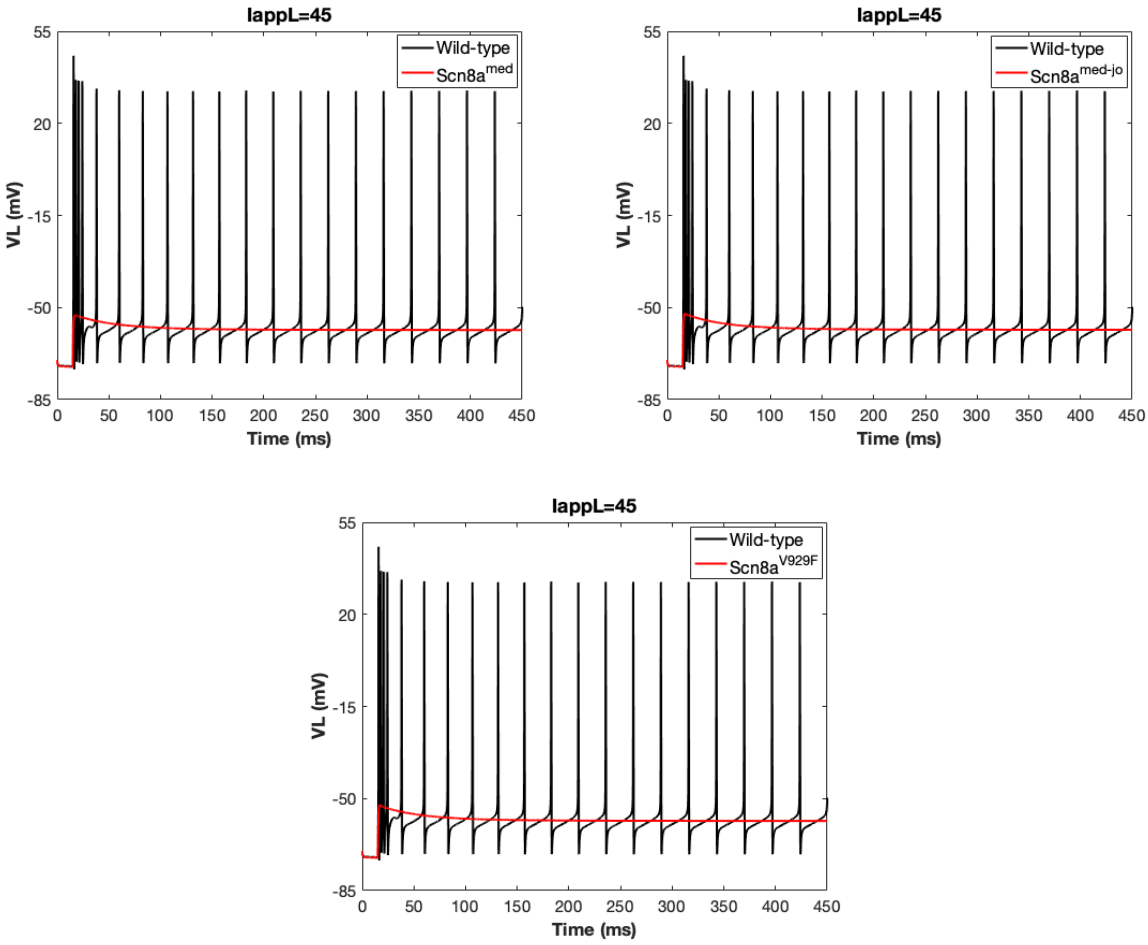

Figure 8.12: Effect on the interneuron by three different modifications of the fast sodium channel, representing three *Scn8a* mutation types.

Next, we investigated the effect on network behaviour following the alterations on the single-neurons as described previously. The idea was to examine under which circumstances, namely due to which mutant variants, our inhibited network from Section 8.3 behaves like the disinhibited one from Section 8.4. Figure 8.13(a)–(c) gives the simulated results with only *Scn8a* variants introduced in the inhibitory interneuron. Figure 8.13(a)–(b) are effectively similar to response of a network without inhibition (with some subtleties) since the firing of the interneuron is diminished with the inclusion of $Scn8a^{med}$ and $Scn8a^{med-jo}$ into the model. In our "disinhibited network", inhibition was eliminated by the removal of synapses from the interneuron to pyramidal neurons. However, feedback to the interneuron ensured that the interneuron was responsive with burst discharges. On the contrary, in these two variant cases, even with normalcy in the kinetics of feedback to the interneuron, it is unresponsive, and in particular, feedback to the interneuron is reduced by approximately 75% as compared to the normal case. The most interesting result however is the one shown in Figure 8.13(c). There are multiple frequencies appearing here, with burst discharges and single spikes existing periodically. This behaviour is surprising because the interneuron as an isolated neuron at most responded with a single action potential. Therefore, it was unexpected that the interneuron would fire any action potentials at all. It seems to be the case that the lack of inhibition to the pyramidal neurons results in a burst discharge which is able to provide sufficient feedback to the interneuron to evoke an action potential. In turn, the interneuron inhibits the bursting response of the pyramidals, and with a delay which is unsurprising in oscillatory responses, the cycle of bursts and single spikes starts over.

Although not shown here, introduction of only *Scn2a* into the model shows minimal changes to the overall network behaviour. The network exhibits synchronized regular spiking with the first couple of spikes occurring at approximately the same time as in the normal network case (one without any mutations). The spikes that follow are delayed in comparison to the normal network. This is not surprising, given the effects of the *Scn2a* mutation on individual pyramidal neurons, where firing following an initial couple of spikes, occurs with a delay in all neurons, as shown in Figure 8.11.

Given in Figure 8.14(a)–(c) are results of both *Scn2a* and *Scn8a* variants introduced into the model. As labelled on each simulation, $Scn2a^{KO/+}$ is in combination with each of the three *Scn8a* mutant alleles. Qualitatively, Figure 8.14(a)–(b) is very similar to Figure 8.13(a)–(b) with some minor differences. Once again, the effect of $Scn8a^{V929F}$ allele on the network is surprising (see Figure 8.14(c)). Here we observe an initial spike, followed by a pronounced burst discharge of all pyramidal neurons, with subsequent firing consisting of a single action potential by all expect for the layer 6 neuron, which exhibits two-spike bursting. The inclusion of $Scn2a^{KO/+}$ into the model seems to have transformed

the network into a state in which there is sufficient feedback to the interneuron constantly which in turn inhibits the response of the previously existing burst discharges to single or double spikes.

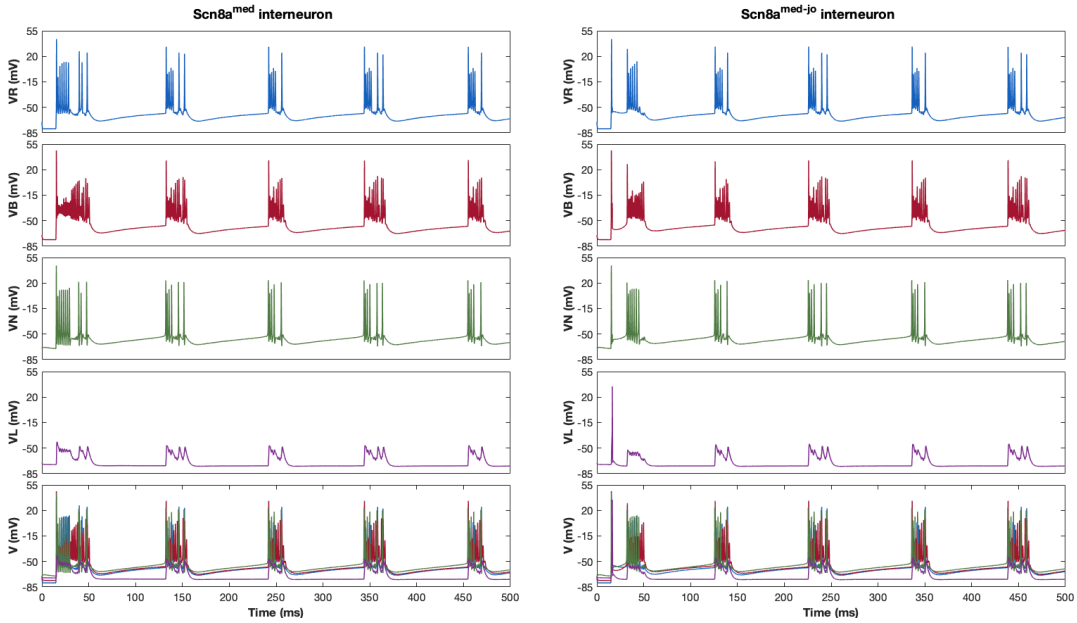

(a) (b)

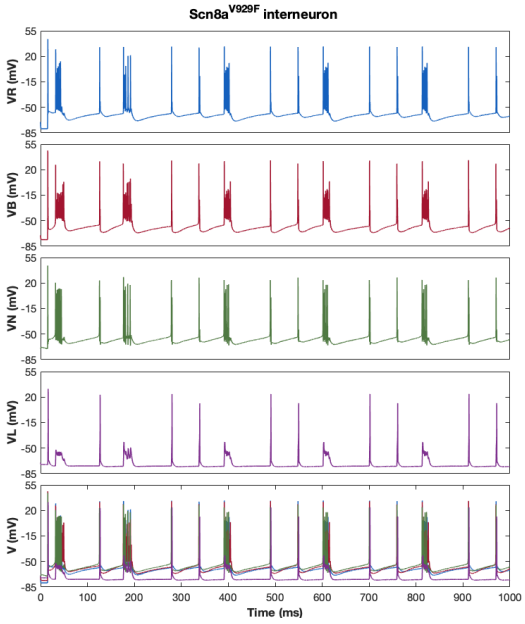

(c)

Figure 8.13: Network behaviour following the introduction of *Scn8a* mutant variants. (a)–(c): *Scn8a* variants introduced in the deep layer interneuron only ($Scn8a^{med}$, $Scn8a^{med-jo}$, $Scn8a^{V929F}$).

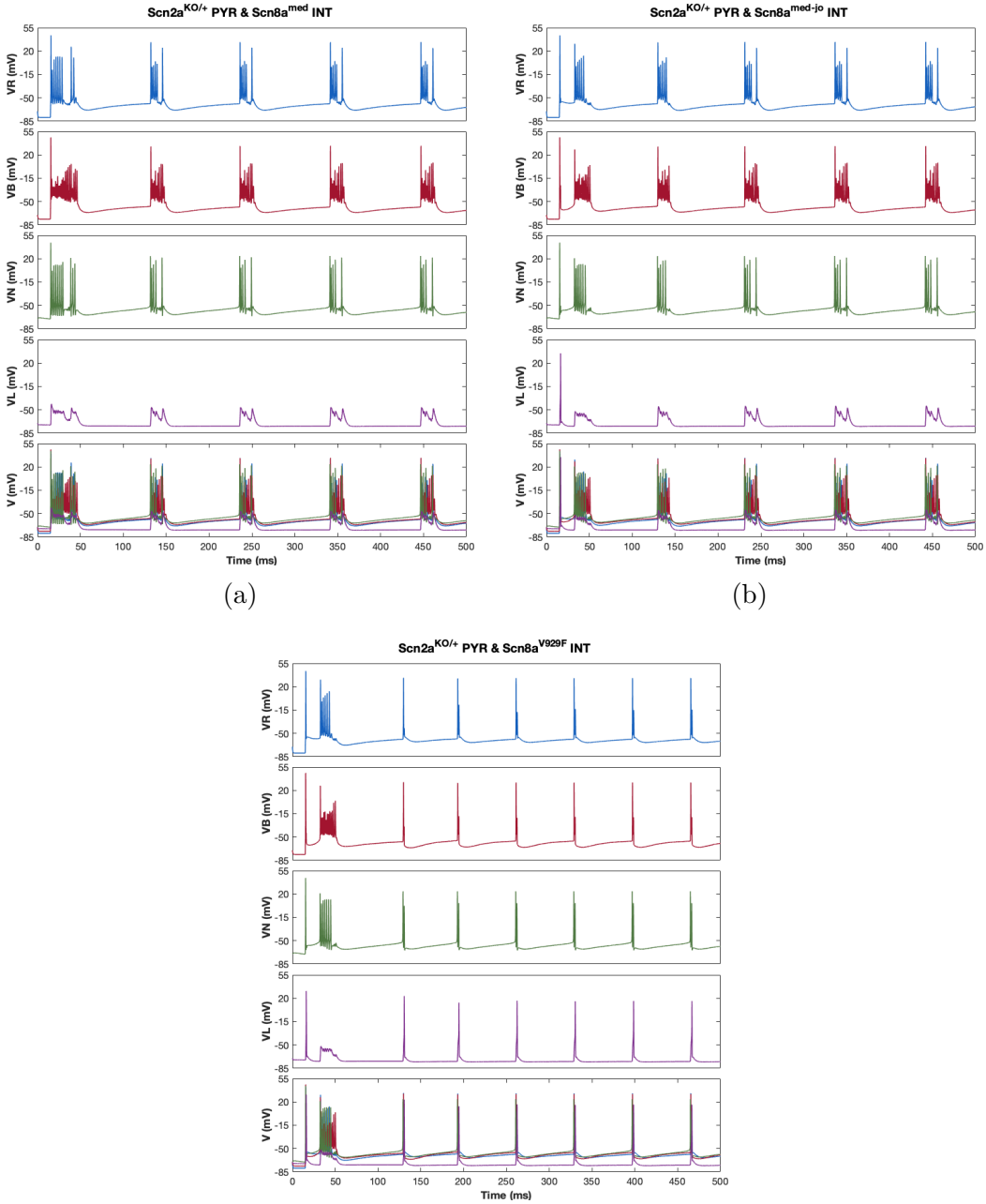

(a) (b)

(c)

Figure 8.14: Network behaviour following the introduction of $Scn2a$ and $Scn8a$ mutant variants. (a)–(c): $Scn2a$ mutation introduced in all pyramidal neurons and $Scn8a$ variants in interneuron ($Scn2a^{KO/+}$ & $Scn8a^{med}$, $Scn2a^{KO/+}$ & $Scn8a^{med-jo}$, $Scn2a^{KO/+}$ & $Scn8a^{V929F}$).

Chapter 9

Conclusion

Epilepsy is suspected of resulting from mutations in genes which encode ion-channels including particular Na^+ channels. Our purpose in this thesis was to explore how some of the mutations mentioned in the literature alter the function of neurons (particularly in the cortex) and contribute to network activity associated with childhood absence epilepsy. Our approach was to first determine normal neuronal network activity in the cortex. The first question to answer was, what do we mean by "normal"? The second question to consider was, how do we know then what is "abnormal", and in particular, what does a hyperexcitable (abnormal) network look like?

To answer the first part, we created a definition based on cortical networks from the literature. Accordingly, a normal network referred to a synchronized response consisting of regular (namely, tonic) firing of neurons. To define what an abnormal network looks like, we considered a signature electrographic feature associated with absence epilepsy, known as spike-wave discharges (or SWDs). These oscillations refer to prolonged discharges of cortical and thalamic neurons during the *spike* component, and periods of quiescence or an inhibited response, during the *wave* component. In fact, it has been noted that an increase in burst firing in cortical neurons causing an increase in synchronized response of firing in thalamocortical networks is an underlying factor of the appearance of SWDs [51]. Thus, accordingly, an abnormal cortical network was defined as one exhibiting synchronized burst discharges. Our cortical network consisted of deep layer pyramidal neurons and an interneuron. In particular, deep layers referred to layers 5 and 6 of the cortex, based on evidence of onset of absence seizures being specific to these layers. A first step in forming a network involved determining individual neuron models. In this regard, we used single-compartment Hodgkin-Huxley type models where each neuron possessed an intrinsic firing behaviour such as tonic firing or bursting. Next, synapses from one neuron to another

were modelled using the formalism by Destexhe and others [71]. By setting biologically plausible synaptic coupling parameters, a normal cortical network was created.

Next, we wanted to investigate what factors convert a normal network into a hyperexcitable one. For this, we considered two factors: impairment of $GABA_A$ synapses, and defects in ion channel function particularly sodium channels, as a result of mutations in the *Scn* genes.

Following evidence of impaired GABA inhibition in the case of absence epilepsy, it was a reasonable approach to model this by reducing the maximal GABA conductance strength for synapses from the interneuron to pyramidal neurons. In this case, we observed that this results in hyperexcitability of the cortical network, consisting of synchronized bursting (including square-wave bursting and parabolic bursting) of all neurons. In addition, the firing frequency of the network reduced significantly by 61% and qualitatively, the nature of firing transformed from regular spiking to slower-frequency bursting. Our interpretation of this behaviour is that it is analogous to the appearance of SWDs in a thalamocortical network in which a normal neuronal network switches to a hypersychronized network. In particular, high-frequency oscillations are converted to slow hypersynchronized oscillations. In addition, burst discharges were discovered to be a network-induced response in neurons exhibiting only tonic-firing otherwise. This was shown by removal of the intrinsically bursting neuron from our network. Its removal also indicated that perhaps it is not necessary for a bursting neuron to be included for the generation of a hyperexcitable network. Our results are interesting in that our cortical network is able to produce its own spike-and-wave oscillations. This network behaviour can be useful for further investigation, especially if we were to consider connectivity of this network in the cortex with one in the thalamus. It would be worth investigating if such spike-and-wave oscillations are also sustained in a thalamocortical network model.

Exploring hyperexcitability of our cortical network further, we modelled sodium channel defects based on literature on *Scn*2*a* and *Scn*8*a* (genes encoding Nav1.2 and Nav1.6 sodium channels) mutations associated with absence epilepsy. While we are aware of mutations in genes that encode h-channels as well as Ca^{2+} channels, we limited our focus to sodium channels especially based on knowledge of voltage-gate sodium channels underlying bursting in neurons. In our model, variants of *Scn*8*a* were introduced for the inhibitory interneuron only, while the *Scn*2*a* variant was introduced in all pyramidal neurons only. Alterations in the interneuron model were specific to the transient Na^+ current, I_{Naf} while alterations in models of pyramidal neurons were specific to the persistent Na^+ current, I_{Nap}, both based on experimental data on effects of the mutations on these sodium channels. To model the *Scn*2*a* mutation, we reduced the maximal conductance of the persistent Na^+ current in individual pyramidal neurons (i.e. as isolated neurons) by 40%. The result

was a reduction in the firing frequency of all neurons, while there was no change in their peak amplitudes. From a dynamical systems point of view, this suggests that as compared to wild-type channels, the closed state is more stable in mutant channels, resulting in a requirement of stronger depolarization to evoke activation and consequently similar firing response to those neurons without any mutations. The modelled $Scn8a$ mutations were of three types- med, $med-jo$, $V929F$. The med variant being a null mutation was modelled by setting the conductance of the transient Na^+ current to 0. To model the other two variants, shifts in voltage-dependence of activation and inactivation of the transient Na^+ current were introduced according to experimental data on electrophysiological effects of the concerned mutations. Both of these alterations included depolarizing shifts in voltage-dependence of activation, while for the $V929F$ variant only, a hyperpolarizing shift in inactivation was also included. These alterations indicate a decrease in the fraction of mutant channels that activate in response to depolarizing input as compared to wild-type (control) channels. To investigate effects of introduction of these variants into our full network model, effects of $Scn8a$ and $Scn2a$ variants were tested individually as well as in combination with each other. In summary, the hierarchy of effects evoking a deteriorating (towards an epileptic network) response of the network is as follows:

$$\boxed{Scn2a} < \boxed{\begin{matrix} Scn2a \\ + \\ Scn8a^V \end{matrix}} < \boxed{Scn8a^V} < \boxed{\begin{matrix} Scn2a \\ + \\ Scn8a^{m-j} \end{matrix}} < \boxed{\begin{matrix} Scn2a \\ + \\ Scn8a^m \end{matrix}} < \boxed{Scn8a^{m-j}} < \boxed{Scn8a^m}$$

Note: $Scn2a = Scn2a^{KO/+}$, $Scn8a^m = Scn8a^{med}$, $Scn8a^{m-j} = Scn8a^{med-jo}$, $Scn8a^V = Scn8a^{V929F}$

Network behaviour following an introduction of $Scn2a$ variant only showed minimal changes, such that all neurons continued to exhibit synchronized regular spiking. On the contrary, introduction of $Scn8a^{med}$ and $Scn8a^{med-jo}$ individually as well as in combination with $Scn2a^{KO/+}$ resulted in burst discharges in all pyramidal neurons. However, $Scn8a^{V929F}$ alone produced network behaviour consisting of alternating burst discharges and single spikes, while in combination with $Scn2a^{KO/+}$ produced a single burst followed by single spikes.

These results are quite satisfactory in that they are able to provide insight on possible mechanisms and the role of various genetic mutations underlying hyperexcitable cortical networks associated with childhood absence epilepsy. It is important to note that for all the mutations considered in this work, the functional consequences are a decrease in the excitability of individual neurons. The effect on network behaviour due to changes at the single-neuron level are therefore dependent on the type of neurons that are altered. In

this regard, alterations due to a mutant variant in (excitatory) pyramidal neurons result in an overall decrease in excitation of the network, while alterations in the (inhibitory) interneuron results in an overall increase in network excitation. While reduced excitation suggests a decreased likelihood of generation of SWDs, functional changes affecting excitatory pyramidal neurons resulting in no excitation at all would no longer be in the regime of a normal cortical network either. Furthermore, our results indicate that deficiency in inhibition due to impaired GABA synapses as well as genetic mutations, gives rise to a hyperexcitable network. Interestingly, when mutations are present together in both pyramidal neurons and the interneuron, our network tends towards a hyperexcitable state as well. This suggests that some mutation types are more debilitating than others. In particular, changes in the interneuron are more dominant than changes in pyramidal neurons, to achieve net hyperexcitability. In addition, these results also suggest that it is possible for multiple mutations to co-exist and increase or decrease the likelihood of giving rise to an epileptic network.

9.1 Limitations and future directions

One of the limitations of this model and results is in the way genetic mutations were modelled. In this regard, it was an extreme case in which all neurons in our population were affected and modelled in the same way. However it is likely that in a larger population size (multiple cells of each type) that there exists some variability in the effects of mutated genes. Furthermore, since neuronal responses due to other neurons are an integrative process, it is possible for a neuron to be unresponsive to feedback from another neuron at all times (particularly, for post-synaptic neuronal spiking to be evoked). Therefore, one other improvement to the existing model would be to consider including a connection probability for the synapses, especially connectivity of a neuron to itself (which is meant to simulate synapses from one neuron to other neurons of the same type). A next step in the more predictable direction would be connectivity with the thalamus to create a thalamocortical network, since the thalamus is a major component in the absence circuitry. A thalamic network consisting of both excitatory and inhibitory neurons would provide additional excitatory and inhibitory feedback with different dynamics, which would be meaningful to explore. In particular, investigating whether SWDs can be sustained in a thalamocortical network under similar conditions as those considered for the cortical network may also be an important step. This is based on knowledge of the importance of the cortex in initiating spike-wave activity followed by the recruitment of the thalamic network in sustaining spike-wave oscillations. The role of genetic mutations can also be

extended to the thalamic network as there is evidence of Ca^{2+}-channel and h-channel mutations in thalamocortical neurons as well as the thalamic reticular neurons giving rise to an epileptic network.

References

[1] R. D. Traub, D. Contreras, M. O. Cunningham, H. Murray, F. E. LeBeau, A. Roopun, A. Bibbig, W.B. Wilent, M. J. Higley, and M. A. Whittington. Single-column thalamocortical network model exhibiting gamma oscillations, sleep spindles, and epileptogenic bursts. *Journal of Neurophysiology*, 93:2194–2232, 2005.

[2] M. O. Cunningham, M. A. Whittington, A. Bibbig, A. Roopun, F. E. LeBeau, A. Vogt, H. Monyer, E. H. Buhl, and R. D. Traub. A role for fast rhythmic bursting neurons in cortical gamma oscillations in vitro. *Proceedings of the National Academy of Sciences of the United States of America*, 101(18):7152–7157, 2004.

[3] Sirven JI editors Bromfield EB, Cavazos JE. *An Introduction to Epilepsy [Internet]*, chapter Chapter 1, Basic Mechanisms Underlying Seizures and Epilepsy. American Epilepsy Society, 2006.

[4] H. Gray. *Anatomy of the Human Body*. Lea and Febiger, Philadelphia and New York, 20 edition, 1918.

[5] L. Danober, C. Deransart, A. Depaulis, M. Vergnes, and C. Marescaux. Pathophysiological mechanisms of genetic absence epilepsy in the rat. *Progress in Neurobiology*, 55(1):27–57, 1998.

[6] World Health Organization. Fact sheets: Epilepsy. http://www.who.int/news-room/fact-sheets/detail/epilepsy.

[7] R. S. Fisher, C. Acevedo, A. Arzimanoglou, A. Bogacz, J. H. Cross, C. E. Elger, J. J. Engel, L. Forsgren, J. A. French, M. Glynn, D. C. Hesdorffer, B. I. Lee, G. W. Mathem, S. L. Mosh e, E. Perucca, I. E. Scheffer, T. Tomson, M. Watanabe, and S. Wiebe. Ilae official report: a practical clinical definition of epilepsy. *Epilepsia*, 55(4):475–482, 2014.

[8] M. De Curtis and M. Avoli. Initiation, propagation, and termina- tion of partial (focal) seizures. *Cold Spring Harbor Perspectives in Medicine*, 5(7), 2015.

[9] Epilepsy Ontario. Types of seizures. http://epilepsyontario.org/about-epilepsy/types-of-seizures/.

[10] WebMD. Types of seizures and their symptoms. https://www.webmd.com/epilepsy/types-of-seizures-their-symptoms#2.

[11] MedicineNet. Epilepsy: Types of seizures and their symptoms. https://www.medicinenet.com/seizuressymptomsandtypes/article.htm#clonicseizures.

[12] E. Posner. Absence seizures in children. *BMJ Clinical Evidence*, 0317, 2008.

[13] J. R. Tenney and T. A. Glauser. The current state of absence epilepsy: Can we have your attention? *Epilepsy Currents*, 13(3):135–140, 2013.

[14] J. Buchhalter. Treatment of childhood absence epilepsyan evidence-based answer at last! *Epilepsy Currents*, 11(1):12–15, 2011.

[15] V. Crunelli and N. Leresche. Childhood absence epilepsy: genes, channels, neurons and networks. *Nature Reviews Neuroscience*, 3(5):371–382, 2002.

[16] Johns Hopkins Medicine. Health library: Electroencephalogram (eeg). https://www.hopkinsmedicine.org/healthlibrary/test_procedures/neurological/electroencephalogram_eeg_92,P07655.

[17] Epilepsy Society. A closer look at eeg. https://www.epilepsysociety.org.uk/closer-look-eeg#.W7UImxNKiog.

[18] A. Depaulis and S. Charpier. Pathophysiology of absence epilepsy: Insights from genetic models. *Neuroscience Letters*, 667:53–65, 2018.

[19] A. M. L. Coenen, W. H. Drinkenburg, M. Inoue, and E. L. J. M. Van Luijtelaar. Genetic models of absence epilepsy, with emphasis on the wag/rij strain of rats. *Epilepy Research*, 12(2):75–86, 1992.

[20] M. Avoli. A brief history on the oscillating roles of thalamus and cortexin absence seizures. *Epilepsia*, 53(5):779–789, 2012.

[21] H. K. M. Meeren, J. P. M. Pijn, E. L. J. M. Van Luijtelaar, A. M. L. Coenen, and F. H. Lopes da Silva. Cortical focus drives widespread corticothalamic networks during spontaneous absence seizures in rats. *Journal of Neuroscience*, 22(4):1480–1495, 2002.

[22] M. R. Islam and J. M. Abdullah. Age-dependent electroencephalographic differences in the genetic absence epilepsy rats from strasbourg (gaers) model of absence epilepsy. *The Malaysian journal of medical sciences*, 21:34–40, 2014.

[23] PubMed Health. How does the nervous system work? https://www.ncbi.nlm.nih.gov/pubmedhealth/PMH0072574/.

[24] Mayfield Brain Spine. Anatomy of the brain. https://mayfieldclinic.com/pe-anatbrain.htm.

[25] Healthline. Thalamus. https://www.healthline.com/human-body-maps/thalmus#1.

[26] Indiana University. Dictionary- cerebral cortex. http://www.indiana.edu/p1013447/dictionary/cercrtx.htm.

[27] Queensland Brain Institute. Lobes of the brain. https://qbi.uq.edu.au/brain/brain-anatomy/lobes-brain.

[28] S. Herculano-Houzel. The human brain in numbers: A lin- early scaled-up primate brain. *Frontiers in Human Neuroscience*, 3:31, 2009.

[29] E. R. Kandel. *Principles of Neural Science*. McGraw-Hill, New York, 2013.

[30] P.E. Ludwig and S. C. Dulebohn. *Neuroanatomy, Neurons*. StatPearls Publishing, Treasure Island, 2018.

[31] Queensland Brain Institute. Axons: the cable transmission of neurons. https://qbi.uq.edu.au/brain/brain-anatomy/axons-cable-transmission-neurons.

[32] H. Lodish, A. Berk, S. L. Zipursky, P. Matsudaira, D. Baltimore, and J. Darnell. *Molecular Cell Biology*. New York: W. H. Freeman, 4 edition, 2000.

[33] B. G. Ermentrout, D. H. Terman, S. S. Antman, J. E. Marsden, L. Sirovich, and S. Wiggins. *Mathematical Foundations of Neuroscience*. Springer New York, 2010.

[34] A. G. Brown. *Nerve Cells and Nervous Systems*. Springer, London, 2001.

[35] B. Fischl and A. M. Dale. Measuring the thickness of the human cerebral cortex from magnetic resonance images. *Proceedings of the National Academy of Sciences*, 97(20):11050–11055, 2000.

[36] H. S. Seung and U. S´umb´ul. Neuronal cell types and connectivity: lessons from the retina. *Neuron*, 83(6):1262–1272, 2014.

[37] H. Markram, M. Toledo-Rodriguez, Y. Wang, A. Gupta, G. Silberberg, and C. Wu. Interneurons of the neocortical inhibitory system. *Nature Reviews Neuroscience*, 5:793–807, 2004.

[38] M. A. Patestas and L. P. Gartner. *Cerebral Cortex*. Blackwell Publishing, Oxford, 2006.

[39] K. I. Van Aerde and D. Feldmeyer. Morphological and physiological characterization of pyramidal neuron subtypes in rat medial prefrontal cortex. *Cerebral Cortex*, 25(3):788–805, 2015.

[40] T. Freund and S. Kali. Interneurons. doi:10.4249/scholarpedia.4720.

[41] V. B. Mountcastle. The columnar organization of the neocortex. *Brain*, 120(4):701–722, 1997.

[42] J. Alonso and Y. Chen. Receptive field. http://doi.org/10.4249/scholarpedia.5393, 2009.

[43] J. C. Horton and D. L. Adams. The cortical column: a structure without a function. *Philosophical transactions of the Royal Society of London. Series B, Biological sciences*, 360(1456):837–862, 2005.

[44] R. T. Narayanan, D. Udvary, and M. Oberlaender. Cell type-specific structural organization of the six layers in rat barrel cortex. *Frontiers in Neuroanatomy*, 11:91, 2017.

[45] C. M. Constantinople and R. M. Bruno. Deep cortical layers are activated directly by thalamus. *Science*, 340(6140):1591–1594, 2013.

[46] A. C. Albuja and P. B. Murphy. *Seizure, Absence*. StatPearls Publishing, Treasure Island, 2018.

[47] R. Fama and E. V. Sullivan. Thalamic structures and associated cognitive functions: Relations with age and aging. *Neuroscience and biobehavioral reviews*, 54:29–37, 2015.

[48] Kenhub GmbH. Thalamic nuclei. https://www.kenhub.com/en/library/anatomy/thalamic-nuclei.

[49] Y. Lam and S. M. Sherman. Functional organization of the thalamic input to the thalamic reticular nucleus. *The Journal of Neuroscience*, 31(18):6791–6799, 2011.

[50] P. Érdi, B. Sen Bhattacharya, and A. L. Cochran. *Computational Neurology and Psychiatry*, volume 6, chapter Outgrowing Neurological Diseases: Microcircuits, Conduction Delay and Childhood Absence Epilepsy, pages 11–47. Springer International Publishing, 2007.

[51] T. Bal, D. Debay, and A. Destexhe. Cortical feedback controls the frequency and synchrony of oscillations in the visual thalamus. *Journal of Neuroscience*, 20(19):7478–7488, 2000.

[52] H. Blumenfeld and D. A. McCormick. Corticothalamic inputs control the pattern of activity generated in thalamocortical networks. *Journal of Neuroscience*, 20(13):5153–5162, 2000.

[53] J. R. Huguenard and D. A. Prince. Intrathalamic rhythmicity studied in vitro: nominal t-current modulation causes robust antioscillatory effects. *Journal of Neuroscience*, 14(9):5485–5502, 1994.

[54] G. K. Kostopoulos. Involvement of the thalamocortical system in epileptic loss of consciousness. *Epilepsia*, 42(3):13–19, 2001.

[55] S. M. Sherman and R. W. Guillery. Functional organization of thalamocortical relays. *Journal of Neurophysiology*, 76(3):1367–1395, 1996.

[56] J. R. Huguenard. Thalamocortical circuits and excitability. *Epilepsy Currents*, 2001.

[57] G. K. Kostopoulos. Spike-and-wave discharges of absence seizures as a transformation of sleep spindles: the continuing development of a hypothesis. *Clinical Neurophsyiology*, 111(Supplement 2):S27–S38, 2000.

[58] H. K. M. Meeren, G. Van Luijtelaar, F. H. Lopes da Silva, and A. M. L. Coenen. Evolving concepts on the pathophysiology of absence seizures: The cortical focus theory. *Archives of Neurology*, 62(3):371–376, 2005.

[59] M. Bazhenov and I. Timofeev. Thalamocortical oscillations. *Scholarpedia*, 1(6):1319, 2006.

[60] M. Steriade, D. A. McCormick, and T. J. Sejnowski. Thalamocortical oscillations in the sleeping and aroused brain. *Science*, 262(5134):679–685, 1993.

[61] A. Destexhe. *Computational Neuroscience in Epilepsy*, chapter Cortico-thalamic feedback: a key to explain absence seizures, pages 184–214. Elsevier, Amsterdam, 2008.

[62] A. Mandal. Epilepsy pathophysiology. https://www.news-medical.net/health/Epilepsy-Pathophysiology.aspx, August 2018.

[63] P. Jiruska, M. de Curtis, J. G. Jefferys, C. A. Schevon, S. J. Schiff, and K. Schindler. Synchronization and desynchronization in epilepsy: controversies and hypotheses. *The Journal of Physiology*, 591(4):787–797, 2012.

[64] I. Osorio, H. Zaveri, M. Frei, and S. Arthurs, editors. *Epilepsy: The Intersection of Neurosciences, Biology, Mathematics, Engineering, and Physics*, chapter 35: Autosomal Dominant Nocturnal Frontal Lobe Epilepsy: Excessive Inhibition?, pages 469–477. CRC Press, 1st edition, 2011.

[65] P. Polack, I. Guillemain, E. Hu, C. Deransart, A. Depaulis, and S. Charpier. Deep layer somatosensory cortical neurons initiate spikeand-wave discharges in a genetic model of absence seizures. *Journal of Neuroscience*, 27(24):6590–6599, 2007.

[66] V. A. Shaposhnik. Walter nernst and analytical chemistry. *Journal of Analytical Chemistry*, 63(2):199–201, 2008.

[67] D. J. Aidley. *The Physiology of Excitable Cells*. Cambridge University Press, Cambridge, 1998.

[68] R. Brette. What is the most realistic single-compartment model of spike initiation? *PLoS Computational Biology*, 11(4), 2015.

[69] U. S. Bhalla. *Multi-compartmental Models of Neurons*, pages 193–225. Springer Netherlands, Dordrecht, 2012.

[70] D. Purves, G.J. Augustine, D. Fitzpatrick, and et al., editors. *Neuroscience. 2nd edition.* Sinauer Associates, Sunderland, 2001.

[71] A. Destexhe, Z. F. Mainen, and T. J. Sejnowski. Synthesis of models for excitable membranes, synaptic transmission and neuromodulation using a common kinetic formalism. *Journal of Computational Neuroscience*, 1(3):195–230, 1994.

[72] M. S. Martin, B. Tang, L. A. Papale, Frank H. Y., William A. C., and A. Escayg. The voltage-gated sodium channel scn8a is a genetic modifier of severe myoclonic epilepsy of infancy. *Human Molecular Genetics*, 16(23):2892–2899, 2007.

[73] H. Vacher, D. P. Mohapatra, and J. S. Trimmer. Localization and targeting of voltage-gated ion channels in mammalian central neurons. *Physiological Reviews*, 88(4):1407–1447, 2008.

[74] N. D. Child and E. E. Benarroch. Differential distribution of voltage-gated ion channels in cortical neurons. *Neurology*, 82(11):989–999, 2014.

[75] A. Escayg and A. L. Goldin. Sodium channel scn1a and epilepsy: muta- tions and mechanisms. *Epilepsia*, 51(9):1650–1658, 2010.

[76] L. A. Papale, B. Beyer, J. M. Jones, L. M. Sharkey, S. Tufik, M. Epstein, V. A. Letts, M. H. Meisler, W. N. Frankel, and A Escayg. Heterozygous mutations of the voltage-gated sodium channel scn8a are associated with spike-wave discharges and absence epilepsy in mice. *Human Molecular Genetics*, 18(9):1633–1641, 2009.

[77] J. E. O'Brien and M. H. Meisler. Sodium channel scn8a (nav1.6): properties and de novo mutations in epileptic encephalopathy and intellectual disability. *Frontiers in Genetics*, 4:213, 2013.

[78] S. L. Jones and T. M. Svitkina. Axon initial segment cytoskeleton: Architecture, development, and role in neuron polarity. *Neural Plasticity*, 2016, 2016.

[79] A. Van Wart and G. Matthews. Impaired firing and cell-specific compensation in neurons lacking nav1.6 sodium channels. *Journal of Neuroscience*, 26(27):7172–7180, 2006.

[80] M. K. Oliva, T. C. McGarr, B. J. Beyer, E. Gazina, D. I. Kaplan, L. Cordeiro, E. Thomas, S. D. Dib-Hajj, S. G. Waxman, W. N. Frankel, and S. Petrou. Physiological and genetic analysis of multiple sodium channel variants in a model of genetic absence epilepsy. *Neurobiology of disease*, 67:180–190, 2014.

[81] W. Hu, C. Tian, T. Li, M. Yang, H. Hou, and Y. Shu. Distinct contributions of nav1.6 and nav1.2 in action potential initiation and backpropagation. *Nature Neuroscience*, 12:996–1002, 2009.

[82] I. Ogiwara, H. Miyamoto, N. Morita, N. Atapour, E. Mazaki, I. Inoue, T. Takeuchi, S. Itohara, Y. Yanagawa, K. Obata, T. Furuichi, T. K. Hensch, and K. Yamakawa. Nav1.1 localizes to axons of parvalbumin-positive inhibitory interneurons: a circuit basis for epileptic seizures in mice carrying an scn1a gene mutation. *The Journal of Neuroscience*, 27(22):5903–5914, 2007.

[83] C. D. Makinson, B. S. Tanaka, J. M. Sorokin, J. C. Wong, C. A. Christian, A. L. Goldin, and J. R. Huguenard. Regulation of thalamic and cortical network synchrony by scn8a. *Neuron*, 93(5):1165–1179, 2017.

[84] I. Ogiwara, H. Miyamoto, T. Tatsukawa, T. Yamagata, T. Nakayama, N. Atapour, and K. ... Yamakawa. Nav1.2 haplodeficiency in excitatory neurons causes absence-like seizures in mice. *Communications biology*, 1(96), 2018.

[85] N. P. Poolos. The h-channel: A potential channelopathy in epilepsy? *Epilepsy Behaviour*, 7(1):51–56, 2005.

[86] C. Wahl-Schott and M. Biel. Hcn channels: Structure, cellular regulation and physiological function. *Cellular and Molecular Life Sciences*, 66:470, 2009.

[87] H. C. Pape. Queer current and pacemaker: the hyper polarization-activated cation current in neurons. *Annual Review of Physiology*, 58:299–327, 1996.

[88] B. Santoro and T. Z. Baram. The multiple personalities of h-channels. *Trends in Neurosciences*, 26(10):550–554, 2003.

[89] B. Santoro, S. Chen, A. Luthi, P. Pavlidis, G. P. Shumyatsky, G. R. Tibbs, and S. A. Siegelbaum. Molecular and functional heterogeneity of hyperpolarization-activated pacemaker channels in the mouse cns. *The Journal of Neuroscience*, 20(14):5264–5275, 2000.

[90] J. C. DiFrancesco and D. DiFrancesco. Dysfunctional hcn ion channels in neurological diseases. *Frontiers in Cellular Neuroscience*, 6:174, 2015.

[91] A. Ludwig, T. Budde, J. Stieber, S. Moosmang, C. Wahl, K. Holthoff, and F. Hofmann. Absence epilepsy and sinus dysrhythmia in mice lacking the pacemaker channel hcn2. *The EMBO Journal*, 22(2):216–224, 2003.

[92] U. Strauss, M. H. Kole, A. U. Bräuer, J. Pahnke, R. Bajorat, A. Rolfs, R. Nitsch, and R. A. Deisz. An impaired neocortical ih is associated with enhanced excitability and absence epilepsy. *European Journal of Neuroscience*, 19(11):3048–3058, 2004.

[93] M. H. Kole, A. U. Bräuer, and G. J. Stuart. Inherited cortical hcn1 channel loss amplifies dendritic calcium electrogenesis and burst firing in a rat absence epilepsy model. *The Journal of Physiology*, 578(Pt 2):507–525, 2007.

[94] Z. Huang, M. C. Walker, and M. M. Shah. Loss of dendritic hcn1 subunits enhances cortical excitability and epileptogenesis. *The Journal of Neuroscience*, 29(35):10979–10988, 2009.

[95] J. R. Huguenard and D. A. McCormick. Simulation of the currents involved in rhythmic oscillations in thalamic relay neurons. *Journal of Neurophysiology*, 68(4):1373–1383, 1992.

[96] M. Martina and P. Jonas. Functional differences in na+ channel gating between fast-spiking interneurones and principal neurones of rat hippocampus. *Journal of Physiology*, 505(3):593–603, 1997.

[97] M. Martina, J. H. Schultz, H. Ehmke, H. Monyer, and P. Jonas. Functional and molecular differences between voltage-gated k+ channels of fast-spiking interneurons and pyramidal neurons of rat hippocampus. *Journal of Neuroscience*, 18(20):8111–8125, 1998.

[98] D. A. McCormick and J. R. Huguenard. A model of the electrophysiological properties of thalamocortical relay neurons. *Journal of Neurophysiology*, 68(4):1384–1400, 1992.

[99] R. D. Traub, H. B. Eberhard, T. Gloveli, and M. A. Whittington. Fast rhythmic bursting can be induced in layer 2/3 cortical neurons by enhancing persistent na+ conductance or by blocking bk channels. *Journal of Neurophysiology*, 89(2):909–921, 2003.

[100] Jefferys J. G. Miles R. Whittington M. A. Tóth K. Traub, R. D. A branching dendritic model of a rodent ca3 pyramidal neurone. *Journal of Physiology*, 481(Pt 1):79–95, 1994.

[101] A. Larkman and A. Mason. Correlations between morphology and electrophysiology of pyramidal neurons in slices of rat visual cortex. ii. electrophysiology. *Journal of Neuroscience*, 10(5):1415–1428, 1990.

[102] M. E. Larkum, J. J. Zhu, and B. Sakmann. Dendritic mechanisms underlying the coupling of the dendritic with the axonal action potential initiation zone of adult rat layer 5 pyramidal neurons. *The Journal of Physiology*, 533:447–466, 2001.

[103] D. Johnston, J. C. Magee, C. M. Colbert, and B. R. Cristie. Active properties of neuronal dendrites. *Annual Review of Neuroscience*, 19:165–186, 1996.

[104] S. R. Williams and G. J. Stuart. Mechanisms and consequences of action potential burst firing in rat neocortical pyramidal neurons. *The Journal of Physiology*, 521:467–482, 1999.

[105] J. R. Gibson, M. Beierlein, and B. W. Connors. Two networks of electrically coupled inhibitory neurons in neocortex. *Nature*, 402:75–79, 1999.

[106] Y. Kawaguchi. Physiological subgroups of nonpyramidal cells with specific morphological characteristics in layer ii/iii of rat frontal cortex. *The Journal of Neuroscience*, 15:2638–2655, 1995.

[107] Y. Kawaguchi. Physiological, morphological, and histochemical characterization of three classes of interneurons in rat neostriatum. *The Journal of Neuroscience*, 13(11):4908–4923, 1993.

[108] S. Hestrin. Different glutamate receptor channels mediate fast excitatory synaptic currents in inhibitory and excitatory cortical neurons. *Neuron*, 11(6):1083–1091, 1993.

[109] C. M. Houston, D. P. Bright, L. G. Sivilotti, M. Beato, and T. G. Smart. Intracellular chloride ions regulate the time course of gaba-mediated inhibitory synaptic transmission. *Journal of Neuroscience*, 29(33):10416–10423, 2009.

[110] P. A. Salin and D. A. Prince. Spontaneous gabaa receptor-mediated inhibitory currents in adult rat somatosensory cortex. *Journal of Neurophysiology*, 75(4):1573–1588, 1996.

[111] W. W. Lytton and T. J. Sejnowski. Simulations of cortical pyramidal neurons synchronized by inhibitory interneurons. *Journal of Neurophysiology*, 1991.

[112] H. J. Luhmann, T. Mittmann, G. Van Luijtelaar, and U. Heinemann. Impairment of intracortical gabaergic inhibition in a rat model of absence epilepsy. *Epilepy Research*, 22(1):43–51, 1995.

[113] I. Lampl and Y. Yarom. Subthreshold oscillations of the membrane potential: A functional synchronizing and timing device. *Journal of Neurophysiology*, 70(5):2181–2186, 1993.

[114] D. C. Kohrman, J. B. Harris, and H. M. Miriam. Mutation detection in the med and medj alleles of the sodium channel scn8a. *Journal of Biological Chemistry*, 271:17576–17581, 1996.

[115] D. C. Kohrman, M. R. Smith, A. L. Goldin, J. Harris, and M. H. Meisler. A missense mutation in the sodium channel scn8a is responsible for cerebellar ataxia in the mouse mutant jolting. *Journal of Neuroscience*, 16(19):5993–5999, 1996.

[116] A. L. Hodgkin and A. F. Huxley. A quantitative description of membrane current and its application to conduction and excitation in nerve. *The Journal of Physiology*, 117(4):500–544, 1952.

[117] David Sterratt, Bruce Graham, Andrew Gillies, and David Willshaw. *Principles of Computational Modelling in Neuroscience*. Cambridge University Press, 2011.

[118] David C. Sterratt. *Goldman-Hodgkin-Katz Equations*, pages 1300–1302. Springer New York, New York, NY, 2015.

[119] D. E. Goldman. POTENTIAL, IMPEDANCE, AND RECTIFICATION IN MEMBRANES. *The Journal of General Physiology*, 27(1):37–60, 1943.

[120] A. L. Hodgkin and B. Katz. he effect of sodium ions on the electrical activity of giant axon of the squid. *The Journal of Physiology*, 108(1):37–77, 1949.

[121] B. Fontaine, J. L. Pea, and R. Brette. Spike-threshold adaptation predicted by membrane potential dynamics in vivo. *PLoS Computational Biology*, 10(4), 2014.

[122] G. S. Yi, J. Wang, K. M. Tsang, X. L. Wei, and B. Deng. Biophysical insights into how spike threshold depends on the rate of membrane potential depolarization in type i and type ii neurons. *PLoS One*, 10(6), 2015.

[123] A. Depaulis, O. David, and S. Charpier. The genetic absence epilepsy rat from strasbourg as a model to decipher the neuronal and network mechanisms of generalized idiopathic epilepsies. *Journal of Neuroscience Methods*, 260:159–174, 2016.

[124] A. Destexhe. *Neuronal Networks in Brain Function, CNS Disorders, and Therapeutics*, chapter 2: Network Models of Absence Seizures, pages 11–35. Academic Press, 2014.

[125] A. Destexhe. Spike-and-wave oscillations. *Scholarpedia*, 2(2):1402, 2007.

[126] Y. Futatsugi and J. J. Riviello Jr. Mechanisms of generalized abence epilepsy. *Brain and Development*, 20(2):75–79, 1998.

[127] S. Herrmann, S. Schnorr, and A. Ludwig. Hcn channels—modulators of cardiac and neuronal excitability. *International Journal of Molecular Sciences*, 16(1):1429–1447, 2015.

[128] J. F. van Brederode and G. L. Snyder. A comparison of the electrophysiological properties of morphologically identified cells in layers 5b and 6 of the rat neocortex. *Neuroscience*, 50(2):315–337, 1992.

[129] K. A. Martin and D. Whitteridge. Form, function and intracortical projections of spiny neurones in the striate visual cortex of the cat. *The Journal of Physiology*, 353:463–504, 1984.

[130] J. G. Pamavelas, R. Luder, S. G. Pollard, K. Sullivan, and A. R. Lieberman. A qualitative and quantitative ultrastructural study of glial cells in the developing visual cortex of the rat. *Philosophical transactions of the Royal Society of London. Series B, Biological sciences*, 301:55–84, 1983.

[131] C. D. Gilbert and T. N. Wiesel. Morphology and intracortical projections of functionally characterised neurones in the cat visual cortex. *Nature*, 280(5718):120–125, 1979.

[132] M. Tjia, X. Yu, L. S. Jammu, J. Lu, and Y. Zuo. Pyramidal neurons in different cortical layers exhibit distinct dynamics and plasticity of apical dendritic spines. *Frontiers in Neural Circuits*, 11:43, 2017.

[133] Z. Xiang, J. R. Huguenard, and D. A. Prince. Cholinergic switching within neocortical inhibitory networks. *Science*, 281(5379):985–988, 1998.

[134] Healthline. Brain anatomy and function. https://www.healthline.com/human-body-maps/brain#anatomy-and-function.

[135] Berkeley University of California. The central nervous system. https://mcb.berkeley.edu/courses/mcb135e/central.html.

[136] Berkeley University of California. The nervous system. https://mcb.berkeley.edu/courses/mcb135e/nervous.html.

[137] C. S. Cheah, F. H. Yu, R. E. Westenbroek, F. K. Kalume, J. C. Oakley, G. B. Potter, and W. A. Catterall. Specific deletion of nav1.1 sodium channels in inhibitory interneurons causes seizures and premature death in a mouse model of dravet syndrome. *Proceedings of the National Academy of Sciences of the United States of America*, 109(36):14646–14651, 2012.

[138] I. Ogiwara, T. Iwasato, H. Miyamoto, R. Iwata, T. Yamagata, E. Mazaki, and K. Yamakawa. Nav1.1 haploinsufficiency in excitatory neurons ameliorates seizure-associated sudden death in a mouse model of dravet syndrome. *Human Molecular Genetics*, 22(23):4784–4804, 2013.